NOTE TO USERS

3-D Simulation of Flow and Sediment Transport during a Controlled Flood in a Short River Reach

Akinbola Olukayode George

A Thesis

in

The Department

of

Building, Civil, and Environmental Engineering

Presented in Partial Fulfillment of the Requirements

for the Degree of Master of Applied Science (Civil Engineering) at

Concordia University

Montreal, Quebec, Canada

January 2005

Your file Votre référence
ISBN: 0-494-04353-9
Our file Notre référence
ISBN: 0-494-04353-9

ABSTRACT

3-D Simulation of Flow and Sediment Transport during a Controlled Flood in a Short River Reach

George, Akinbola Olukayode

Controlled floods are often used in rivers to remove fine sediments that accumulate within gravel particles. Three-dimensional numerical models can predict the flow field and bed shear stress in a very detailed way. In the present study is to use a three-dimensional model is used to predict flow field, assess the effect of inlet conditions, predict bed shear stress, and bed load transport rates during a controlled flood in a natural river. The study site is the Escoumins River (Quebec), where a dam upstream of the studied reach has been used to create control floods. Field measurements (flow and bed load transport) and 2-D simulation results were available, allowing a comparison between the 3-D model, 2-D model and the field measurements. A body-fitted coordinate grid was used and several inlet flow conditions were tested.

Results show that the 3-D model predicts the flow dynamics of a natural river very well. However, the validation of the simulation greatly depends on the mesh generated, inlet conditions, boundary conditions, and the accuracy of the field measurements. Estimates of bed shear stresses in particular cannot be validated easily. Most sediment bed load transport equations greatly under-predict, or over-predict the sediment transport rates. The Eugelund-Hansen stream power equation was deemed to be more reliable for bed load predictions compared to shear stress

based formulae. Hence, this approach was used to compare the predicted sediment transport with the field data. 3-D models have the ability to give better estimates of the bed shear stresses compared to shear stresses estimated from indirect field measurements or from 2-D models. Bed shear stresses obtained from the 3-D model used in the Eugelund-Hansen equation provided the best match with field measurements of bed load rates, when compared to the results based on 2-D simulation shear stress or the indirect estimate of the shear stress based on field measurements.

ACKNOWLEDEMENTS

I wish to express my deepest gratitude and appreciation to Dr. P.M Biron and Dr. A.S Ramamurthy for their advice, during the course of this study. The financial support provided by Dr. P.M Biron is thankfully acknowledged.

I also wish to express my sincere thanks to doctoral students Christian Latulippe and Sangsoo Han for their help and assistance during the course of this research.

In addition, loving thanks to my parents and family for their love and support in each step of my studies.

Above all, I would like to appreciate the Almighty God for seeing me through the course of this research.

TABLE OF CONTENTS

Table of contents....vi
List of Figures....viii
List of Tables....xi
List of Symbols....xiii
1. INTRODUCTION 1
1.0 Background and motivation 1
1.2 Research goals and objectives 3
2. LITERATURE REVIEW 4
2.1 Physical modeling 4
2.2 Field measurements 5
2.3 Numerical modeling 8
2.3.1 Grid generation 9
2.3.2 Boundary conditions 10
2.4 Flow and sediment modeling 12
2.5 Bed load transport 18
3.0 METHODOLOGY 24
3.1 Study reach 24
3.2 Previous field and numerical modeling work 27
3.2.1 Field measurements 27
3.2.1.1 Bed topography 27
3.2.1.2 Velocity measurements 28
3.2.1.3 Bed shear stress estimates 28
3.2.1.4 Sediment transport 32
3.2.2 Two-dimensional numerical simulation 32
3.3 Three-dimensional modeling for flow and sediment transport 35
3.3.1 Mesh generation 35
3.3.2 Computational modeling 42
3.3.2.1 Numerical solution 43
3.3.3 Boundary conditions of 3-D simulation 45
3.3.3.1 Downstream simulations 46
3.3.3.2 Upstream simulations 48
3.3.3.3 Combined simulations 50
3.3.4 Bed load equations 52

4.0 RESULTS **54**

4.1 Flow field 54

4.2 Validation of results 61

4.2.1 Velocity data 61
4.2.2 Bed shear stress distribution 73
4.2.2.1 Shear stress based on Log-law 73
4.2.2.2 Shear stress based on quadratic stress law 75
4.3 Bed load transport 78

5.0 DISCUSSION OF RESULTS **87**

5.1 Discussion 87

5.1.1 Flow field 87
5.1.2 Bed shear stress 87
5.1.3 Bed load transport 88
6.0 SUMMARY, CONCLUSIONS AND RECOMMENDATIONS **93**

6.1 Summary 93

6.2 Conclusions 94

6.2 Recommendations 94

REFERENCES **96**

LIST OF FIGURES

Fig. 2.1 An illustration of the effect of the upstream boundary condition specification upon flow field prediction. 13

Fig. 2.2 Simulated near surface and near bed flow patterns with outer bank 14

Fig. 2.3 Simulated velocity distribution in the top and bottom layers of Interpolated filled contour estimated bed shear stress using the (a) third cell (assumed near bed) (b) fourth cell (depth-averaged) computational cells in CFD models. 15

Fig. 2.4 Simulated secondary circulation at selected cross-sections of two bends 16

Fig. 2.5 Comparison between calculated and measured bed load discharge 20

Fig. 2.6 Predicted and observed gravel transport rates along the Vedder River 22

Fig. 3.1 Site location 25

Fig. 3.2 Bed topography of the Escoumins Rivers and limit of study reach 26

Fig. 3.3 Interpolated filled contours of velocity distribution near the bed and the depth-averaged 29

Fig. 3.4 Interpolated filled contours of bed shear stress based on the near bed method and the depth-averaged method 31

Fig. 3.5 Location of sediment traps in the study reach 33

Fig. 3.6 Simulation results for velocity distribution using the Manning and Limerinos equations 36

Fig. 3.7 Simulation results for bed shear stress distribution using the Manning and Limerinos equations 37

Fig. 3.8 Multi-block grid used in the study 39

LIST OF FIGURES

Fig. 3.9	Grid angles at apex P	41
Fig. 3.10	Study section and the upstream section	46
Fig. 3.11	Study reach as in Fig. 3.10 and inlet velocities	47
Fig. 3.12	Entire upstream section of the study reach	49
Fig. 3.13	Upstream simulation from mid-channel bar	49
Fig. 3.14	Upstream simulation without mid-channel bar	50
Fig. 3.15	Combined simulation sections as in Fig. 3.11 and inlet velocities	51
Fig. 4.1	Depth-averaged velocity distribution for study reach using uniform inlet velocity, dual inlet velocity, and three inlet velocity values	55
Fig. 4.2	Cross-sections showing secondary flow for sections 1-1′, 2-2′, and 3-3′ of Fig. 4.1	56
Fig. 4.3	Depth-averaged velocity distribution using outlet velocities from upstream section as inlet velocities of study reach for entire upstream section, from the mid-channel bar, and before mid-channel bar	57
Fig. 4.4	Cross-sections showing secondary flows for sections 4-4′, 5-5′, and 6-6′ of Fig. 4.3	59
Fig. 4.5	Depth-averaged velocity distribution using inlet velocities as in Fig. 3.15b, Fig. 3.15c, and Fig. 3.15d	60
Fig. 4.6	Cross-sections showing secondary flows for sections 7-7′, 8-8′, and 9-9′ of Fig. 4.5	62

LIST OF FIGURES

Fig. 4.7	Comparison of interpolated filled contours of the depth-averaged velocity distribution of the field measurements and the 3-D simulation for study section with inlet conditions as in Fig. 4.5c	64
Fig.4.8	Correlation results of the depth-averaged velocity between field measurements and the 3-D model results	65
Fig. 4.9	Correlation results of the depth-averaged velocity between field measurements and the 2-D model results	65
Fig. 4.10	Study reach section showing the outliers of Fig. 4.8	67
Fig. 4.11	Correlation results of the depth-averaged velocity between the field measurements and 3-D model results after elimination of the outliers	68
Fig. 4.12	Interpolated filled contour for the near bed velocity distribution for the field measurements and the 3-D model	70
Fig. 4.13	Correlation results between the field measurement near bed velocity measurements and the 3-D model results	71
Fig. 4.14	Correlation results the field measurement near bed velocity measurements and the 3-D model results after the elimination of the outliers in Fig. 4.10	71
Fig. 4.15	Comparison between the estimated bed shear stress interpolated filled contour between field measurements and 3-D model using the combined simulation results as in Fig. 4.5c	73
Fig. 4.16	Interpolated filled contour estimated bed shear stress using the third and fourth cells	75

LIST OF FIGURES

Fig. 4.17 Correlation results between the estimated bed shear stresses from 3-D model and field measurements (a) using the third cell (assumed near bed) velocities and comparing with results in field measurement using equation 4.2 (b) using the depth-averaged velocities (fourth cell) and comparing with results in field measurement using equation 4.2 75

Fig. 4.18 Bed load comparison between using the different bed shear stresses in the Eugelund-Hansen stream power equation and the actual field measurement (a) for the traps (b) correlation results 82

Fig. 4.19 Field measurements of the bed load transport for the traps and the estimated bed shear stress from field measurements. 83

Fig. 4.20 Field measurements of the bed load transport for the traps and the estimated bed shear stress from 2-D model. 84

Fig. 4.21 Field measurements of the bed load transport for the traps and the estimated bed shear stress from 3-D model. 85

LIST OF TABLES

Table 3.1	Controlled floods in 1999	27
Table 3.2	Computed sediment transport for control flood 6	33
Table 4.1	Summary of simulation	63
Table 4.2	Correlation results of 3-D models of natural rivers	68
Table 4.3	Estimated bed load transport using different equations and different diameters	78
Table 5.1	Estimates of bed load transport using estimated bed shear stress from field measurements	90
Table 5.2	Estimates of bed load transport using estimated bed shear stress from 2-D model	91

LIST OF SYMBOLS

μ = Dynamic viscosity

ϕ = Latitude of the site in study

ω = Rotational acceleration of the earth

κ = Von Karman's constant

ρ = Water density

B = Porosity

c = Celerity waves

C_D = Drag coefficient

C_d = Sediment coefficient

D = Flow depth

d, d_m, d_{50}, d_{84} = grain size diameter

E = Roughness parameter

f_c = Coriolis factor

g = gravitational acceleration

h = Water surface level

k_s = Sand grain roughness height

k and k′ = Reciprocals of Manning's coefficient

n = Manning coefficient

p = Pressure

q = Water discharge

q_b = Bed load discharge

R = Hydraulic radius

LIST OF SYMBOLS

R^2 = Coefficient of determination

s = ratio of mass density of sediment to mass density of water

S = Total energy

t = time

u, v, w = velocity components

u_i =Instantaneous value of the velocity

V = Resultant velocity

V_* = Shear velocity

Y = Normal distance of first grid cell from the wall

z = Velocity distance from the channel bottom

z_c = bed level with respect to a plane

z_o = Bed roughness height

γ = Specific gravity of water

γ_s = Specific gravity of sediment

τ_c = Critical shear stress

τ_o = Shear stress

υ = Kinematic viscosity

1. INTRODUCTION

1.0 Background and motivation

The survival of fish depends on the quality of the fish habitat, which itself is a function of flow conditions, temperature and bed grain size (Tappel and Bjornn, 1983; Heggberget, 1988; Scrivener and Brownlee, 1989; Heede and Rinne, 1990). Sediments are transported during high flows in a river. However, fine sediments can accumulate within the gravel particles and have a negative impact on the survival rate of fish eggs in the substrate (Alexander and Hansen, 1986; Rinne and Medina, 1989; Heed and Rinne, 1990). In many rivers, changes in land use or dam construction have resulted in increased deposition of fine particles on the bed. In these cases, controlled floods can be used to remove fine sediments that accumulate within the gravel of a riverbed (Milhous, 1998; Andrews and Pizzi, 2000; Schmidt et al., 2001).

In order to determine whether a given discharge can create sufficient sediment transport to remove the fine particles, accurate estimates of bed shear stress are required (Paquier and Khodashenas, 2002). The spatial pattern of bed shear stress distribution is dependent on the spatial distribution of resistance to flow (Bennett, 1995). Numerical models, particularly 3-D models have been shown to predict the flow field reasonably accurately in natural rivers (Lane et al., 1999; Ferguson et al., 2003). However, the prediction of sediment transport is much more complex. Estimates of sediment transport can be accomplished with the use of various dynamic transport equations, based on bed shear stress or stream power (DuBoys, Shields, Einstein bed load function, Meyer-Peter-Muller, Einstein Brown and Parker et al., 1982). Because 3-D numerical models can

predict the flow field and shear stress very close to the bed in a detailed way, they are promising tools to determine potential zones of bed load transport, particularly in complex river reaches such as meandering rivers. Meandering rivers are ubiquitous in the fluvial system and have so far been examined mainly using field studies and physical modeling (Odgaard and Bergs, 1988; Whiting and Detrich, 1993; Bathurst et al., 2002). There are, however, several limitations in these studies due to factors such as the restricted range in flow conditions, and flow measurements based on a limited number of point measurements.

Flow and sediment transport calculations in a river are one of the most important tasks in river engineering and related areas. The estimation of the flow and sediment transport is very difficult, since the flow in open channels is turbulent. The flow passes through the stream cross-section, which is irregular in geometry and varies with time and the sediment transport phenomena itself is complex (Wu et al., 2000). Numerical models of flow and sediment transport in a river have mostly been carried out using 1-D and 2-D simulations (Wu et al., 2000). These approaches neglect the influence of secondary flows such as those present in meandering rivers (Andrew and Nelson, 1989; Shimizu and Itakura, 1989; Tingsanchali and Maheswaran, 1990; Bridge and Gabel, 1992; Lane et al., 1995; Butler et al., 2001; Korman et al., 2004). When studies are to be carried out at the scale of a river reach, and the geometry is complex, at least the 2-D or even a 3-D approach will be required (Hodskinson and Ferguson, 1998; Lane and Ferguson, 2004). Influence of secondary flows is significant for the main flow and sediment transport and can only be accounted for realistically with 3-D models (Weerakoon et al., 1989, 1991;

Bradbrook et al., 1998; Lane et al., 1999, 2000a, b; Meselhe and Sotiropoulos, 2000; Nagata et al., 2000; Wu et al., 2000).

The major problem in using the 3-D numerical modeling for flow and sediment transport in a river is the increased complexity in the representation and validation of the simulations. Generating a numerical mesh for a complex river topography is one of the most difficult challenges. This is further complicated when the specification of a correct sediment transport function is required (Vanoni, 1984; Guo et al., 1999).

1.2 Research goals and objectives

In order to determine the appropriate discharge of a controlled flood to remove sediments of different sizes, a better understanding of the near bed flow dynamics is required. The objectives of the research are as follows:

1. To assess the validity of a three-dimensional model (Phoenics) of a complex natural river meandering reach (River Escoumin) to predict the flow field and the bed shear stress distribution during a controlled flood, and compare the results with shear stress estimates based on field measurements and 2-D numerical simulations.
2. To assess the effect of inlet conditions in 3-D numerical modeling.
3. Based on the shear stress distribution, to estimate bed load transport using various bed load equations and to compare these estimates with field measurements.

2. LITERATURE REVIEW

The study of flow and sediment transport in natural rivers is based on empirical formulae, analytical theories, engineering judgment, physical models, field measurements and more recently, numerical models (Odgaard and Bergs, 1988; Whiting and Detrich, 1993; White, 1998; Shams et al., 2002). The understanding of the complex flow field in natural rivers has improved remarkably over the last few years. However, linking the flow field and bed load transport remains problematic as most formulae have error levels greater than the predicted transport rate (White and Inmam, 1989a, b; Schoonees and Theron, 1994; White, 1994). The accurate prediction of bed load transport becomes even more complex while dealing with complex planforms and bed geometry such as those observed in meander loops where secondary circulation is important.

2.1 Physical modeling

Physical modeling has been carried out with the use of prismatic channels to investigate the flow structure, bed morphology and sediment transport of meandering rivers. However, the representation of the complexity of a meandering river is never entirely achieved in these studies. Odgaard and Bergs (1988) estimated flow and sediment transport experimentally by using a 180^{o} laboratory channel bend, which indicated a scour channel near the outer bank, point bar near the inner bank and the presence of secondary flow. Shams et al. (2002) also established experimentally that flow through meandering rivers was three-dimensional, with secondary flow at river bends that affect particle deposition. Shiono and Muto (1998) investigated the flow in a meandering channel with an overbank flow. They established the following: 1) The flow behavior at

the water surface is closely related to the upper-layer flow structure when depth of the flooding is low, but is not related to complex internal flow structure, when the depth of flooding is high. 2) The most important feature of secondary flow structures in meandering channels is the opposing sense of rotation of the secondary flow cells at bend apexes before and after inundation. Bathurst et al. (2002) illustrate the ability of a flume study to model overbank deposition across the meander tongue.

In physical modeling of sediment transport in meandering rivers, however, violating the scaling laws is inevitable due to simultaneously needing to model more than one transport mode under the physical constraints of a flume, and modeling cohesionless sediment with cohesive sediment (White, 1998). Hughes (1993) even concluded that accurate estimates of sediment transport might probably never be achieved in physical models. As a result of the inaccuracy and unreliabity of alternatives, field measurements, which are often much more expensive and difficult than laboratory experiments, have been employed for sediment transport in river channels (White, 1998).

2.2 Field measurements

Several instruments and methods are used in the field to collect data related to the river morphology and processes. Examples of these instruments and methods are sediment traps, tracers, Helley-Smith sampler and optics for sediment transport, total station or global positioning systems for bed topography, electromagnetic current meter (ECM) and acoustic Doppler velocity meter (ADV) for flow velocity (Hodskinson and Ferguson, 1998; White, 1998; Ferguson et al., 2003). White (1998) showed that field measurements

are the most reliable form of estimating sediment transport in a river. However, field measurements suffer two great limitations: 1) obtaining data at all times and at the location of interest is nearly impossible (Hodskinson and Ferguson, 1998), and 2) measurements can be expensive and difficult at the high flow stage (White, 1998). These factors serve as a great disadvantage in studying complex meandering rivers effectively, using field measurements.

Despite these difficulties, field studies have been carried out to investigate river dynamics in a meandering river. The most important feature of meandering rivers was found to be the behavior of secondary flows, which has important impacts on bed load transport (Shiono and Muto, 1998). Problems arise when one is attempting to identify the secondary flows along a meandering river during field studies where the direction of primary flow is not parallel to the channel centerline (Lane et al., 2000). This is particularly problematic because changes in section orientation can result in major changes in the appearance of the secondary circulation field (Dietrich and Smith, 1983). However, Perkins (1970) studied river bends and established that strong secondary flows are caused by skewing of cross-stream vorticity, where there is a change in the channel geometry such as a channel bend or a rapid change in cross-sectional shape. Further field studies showed that the skew induced secondary cell does not extend to the inner bank of a meander bend (Dietrich et al., 1979; Thorne et al., 1985; Markham and Thorne, 1992).

Field studies on river bends have also shown that the main flow can become separated from the channel boundary, either just upstream of the bend apex at the outer bank, or

just downstream of the apex at the inner bank. The low velocities in these regions allow the progressive deposition of fine-grained sediments at the inner bank as a point bar (Hickin, 1977, 1986; Page and Nanson, 1982; Reid, 1984; Hattingh and Rust, 1993). Leopold and Wolman (1960), Jackson (1975), and Dietrich and Smith (1983) studied the flow pattern in a meandering river and established a high velocity core that shifts from the inside to the outside channel with distance through the bend. Their studies showed that regions of outward flows are strongly correlated with point bars. Ferguson et al. (2003) studied flows in meander bends and established that separated flows at the inner bank creates a recirculation eddy with weak upstream flow, which affects the sediment dynamics of the system, and act to accumulate patches of fine sediment.

Dietrich and White (1983) measured the sediment transport along a meandering river and established that the downstream decrease of high boundary shear stress near the inside bank must cause sediment transport rate to diminish, and net deposition of sediment must occur at the downstream end of the bend. Dietrich and White (1989) measured the bed load transport rate of a meandering river to establish a relationship between boundary shear stress, bed load, suspended load and grain sorting processes through a bend. Leopold and Emmett (1984) measured the bed load transport rate of a meandering river and established that the average local boundary shear stress and the grain size distribution at the riffle and pools were nearly the same.

Although field measurements are often a preferred alternative to laboratory physical modeling, difficulties are encountered when observing bed load entrainment and its

movement in rivers. These difficulties include field efforts required during bed load measurement, and the high spatial and temporal variability associated with bed load movement (Hubbell, 1987). Obtaining data at all times and locations of interest are impossible (White, 1998) as stated earlier.

2.3 Numerical modeling

Numerical models have been used extensively in recent years to improve our understanding of river flow dynamics. The turbulent nature, irregular geometry of river channels, their time dependence, and complex sediment transport phenomena makes the prediction of flow in natural channels a challenging task. Paquier and Khodasheuas (2002) established that 1-D simulations are insufficiently complete, as they do not take into account the important lateral variability of river reaches. Ghanem et al. (1996) obtained a more accurate representation of spatial patterns of velocity with a 2-D model than with a 1-D model for assessing the habitat suitability. The use of 1-D models in numerical modeling of reach scale flow, morphodynamics and habitat problems has been replaced recently by 2-D and 3-D models (Lane and Ferguson, 2004).

The use of 2-D or 3-D models in fluvial geomorphology and engineering depends on the scale and aims of the study (Lane and Ferguson, 2004). Both types of models can include unsteady flows, sediment transport, and morphodynamics in natural rivers (Lee et al. 1997; Ma et al., 2002; Korman et al., 2004; Shapiro et al, 2004). In comparison with 2-D models, there are fewer applications of 3-D models to rivers, although these are increasingly being used, even for long study reaches (Dargahi, 2004). However, fluid

dynamics problems are represented explicitly in 3-D models, providing a marked advantage (e.g. Weerakoon et al., 1989, 1991; Bradbrook et al., 1998; Hodskinson and Ferguson, 1998; Lane et al., 1999; Wu et al., 2000; Rodi, 2000; Ferguson et al., 2003; Olsen, 2003; Dargahi, 2004).

2.3.1 Grid generation

Grid generation is an integral part of solving complex computational fluid dynamics problems. Grid generation strongly affects the accuracy of a numerical simulation (Jordan and Spaulding, 1993; Yu et al., 1997). Computational processes for numerical system solution require powerful discretization methods based on the use of appropriate grids. These consist of a discrete set of points representing the geometry of the definition domain (Conti et al., 2004). The domain discretization is often difficult for natural rivers due to the irregular and variable shape of cross-sections, which prevent the use of an orthogonal coordinate systems (Yu et al., 1997). One of the greatest tasks for engineers is to search for an adaptable grid system, which efficiently makes use of geographical information such as shorelines and the bed topography, and at the same time to achieve higher quality numerical results (Yu et al., 1997).

A general approach to discretization of domains with complex geometry is the generation of boundary-fitted coordinate systems by solution of elliptic partial differential equations known as the finite difference or finite volume methods (Sinha, 1997). Ability of finite difference or finite volume methods to model natural river flows in such a formulation depends on the adequacy of the numerical grid (Sinha, 1997). Grids are required to

satisfy some properties like smoothness and boundary orthogonality, which affects the solution accuracy (Zhu, 1990; Khamayseh et al., 1999). Non-orthogonal boundary–fitted grid can be generated to model complex river reaches using a variety of techniques such as the difference methods or the algebraic methods (Sinha, 1997). Conti et al. (2004) showed that coupling advanced algebraic methods with elliptic generation are advantageous in achieving good grid properties. Zhu (1990) proposed the use of hybrid method in which both the difference method and the algebraic method are combined to yield a final grid which is efficient for a variety of flow configuration, and which meets requirement of orthogonality, and smoothness.

2.3.2 Boundary conditions

Implementing boundary conditions for finite volume method requires that the flux at the boundaries is physically correct. These boundary conditions are the water surface, the bed surface, extent of domain, and the inflow characteristics (Ferguson et al., 2003). The water surface is defined as a plane of symmetry, which implies that the normal velocity and the normal gradient of all variables are zero at the plane of symmetry (Ferguson et al., 2003; Argali, 2004). However, the water surface may be depressed or super elevated, for example in the separation zone and near the apex of an open channel junction flow (Best and Reid, 1984; Whereon and Tami, 1989, Rhoads, 1996; Byron et al., 2002). This surely influences the flow field. Although it is necessary to identify the relationship between water surface geometry and the flow field, it is quite difficult to collect actual free surface elevation data for large-scale natural channels. One of the methods to trace

the free surface geometry in numerical models is to use the porosity correction concept (Ouillon and Dartus, 1997; Bradbrook et al., 2000a, b; Biron et al, 2002).

Bed surfaces are treated by assuming that they are in the wall region and that the standard law of the wall applies (Wu et al., 2000). In this procedure, a roughness height is adopted. It is usually estimated from the grain size of bed particle (Ferguson et al., 2003). Bed and bank roughness are often parameterized using Launder and Spalding (1974) non-equilibrium version of the law of the wall in the layers of cells touching the rough boundaries (e.g. Lane et al., 1999; Ferguson et al., 2003; Dargahi, 2004). The extent of the domain is described by the river bed and the water's edges, which must remain fixed (Lane et al., 1999; Ferguson et al., 2003; Dargahi, 2004). The inlet conditions require the values of the velocity and turbulence properties at the furthest upstream cross-section (Lane et al., 1999; Dargahi, 2004). A good knowledge of upstream boundary specification is required in 3-D models, particularly in terms of inflow data, and difficulties in such specification may provide fundamental limitations in the predictive ability of a model (Lane et al., 1999). Lane et al. (1999) effectively illustrated this by comparing two boundary condition specifications upon flow field prediction for a river confluence. Fig. 2.1a shows the grid plan and a cross-section showing the predicted flow field downstream from the junction. Fig 2.1b shows the same grid plan as in Fig. 2.1a but it includes an upstream curvature in the tributary channel, which affects the flow field as seen in the cross-section downstream.

2.4 Flow and sediment modeling

Several numerical models have been developed to establish the link between flow field and sediment transport (Wang and Adeff, 1986; Van Rijn, 1987; Demuren, 1989, 1991; Lin and Falconer, 1996; Wu et al., 2000; Dargahi, 2004). Most of these studies were examining simple bed geometry and only a few have looked at meandering rivers (Ferguson et al., 2003; Olsen, 2003; Dargahi, 2004). In these rivers, secondary flows and flow separation can significantly affect sediment transport (Odgaard, 1989a, b; Shams et al., 2002; Ferguson et al., 2003; Olsen, 2003; Dargahi, 2004).

Hodskinson and Ferguson (1998) used a 3-D model, based on time average flow in an idealized channel bend to investigate geometric controls on flow separation. They showed that the existence and extent of concave bank flow separation is affected by the channel curvature, point bar topography, and upstream planform (Fig. 2.2). The erosion of the upstream part of the point bar leads to a redistribution of flow in the bend and enlargement of the separation zone at the outer bank. Ferguson et al. (2003) also investigated flow in sharp meandering bends, with recirculation at the inner banks. By simulating the 3-D flow field in two bends having different channel curvatures, it was established that free stream exists at the outer bank within which helicity first increases, and then decays through vortex stretching. The presence and nature of the recirculation was dependent on the channel curvature, inflow distribution to the bend, and bend topography (Fig. 2.3). Strong secondary flow experienced in meandering bends was well predicted by their 3-D model (Fig. 2.4). The inner bank zones of slower moving flow in

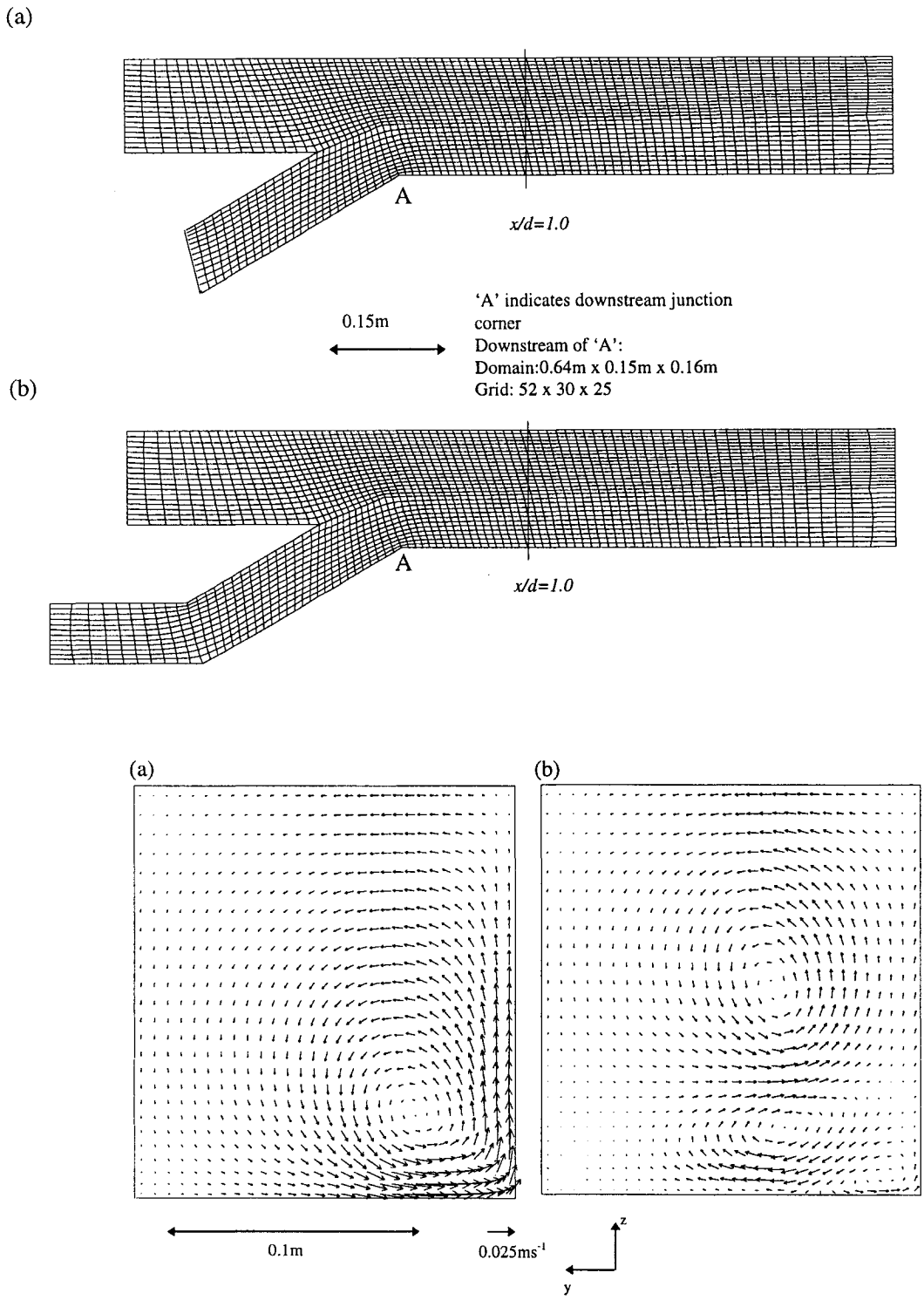

Figure 2.1. An illustration of the effects of upstream boundary condition specification upon flow field prediction (a) initial grid (b) new grid with upstream curvature in the tributary channel (Lane et al., 1999).

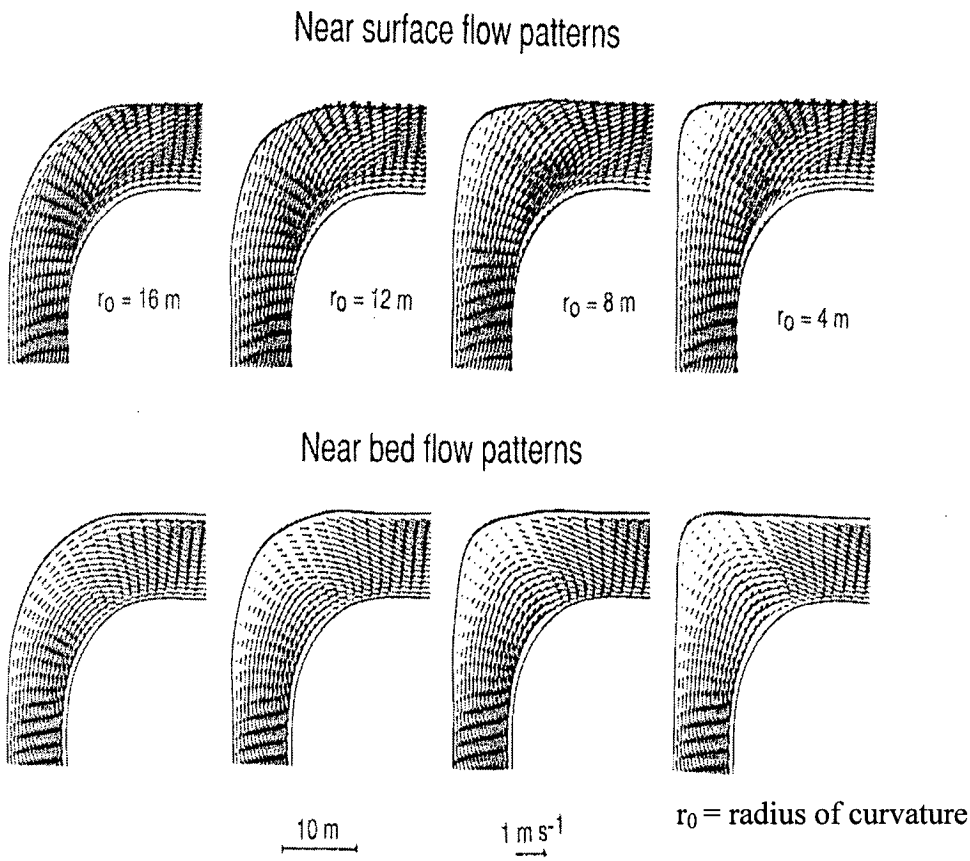

Figure 2.2 Simulated near-surface and near bed flow patterns with outer bank curvature and apex width (Hodskinson and Ferguson 1998)

meandering bends severely affect the sediment dynamics and act to accumulate patches of fine sediments (Ferguson et al., 2003).

Studies on sediment transport using 3-D models are limited. However, Wu et al. (2000), Shams et al. (2002), and Dargahi (2004) investigated the potential of 3-D numerical models for flow and sediment transport in the river. These studies calculated the flow by solving the full Reynolds-averaged Navier stokes equation with a k-ε turbulence model. The bed load model used by Wu et al. (2000) was based on the mass balance equation for non- equilibrium bed load transport, a median diameter of 0.3mm, and an open channel

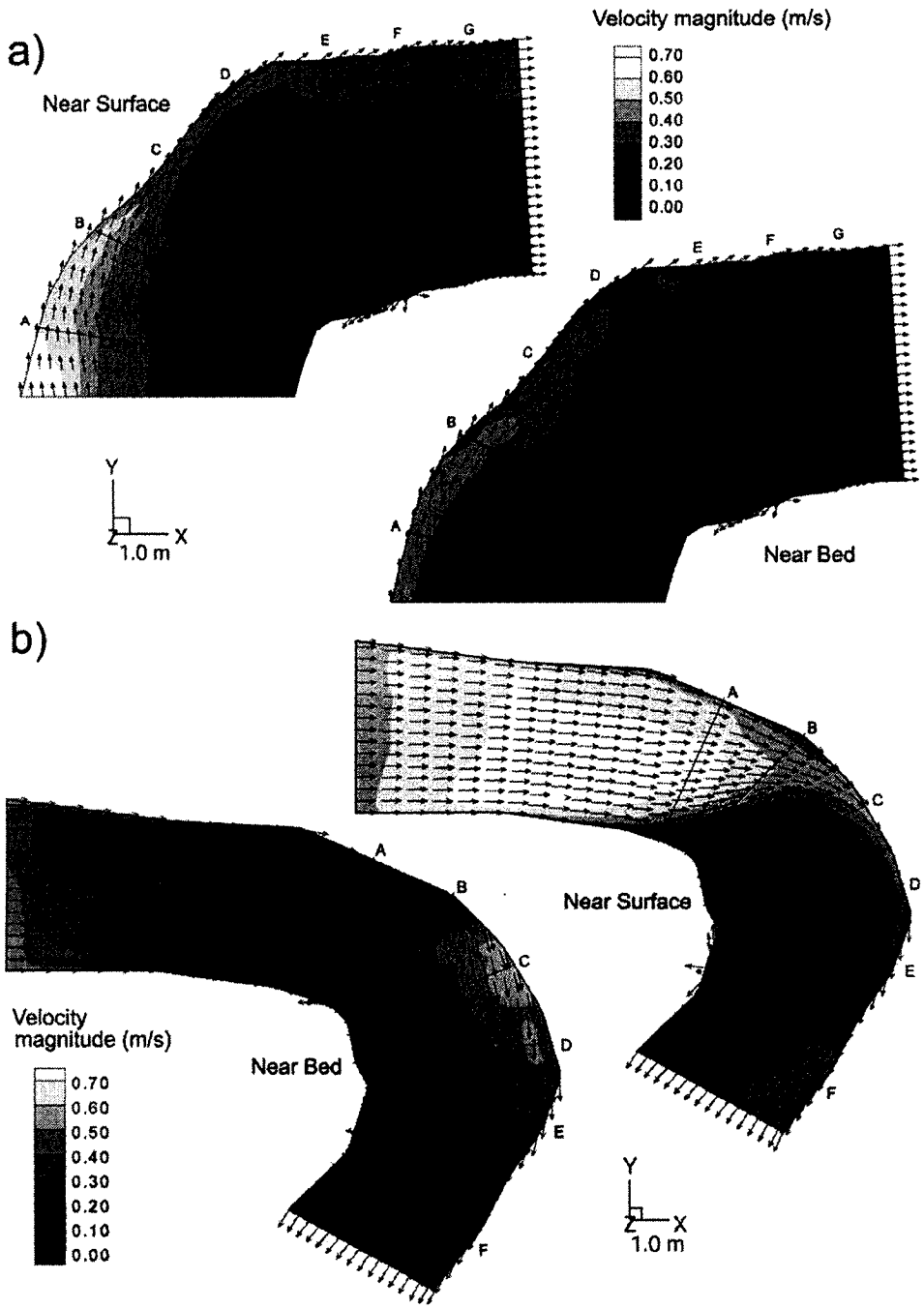

Figure 2.3 Simulated velocity distribution in the top and bottom layers of computational cells in CFD models of two bends a and b (Ferguson et al., 2003).

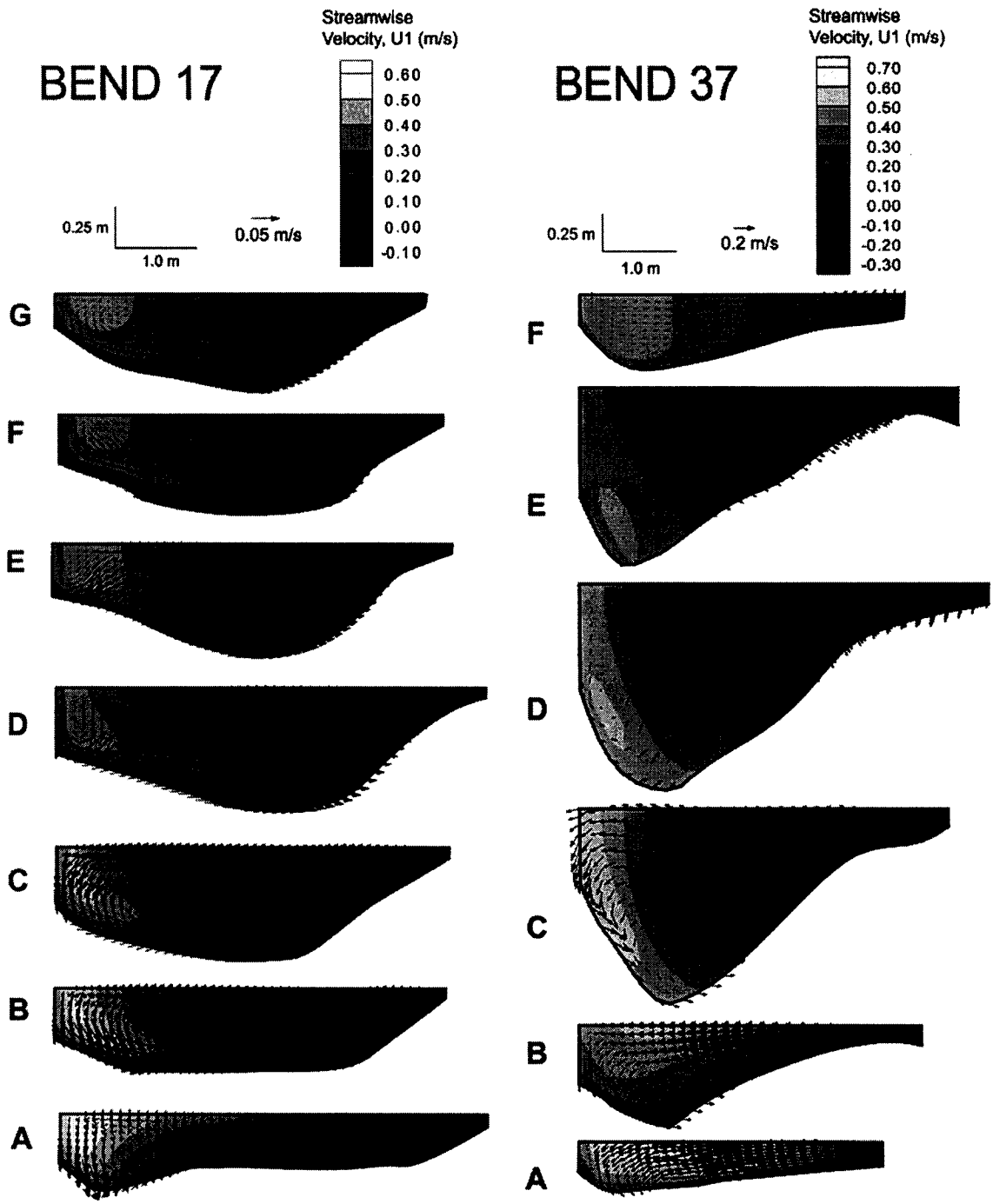

Figure 2.4 Simulated secondary circulations at selected cross-sections of two bends. Section location are shown in Figure 2.3 (Ferguson et al., 2003)

bend (180°). Though Wu et al. (2000) model of reproduced the general features, specifically the development of scour channel near the outer bank, point bar near the inner bank and secondary flow, the model needs to be tested for situations where suspended load is significant and applied to a real river situation.

Shams et al. (2002) used a 3-D approach to analyze the flow, sediment transport, and deposition of a meandering river model, which is identical to the river model used by Shiono and Muto (1998). These analyses were accomplished with the aid of a laboratory scale model having a Froude number identical to the physical scaled meandering river model. Shams et al. (2002) applied the particle equation of motion that includes the effects of nonlinear drag and gravitational forces for the sedimentation transport model. The equation requires knowledge of the instantaneous turbulent fluid velocity at the location of each particle at every instance of time. The model was applied to a meandering river channel with varying grain sizes (1-3000μm). The comparison of their results with data of laboratory experiment (Shiono and Muto, 1998) showed that the flow patterns were comparable. The agreement for sedimentation rates good because sedimentation process did not satisfy the similarity rule.

Dargahi (2004) studied the flow and sediment transport in a meandering river (River Klarälven) using a 3-D model. The 3-D flow model was carried out with the use of RNG k-ε turbulence model and a non-equilibrium wall function. The sediment transport model solved the sediment continuity equations to find the general sediment transport pattern in the river reach, and rate of average total transport load was calculated using the Ackers-

White equation. Dargahi (2004) results successfully predicted the flow structures along the river reaches. The study also showed that the localized sediment transport occurred in the river bends in regions of high bed shear stress. Calculated sediment transport patterns were closely related to the velocity vectors and the distribution of bed shear stresses.

2.5 Bed load transport

Bed load is defined as the component of the total load that moves in at least intermittent contact with the bed (Martin, 2003). Bed load transport occurs when the bed shear stress exceeds a critical value (Chanson, 1999). The estimation of bed load transport has been achieved with the use of several predictive formulae based on several factors, which includes hydraulic parameters and bed characteristics (Chang, 1988). Although sediment transport is affected greatly by bed characteristics (Church et al., 1998), they have not generally been incorporated in the bed load formulae, which may limit their predictive capability. Despite these limitations, a wide range of bed load formulae continues to be used in geomorphological studies (Gomez and Church, 1989; Martin, 2003). However, a successful universal solution for predicting bed load transport has not yet been found (Ham and Church, 2000).

Bed load equations that are based on shear stress approach include DuBoys, Shields, Meyer-Peter, Meyer-Peter and Muller, Bagnold, Einstein, Nielsen, Parker et al., Sato et al. formulae (Vanoni, 1975; Garde and Ranga Raju, 1985; Chang, 1988; Chanson, 1999). Stream power approaches include Schoklitsch, Eugelund-Hansen, Laursen, Blench Regime, Inglis-Lacey, Toffaleti and Ackers-White, and an example of the parametric

approach is the Colby relation formula (Vanoni, 1975; Garde and Ranga Raju, 1985; Chang, 1988; Chanson, 1999). Limited numbers of field studies are available for the validation of these formulae (Habersack and Laronne, 2002; Martin, 2003). However, the use of prototype data has allowed for a more realistic evaluation of these bed load equations. In many of these evaluations, the results were generally good but no universal relationship can be established between bed load discharge and hydraulic conditions (Habersack and Laronne, 2002; Martin, 2003).

Gomez and Church (1989) assessed sediment transport equations for gravel bed rivers with the use of various available field data. A range of 0.04-102mm grain size diameter was used in this study. The formulae considered fell into two categories; those developed for gravel bed channels and those applicable to both sand and gravel bed channels. Gomez and Church (1989) established the following:

1. If the hydraulic information is limited, the stream power equations and in particular Bagnold equation should be used.
2. When local transport estimates are required and local hydraulic information is available, a formula should be selected that is sensitive to bed state or grain size distribution.

Habersack and Laronne (2002) evaluated bed load discharge based on the Helley-Smith sampling in an Alpine gravel bed river. The field data used in the evaluation are bed width, subsurface mean diameter (39mm), and the mean annual discharge. Habersack and Laronne (2002) provide a comparison (Fig. 2.5) between calculated and measured bed

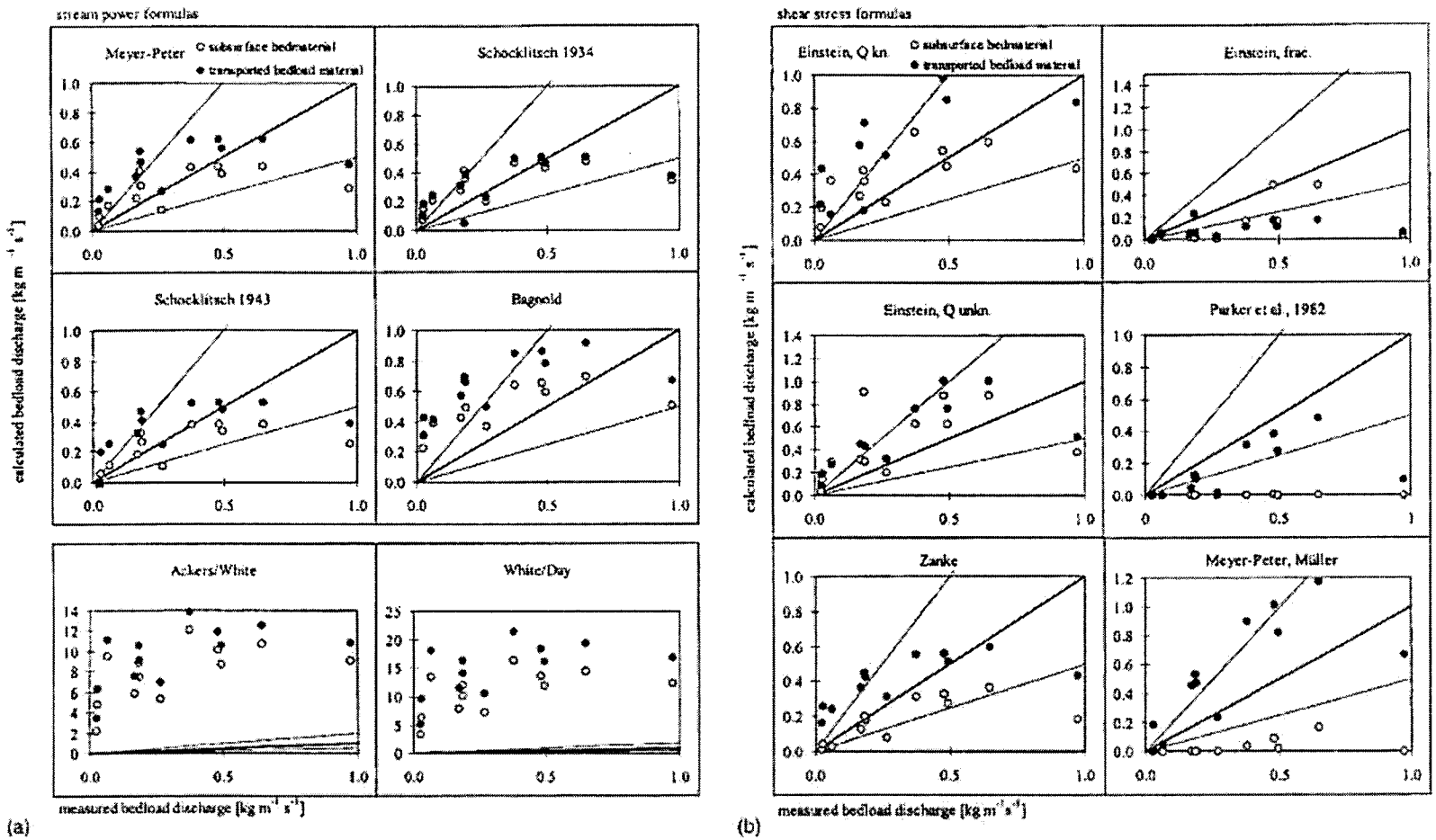

Figure 2.5 Comparison between calculated and measured bed load discharge; (a) stream power formulae and (b) shear stress formulae (Habersack and Laronne, 2002)

load discharge. The study established that shear stress based formulae do not perform as well as stream power equation (Bagnold equation) in bed load estimation. However, for a weak bed load discharge, shear stress formulae perform better when used with representative grain size distribution of the transported bed.

Martin (2003) evaluated the bed load equations using field data from the Vedder River of British Columbia. The study reach had four distinct morphological reaches with bank-to-bank widths varying from 50 m to several hundred meters in the braided reaches. Variables used in the various equations include the mean annual discharge, grouped widths, and depths for the four morphological reaches. Grain size decreased systematically along the study reach. Martin (2003) established that the stream power correlation was quite good in comparison to the other formulae for both gravel and total bed load transport. The only defect with the formula is that it does not account for grain size variation, and this serves as a potential weakness as changes occur in particle size. The Bagnold-type formula and Meyer-Peter and Muller formula do not adequately simulate the magnitudes and pattern for the Vedder River. Fig. 2.6 illustrates the predicted and observed gravel transport rate along the Vedder River. The study also showed that the use of the equations should be approached with caution as they may significantly overestimate bed load transport.

Bed load equations will predict that larger particles are less eroded than the smaller ones. As a result of this, the top layer in a gravel bed river is made up of coarser material than the original bed. This top layer would have a protective action on the underlying ones,

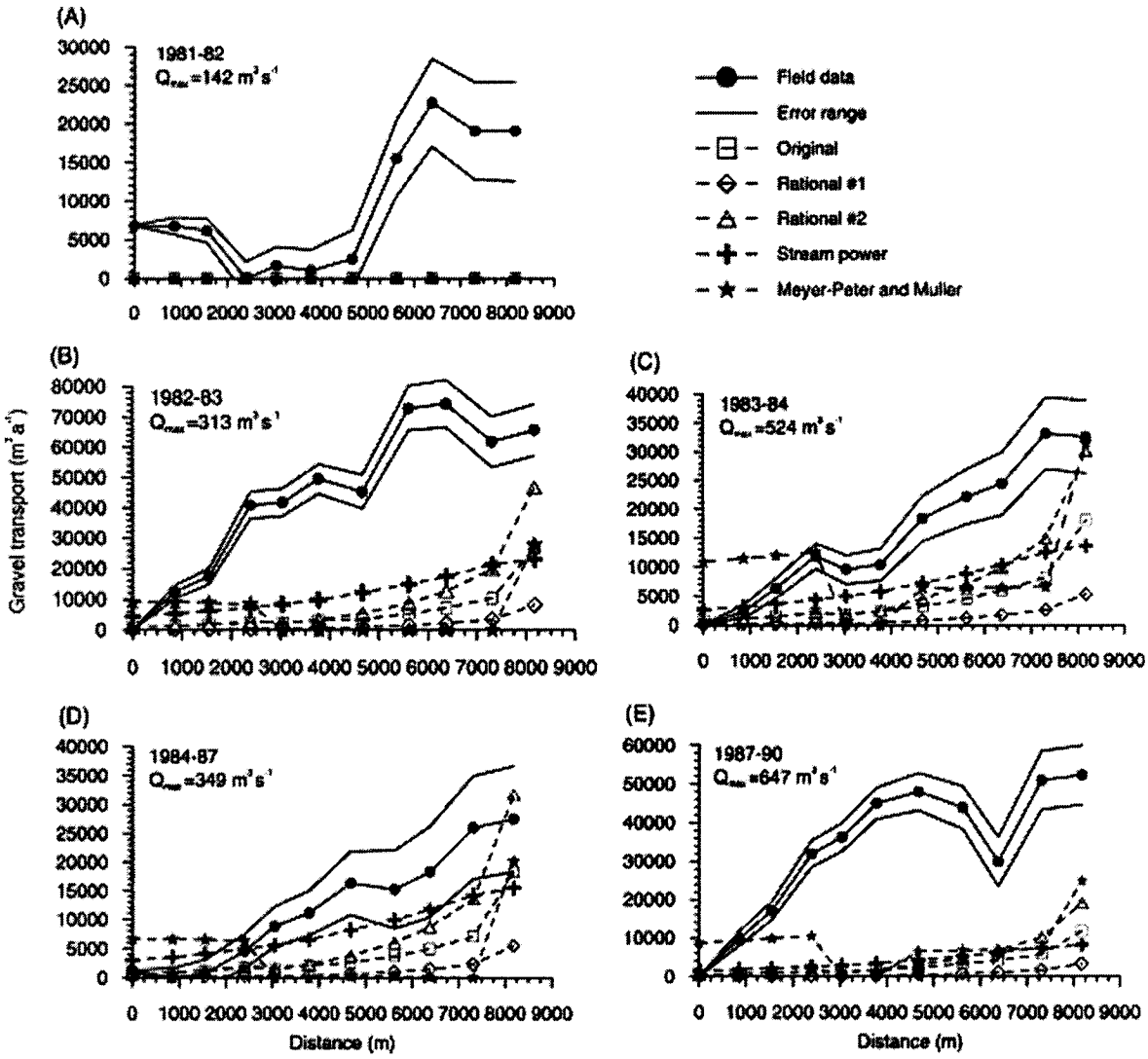

Figure 2.6 Predicted and observed gravel transport rates along the Vedder River. The maximum in each period is shown. (Martin, 2003)

which might result in a zero transport. This action is known as armoring (Graf, 1971). The effect of armoring on a gravel bed river causes transport predictions to be particularly sensitive to the accuracy of shear stress (Barry et al., 2004). Barry et al. (2004) used a large amount of observations (2104 bed load transport data) in 24 gravel bed river in idaho to assess the performance of eight different formulations of four bed load transport equation (Meyer-Peter and Muller, Ackers and White, Bagnold, Parker et al.). Their results indicate that these formulae lack inconsistency and fail to predict bed load transport rates. In particular, formulae having a transport threshold were found not to be capable of predicting bed load transport rates properly. They conclude that bed load transport rates are well predicted by a simple power function of discharge. Hence, in the present study the Eugelund-Hansen stream power equation, which is based on the stream power concept, is used to validate the bed load transport rate predictions of the 3-D model.

3.0 METHODOLOGY

3.1 Study reach

The study reach is the Escoumins river located downstream of Des Coeurs river, flowing into the St-Lawrence river near Tadoussac in Quebec, Canada (Fig. 3.1a). The studied section is located at the downstream end of this reach (Fig. 3.2). The width of the river varies between 20m and 30m. The slope is 0.3 % and the length of the modeled section is about 96m. The modeled reach consists of a riffle-pool-riffle sequence with a point bar on the right bank at the downstream end (Fig. 3.2). In the section upstream of the bridge (Fig. 3.2), the river flows between two engineered banks, and the gravel bed is composed mainly of coarse gravel with a median diameter (d_{50}) of 50mm. A mid-channel bar exists downstream of the bridge (Fig. 3.2), which divides the flow into two, with most of the discharge going through the right channel. The study reach has a bed sediment d_{50} of 40mm upstream and d_{50} of 20mm downstream. The channel is also curved as seen in Fig. 3.2.

Control floods were created at the study reach with the aid of the dam at Des Coeurs Lake (Fig. 3.1b). This was achieved by opening the gates of the dam from 6 hours to 25 hours. The discharge was monitored at the bridge (Fig. 3.2), by observing the velocities and stage across the entire cross-sections immediately downstream of the bridge. Seven control floods of various duration and strength were carried out in 1999 (Table 3.1) ranging from 0.37 to 1.23 times the bank full discharge ($20m^3/s$). For this study, flood 6, slightly greater than the bank full discharge, was investigated.

a)

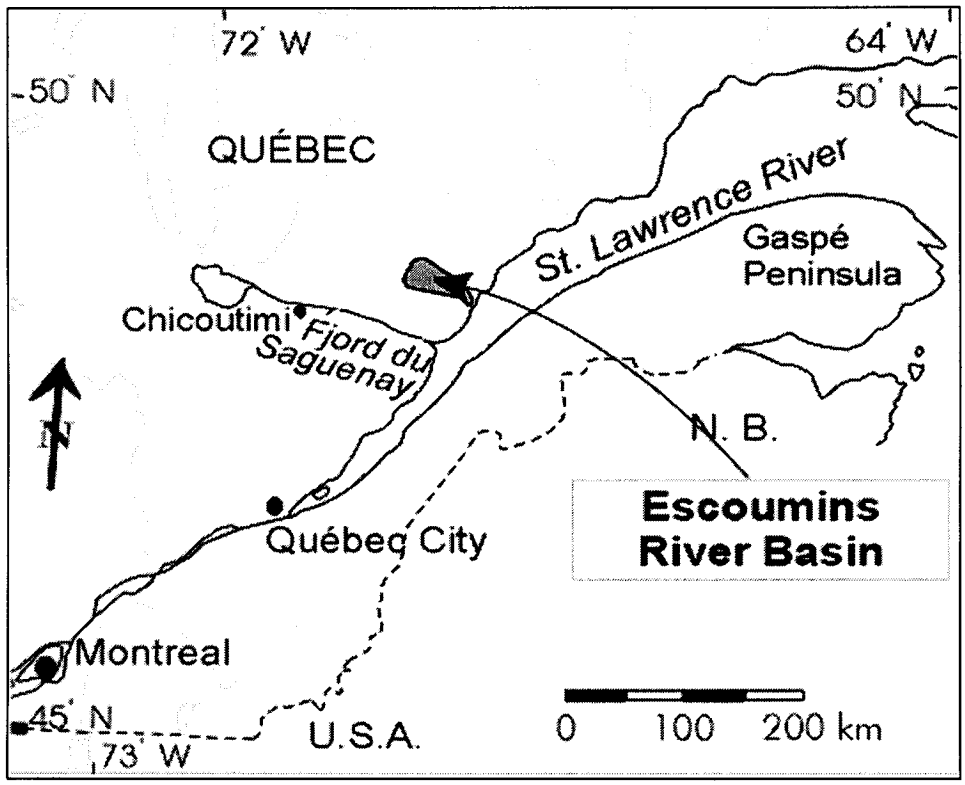

b)

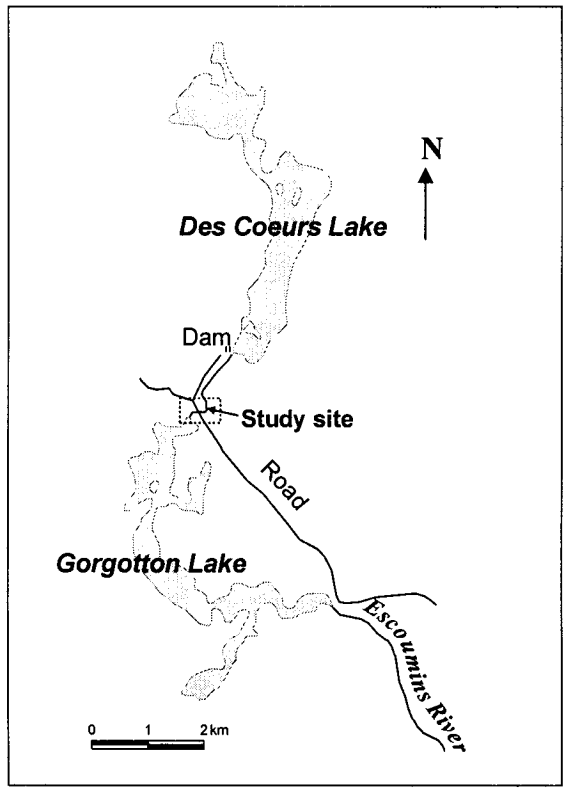

Figure 3.1 Site Location

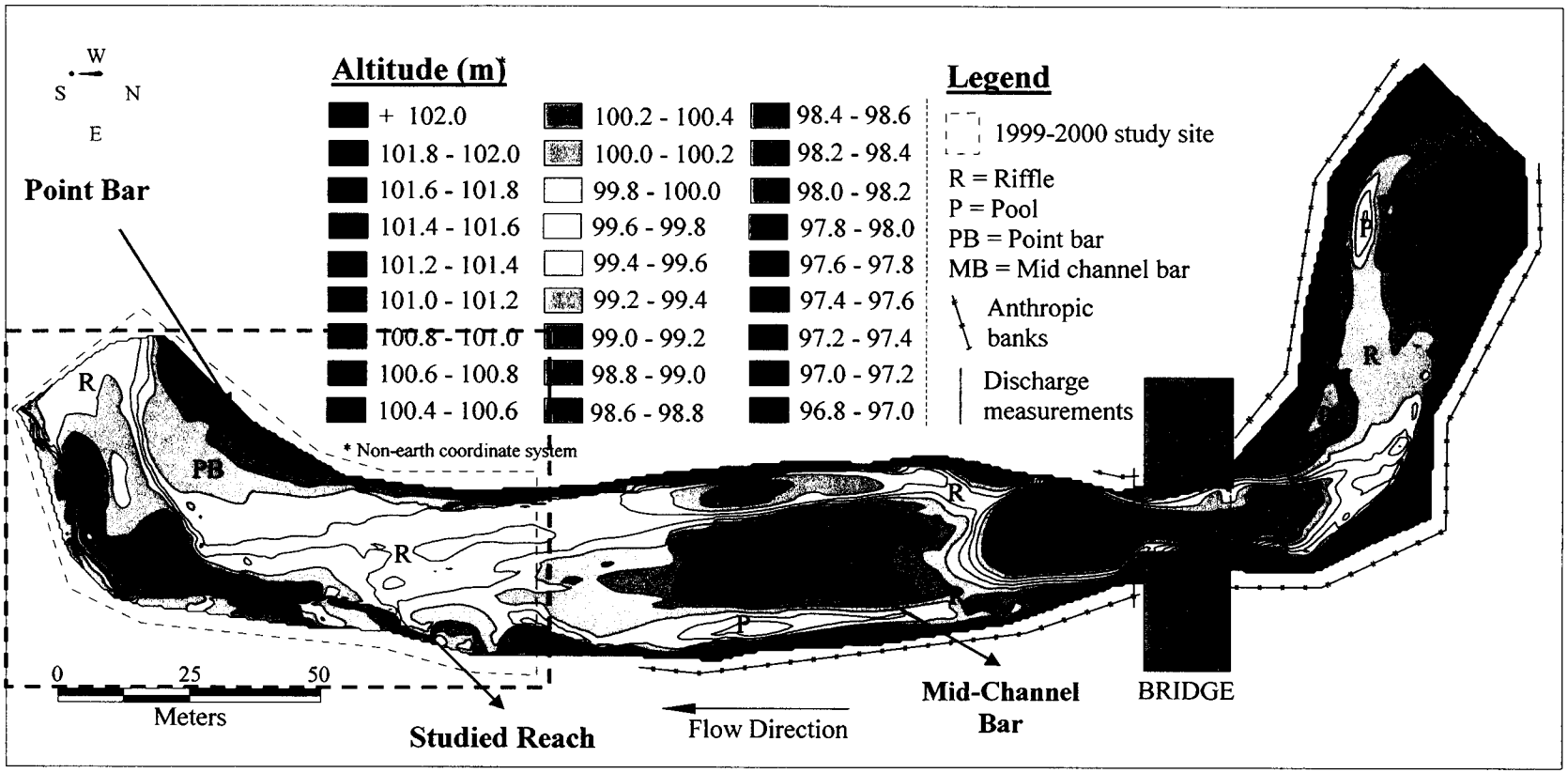

Figure 3.2 Bed topography of the Escoumins River and limit of study reach

Table 3.1 Controlled Floods in 1999

No	Discharge (m^3/s)	Duration (hrs)
1	22.8	6
2	24.5	6
3	11.1	25
4	17.1	10
5	7.4	24
6	20.6	8
7	15.5	8

3.2 Previous field and numerical modeling work

3.2.1 Field measurements

One of the objectives of this research is to verify the accuracy of a 3-D model compared to field measurements. Christian Latulippe (Ph.D student, Department of Geography, McGill University) has collected morphological, sedimentological, and hydraulic data in the study reach during the sequence of controlled floods. These data include measurements of bed topography, velocity distribution, bed load transport, and estimation of bed shear stress distribution, along the study reach. Measurements were taken during all the control floods listed in Table 3.1. However, only data on flood 6 are examined in this study.

3.2.1.1 Bed topography

The bed topography survey of the study reach was carried out using an electronic theodolite (total station). Surveys were performed before the first control flood, between each control flood and after the last flood. More than 800 topographical points were taken

for each survey. These data were imported into a geographic information system (MapInfo) to be interpolated and to produce maps of bed elevations such as Fig. 3.2.

3.2.1.2 Velocity measurements

Velocity measurements were taken along vertical profiles using two Price propeller current meters assembled on long graduated rods fixed on each side of a wooden platform installed on a zodiac boat. Measurements of shallow regions and low flows were taken with the Price current meter mounted on a handheld classic rod. The near bed (taken at 22cm from the bed throughout the entire study reach) and the depth-averaged velocities (0.4 of the flow depth) were taken. Fig. 3.3 presents the point values and the interpolated velocities for the controlled flood used in this research.

3.2.1.3 Bed shear stress estimates

Estimates of bed shear stress (τ_o) were calculated following the law of the wall also known as the Prantdl-Von Karman universal velocity law, which assumes that velocity (V) varies with the distance from the channel bottom (z) as

$$V/V* = (1/\kappa) In(z/z_o) \quad (3.1)$$

where $V^* = (\tau_o/\rho)^{1/2}$ is the shear velocity, $\kappa \approx 0.4$ is Von Karman's constant, z_o is the bed roughness length-scale and $\rho = 1000$ kg m^{-3} is the fluid density. Three methods were used to estimate local shear velocity from velocity measurements, from which the local bed shear stress was calculated by $\tau_o = V^{*2}\rho$:

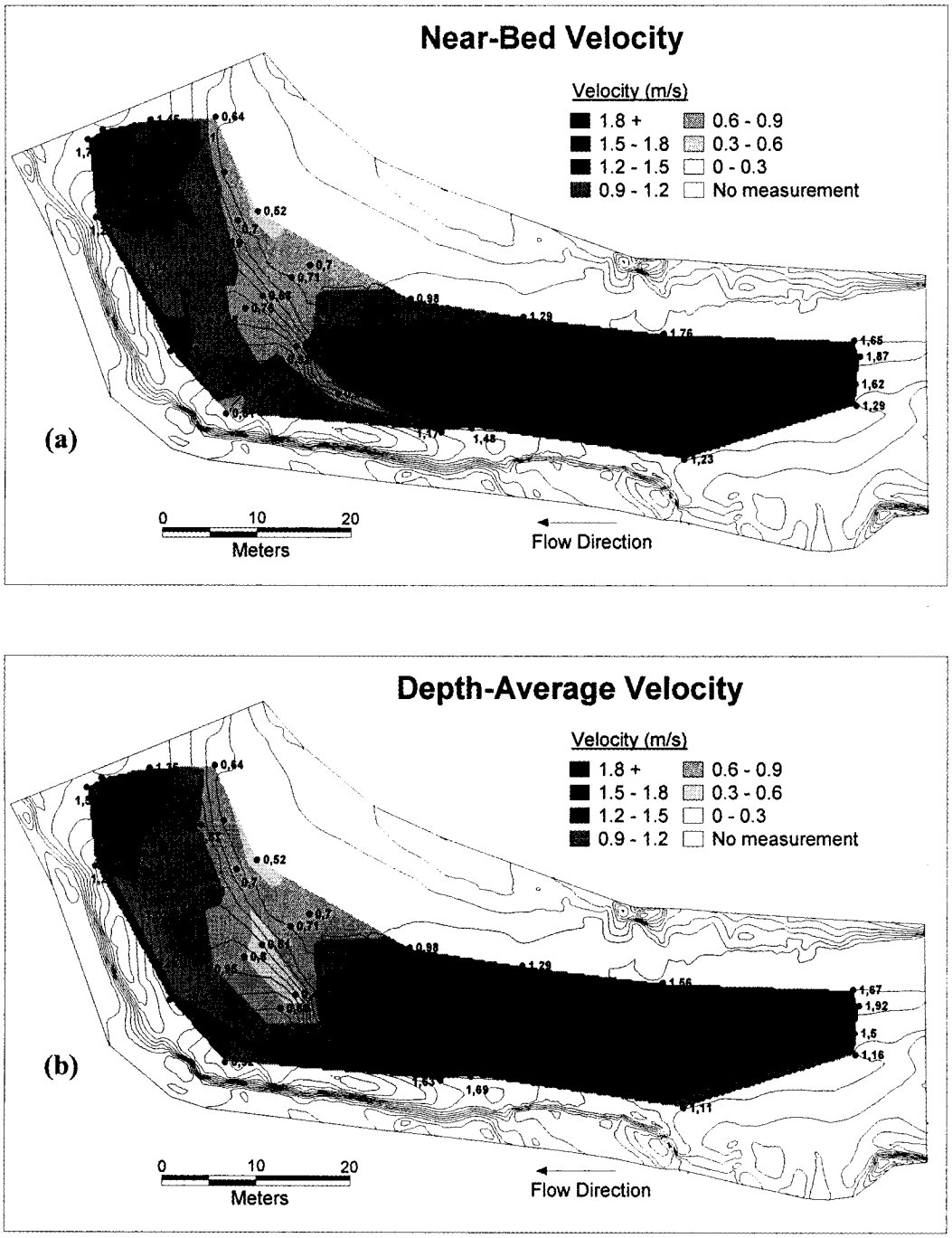

Figure 3.3 Interpolated filled contours of the velocity distribution (a) near the bed (b) depth-averaged (0.4 of the flow depth).

1. Shear velocity using velocity profile (V^*_p) calculated using the slope obtained by a least squares line of multiple observations of V and ln (z), which is V^*/κ (Von Karman Constant) from the derivative $\partial v/\partial$ (ln (z)) of 3.1.

2. Shear velocity using near-bed velocity is defined as follows.

$$V^*_z = \frac{V_z}{In(z/z_o)} \qquad 3.2$$

Here, V_z is one observation of the velocity obtained near the channel bed (z) and z_o is computed as $0.1d_{84}$ Also, d_{84} corresponds to the diameter with 84% of the particles being smaller than that value (Whiting and Dietrich, 1990; Wilcock, 1996).

3. Shear velocity using depth average velocity.

$$V^*_D = \frac{V\kappa}{\ln(D/ez_o)} \qquad 3.3$$

Where D is the total depth, e is the base of the natural logarithms, $z_o = 0.1d_{84}$ and V is the depth average velocity.

Using four replicate observations of velocity profiles at six different locations on the gravel bed river, four values of V^*_p, V^*_z, V^*_D and consequently τ_{op}, τ_{oz}, τ_{oD} were obtained at each location. The standard error (STE) was calculated and results showed that errors in the velocity profile method were higher than the other methods. Because of this, shear velocity and shear stress estimated by the velocity profile method were not used. Fig. 3.4 shows the estimated bed shear stress using the near bed method and depth-averaged

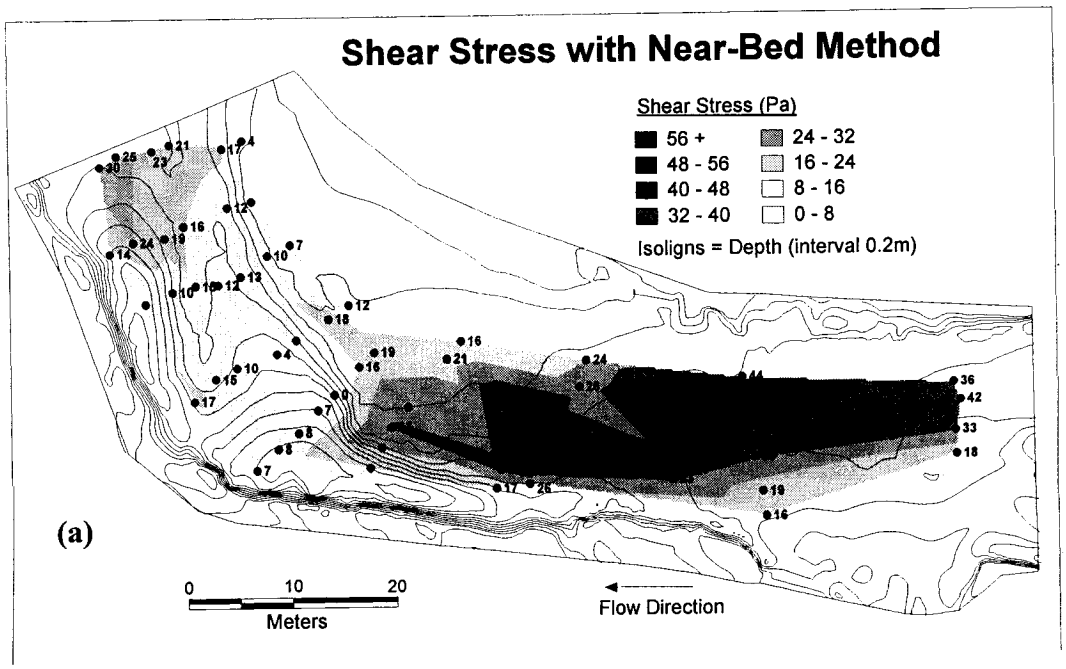

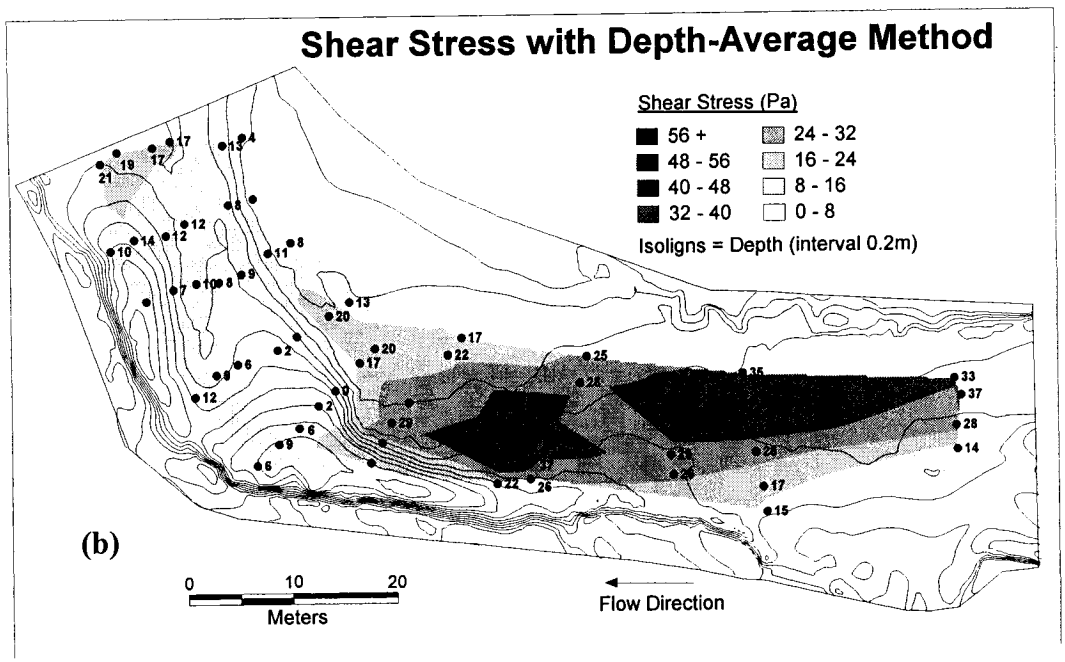

Figure 3.4 Interpolated filled contours of the shear stress distribution based on (a) near bed method (b) depth-averaged method

method. Results of the shear stress distribution were similar only for slight variations in the magnitudes and distribution of the bed shear stress. The results showed that the depth-average velocity method seems to be more precise because it considers the total depth of flow. The hydraulic conditions in which the depth-averaged method can be used are limited to the places where the velocity profile is logarithmic throughout the flow depth.

3.2.1.4 Sediment transport

Bed load transport was measured along the study reach after each controlled flood. This was achieved by embedding seven sediment traps in the river bed (Fig. 3.5). The bed load discharge was computed for masses found in the trap to be greater than 2mm and for the total mass of sediments in the trap. Table 3.2 summarizes bed load transport data for the seven sediment traps.

3.2.2 Two-dimensional numerical simulation

Christian Latulippe (2004) used the hydrodynamic model Hydrosim to perform a 2-D model simulation of the flow field for the study reach. The model simulated flow velocity, flow depth, and bed shear stress. The model used the finite element method to solve the mathematical model of Saint-Venant equations in a horizontal plan. This applies the principle of vertical integration of the 3-D Navier Stokes equations, which involves fundamental theories such as the hydrostatic pressure theory (Heniche et al., 2000). The governing equations for the model are conservation of mass and conservation of momentum equations, which are given below.

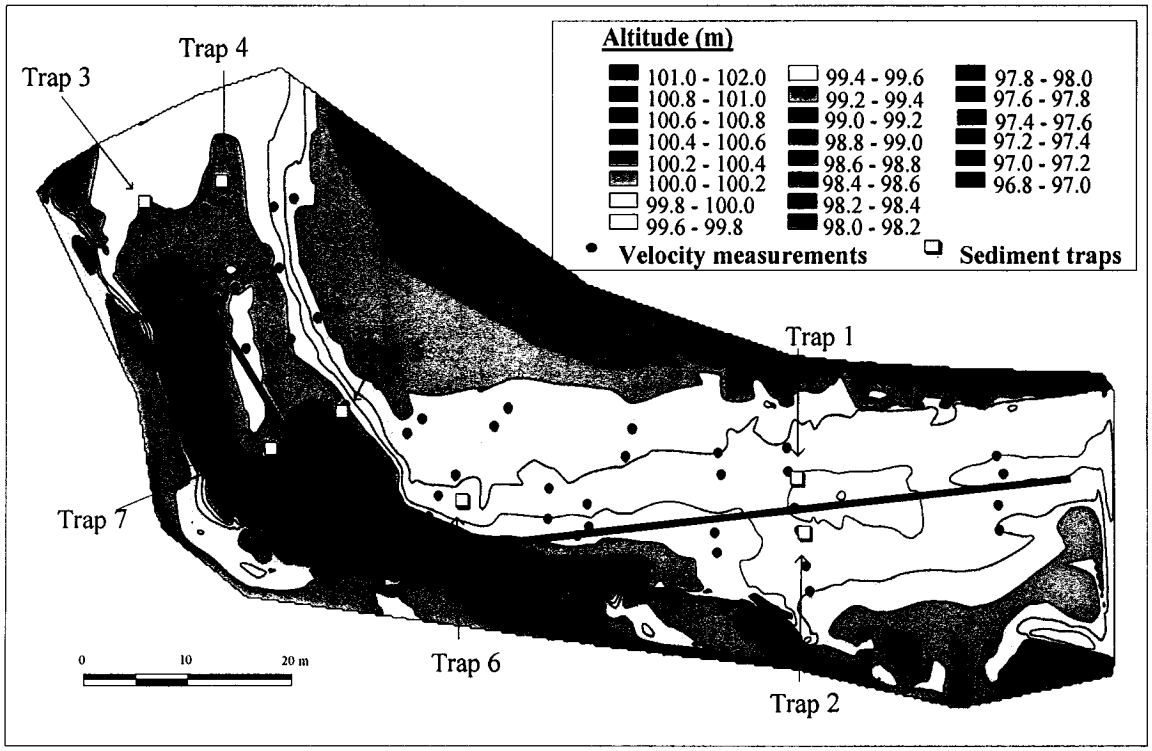

Figure 3.5 Location of sediment traps in the study reach

Table 3.2 Computed sediment transport for controlled flood 6

Trap No.	Trap Width (m)	Time (secs)	Mass > 2mm (kg)	Bed load Discharge (>2mm) (g/m/s)	Total Load (kg)	Bed load Discharge (Total) (g/m/s)
1	0.6098	28800	170.4	9.70	185.40	10.56
2	0.6098	28800	57.20	3.26	68.10	3.88
3	0.6098	3600	77.20	35.17	81.10	36.94
4	0.6098	3600	75.20	34.26	96.70	44.05
5	0.3048	21600	9.57	1.45	66.80	10.15
6	0.3048	28800	88.68	10.10	107.55	12.25
7	0.3048	28800	66.30	7.55	79.10	9.01

Conservation of mass

$$\frac{\partial \mathrm{B}H}{\partial t}+\frac{\partial q_x}{\partial x}+\frac{\partial q_y}{\partial y}=0 \tag{3.4}$$

Conservation of momentum

$$\frac{\partial(\mathrm{B}q_x)}{\partial t}+\frac{\partial}{\partial x}\left(\frac{q_x q_x}{H}\right)+\frac{\partial}{\partial y}\left(\frac{q_x q_y}{H}\right)+c^2\frac{\partial h}{\partial x}-\frac{1}{\rho}\left(\frac{\partial}{\partial x}(H\tau_{xx})+\frac{\partial}{\partial y}(H\tau_{xy})-\tau_x^b+\tau_x^b s\right)-f_c q_y=0$$

$$\frac{\partial(\mathrm{B}q_y)}{\partial t}+\frac{\partial}{\partial x}\left(\frac{q_y q_x}{H}\right)+\frac{\partial}{\partial y}\left(\frac{q_y q_y}{H}\right)+c^2\frac{\partial h}{\partial y}-\frac{1}{\rho}\left(\frac{\partial}{\partial x}(H\tau_{yx})+\frac{\partial}{\partial y}(H\tau_{yy})-\tau_y^b+\tau_y^s\right)-f_c q_x=0$$

(3.5)

Where q (q_x, q_y) is specific discharge, x (x, y) are Cartesian components, t is time, B is porosity, τ is the stress, g is the gravitational acceleration, c the celerity waves ($c = \sqrt{gH}$), ρ is the density of the water, f_c is the Coriolis factor given as $f_c = 2\omega \sin \phi$ where ω is the rotational rate of the earth and ϕ is the latitude of the site under study, D ($= h\text{-}z_f$) the water depth, where h and z_f are, respectively, the water surface level and the bed level with respect to a reference plane.

The boundary condition was given as discharge or water surface level, which was determined at several locations along the study reach. For flow simulation the discharge and water level was specified at the upstream section and water level at the downstream section. Lateral boundaries were not necessary because the model employs a wetting and drying algorithm, which defines the wetted boundary within the channel. The finite element method was used for the discretization where a spatial interpolation technique allowed the division of the flow domain into a number of six-node triangular elements.

This was superimposed over a digital elevation model (DEM) that defines the topography of the study reach. The information of each corner of the triangular element with the boundary conditions allowed for the hydrodynamic simulation. Bed resistance coefficient was obtained using Manning–Strickler equation for gravel bed rivers and Limerinos formula. These equations are represented below respectively

$$n = 0.0151 d_{50}^{1/6} \tag{3.6}$$

$$n = \frac{0.1129 D^{1/6}}{0.9 + 2\log(D/d_w)} \tag{3.7}$$

Here n is the roughness coefficient, d_w is the weighted size of intermediate particle diameter (m) given as $d_w = 0.1\ d_{16} + 0.3\ d_{50} + 0.6\ d_{84}$ and y_d is the flow depth (m). The d_{50} was obtained by a visual characterization technique (Latulippe et al., 2001). The simulation results for the velocity and shear stress using the Manning and Limerinos equations are shown in Figures 3.6 and 3.7. The results showed little or no differences for both the velocity (Fig. 3.6a and b) and bed shear stress distribution (Fig.3.7a and b) along the study section.

3.3 Three-dimensional modeling for flow and sediment transport

3.3.1 Mesh generation

Grid generation is one of the most crucial and time consuming tasks when solving partial 3-D differential equations in a complex shaped domain such as the geometry of a natural river (Spitaleri and Micacchi, 1998). Depending on the way the domain is discretized and the way the grid points are controlled, the solutions obtained using an appropriate

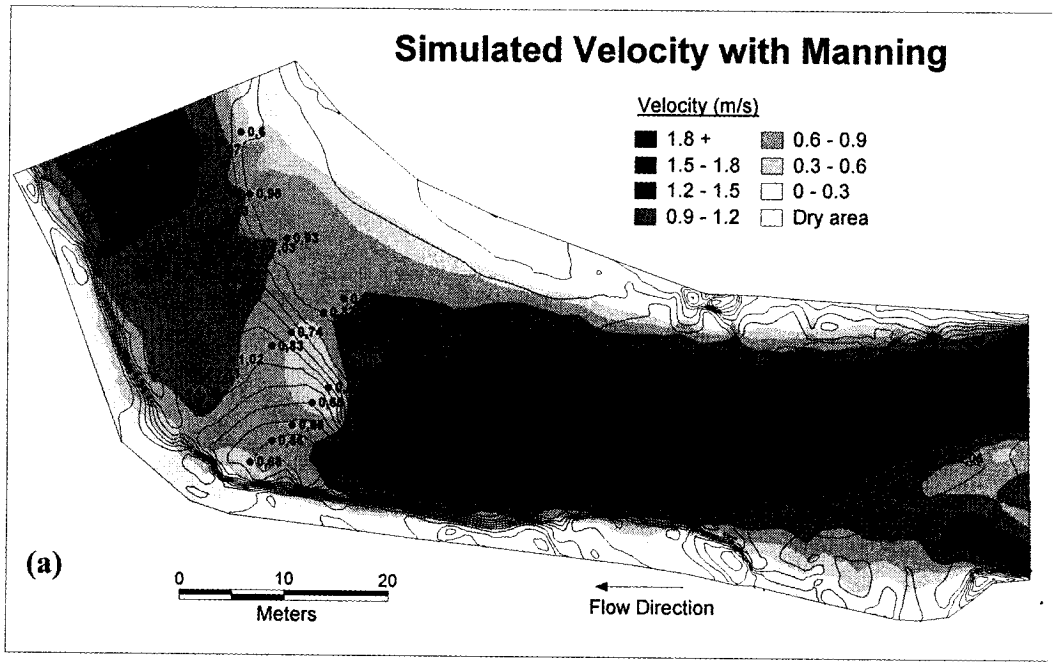

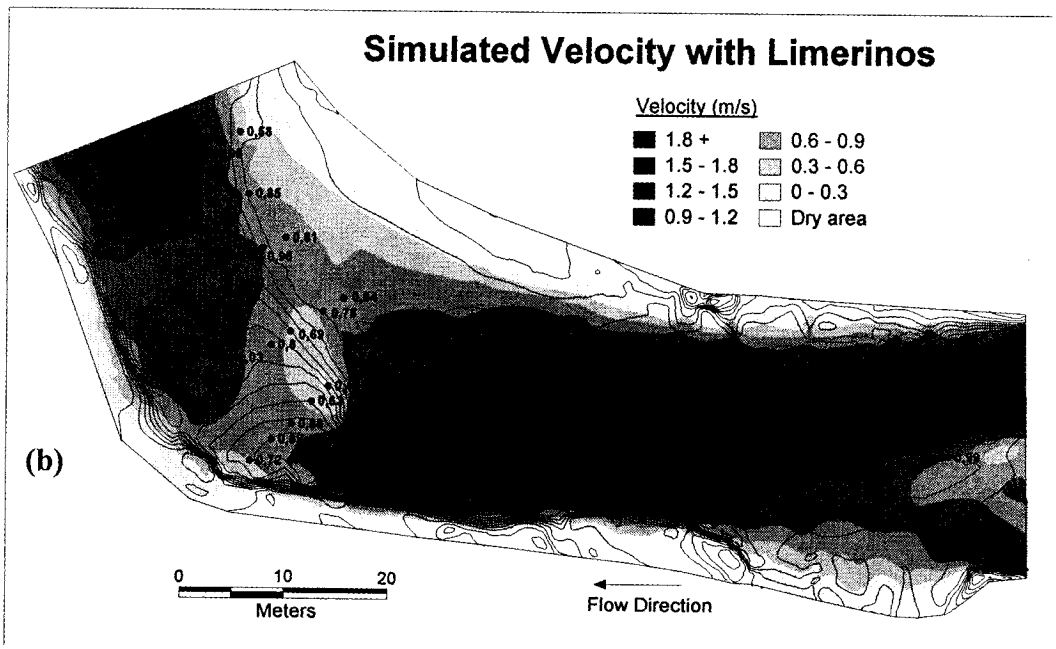

Figure 3.6 Simulation results for velocity using (a) Manning equation (b) Limerinos equation

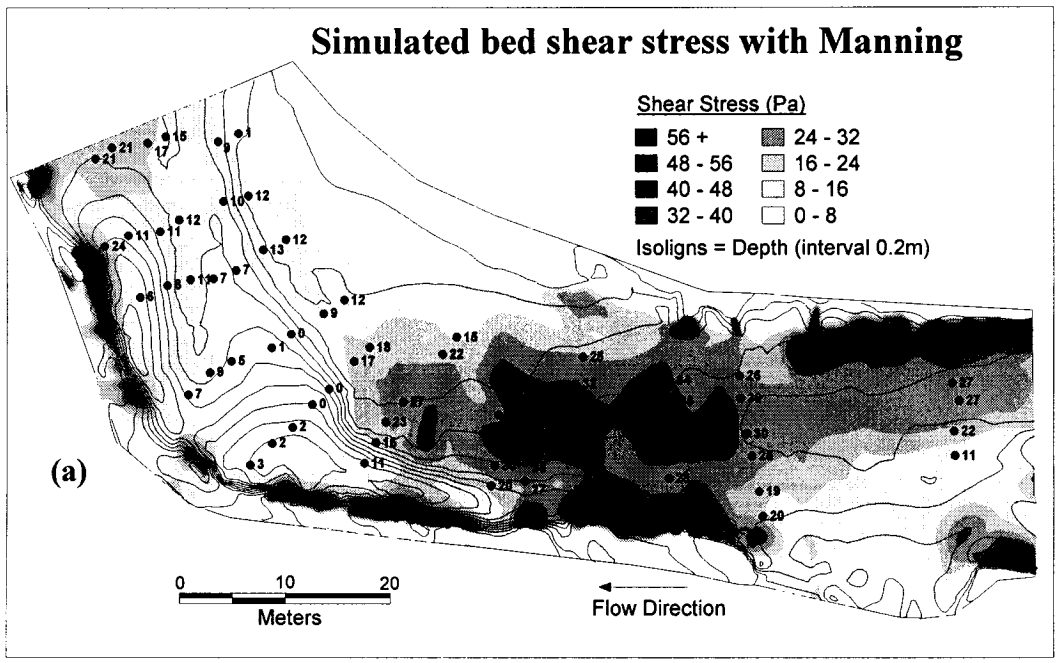

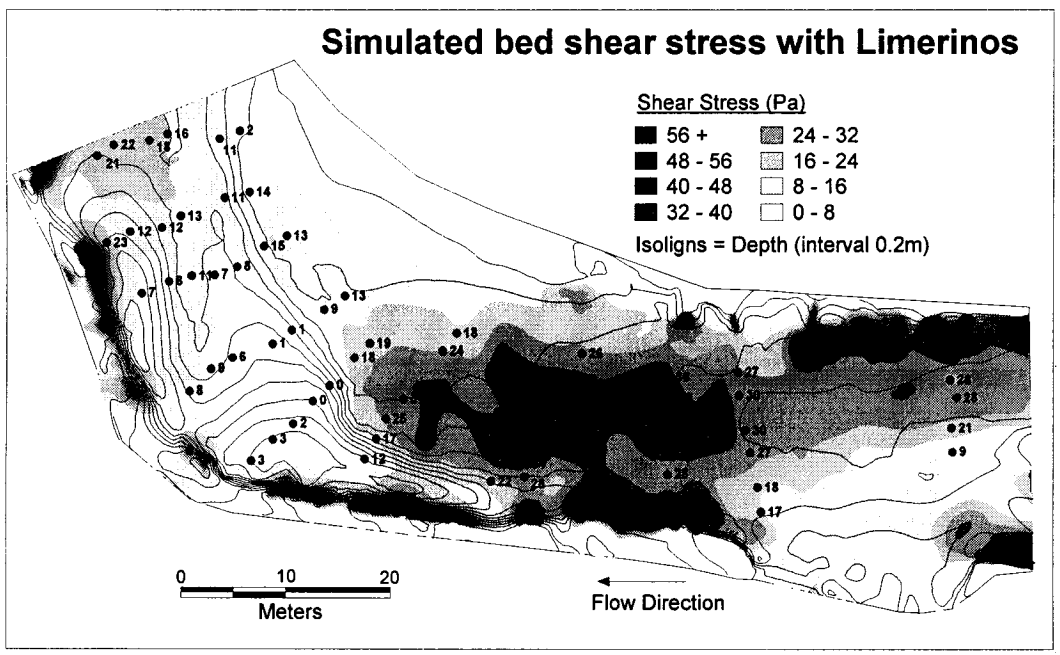

Figure 3.7 Simulation results for shear stress using (a) Manning equation (b) Limerinos equation

solution scheme may not be so accurate. This is due to discretisation and interpolation errors. The Phoenics software uses the finite volume method (FVM) to discretize the domain. A body fitted coordinate (BFC) grid system has been employed for this study instead of a Cartesian grid. This allowed the undulating bed topography to be more accurately represented. Grid generation was achieved by using the GEOGRID software (Computational Sciences, Inc.), which is based on the structured multi-block method. Structured grids are built with a rigid topological framework, whereas the unstructured grids have no underlying structure. Multi-block grids can be considered as an unstructured collection of structured blocks. Structured grids are easy to deal with for application development, computation, and visualization. Further, the computational connectivity of the grid can also be simplified by using a structured grid. This leads to a more efficient computation of the flow field. Fig. 3.8 illustrates the concept of multi-block grid used in this study. The multi-block made it easier to construct the mesh for this study since the complex geometric components were dealt with nearly independently. The generated grid for this study had a dimension of 120 x 30 x 10 (Fig. 3.8).

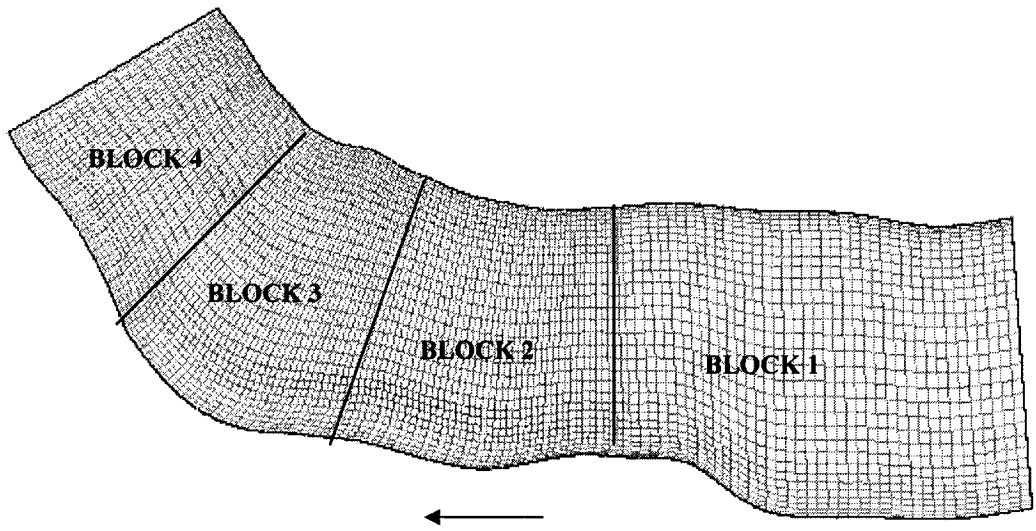

Figure 3.8 Multi-block grid used in the study

As stated earlier in section 2.3.1, the following characteristics were controlled to produce predictions as accurate as possible from the simulation:

a) Local density of the cells

Higher density of cells in the domain improves simulation accuracy. However, it leads to longer computation time and more memory is required. Therefore, the total number of grid points was kept to the minimum needed to obtain solutions with the desired accuracy. To achieve this, a grid dependency test was carried out and the optimal grid was obtained. The grid conformed to the physical boundary of the spatial domain so that finite approximations are accurate, and at the same time, smaller grid cells were placed in areas where gradients of physical variables were expected to be large. This is particularly important for grid cells adjacent to the boundary, where the non-dimensional distance of

each cell from the wall would satisfy: $30 < z^+ < 300$. Here $z^+ = V^* z / \upsilon$, and υ is the kinematic viscosity (Ferguson et al., 2003).

b) Smoothness of the grid distribution (aspect ratio)

The smoothness of the cell distribution was also controlled. The spacing between grid points should change gradually from a region where grid points are concentrated to a region where grid points are sparsely distributed, especially in regions where gradients of the flow are large, since large variations in grid density or shape can cause numerical diffusion. This might lead to inaccurate results or instability.

c) Angle of cells

The grid lines were constructed to intersect as much as possible a boundary perpendicularly, so that the derivative boundary conditions can be implemented more accurately. Inside the numerical domain, the angle of intersection between grid lines was set to be nearly perpendicular. During the construction of the mesh, avoidance of angles less than 30 degrees between grid lines has been implemented (Lane et al., 1999). The mesh was constructed following the bed topography, which imposed challenges on the construction of the river mesh, especially in regions where we have deep to shallow transition and the riverbanks as illustrated in Fig. 3.9. The grid control was carried out by adjusting the size of the cells and by using curves instead of straight lines for grid lines. These procedures were carried out throughout during the grid generation of the study reach.

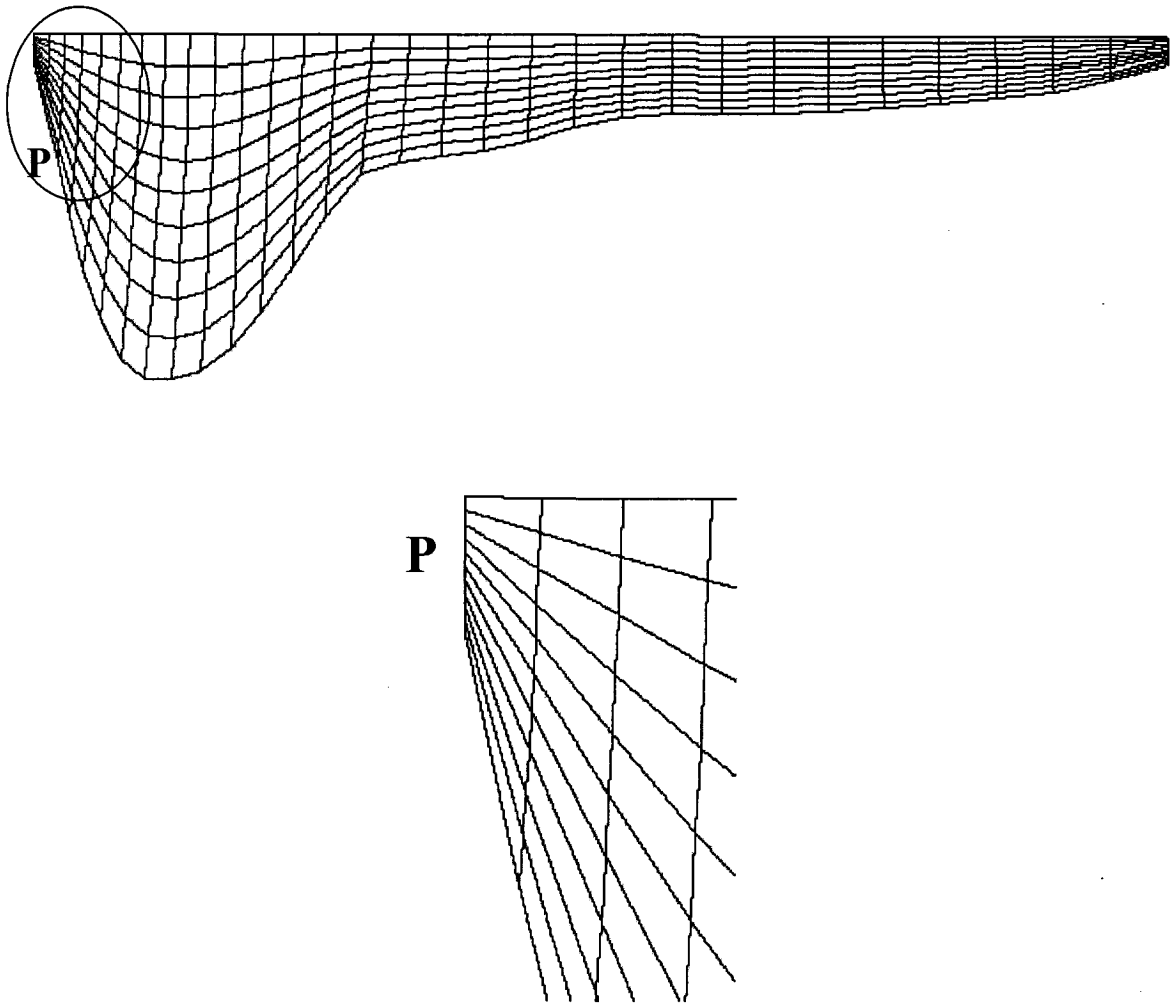

Figure 3.9 Grid angles at the apex P of a deep section 45 m downstream of the study reach

d) Alignment of the grid lines

One set of grid lines was aligned with the flow direction. This condition is important for convection-dominated flows when the aspect ratio of the control volume of each grid point is very high. The grid generation for a complex system such as the study reach requires numerous trials to meet the conditions stated above, in particular, for the skewness of the cells at the riverbanks and in deep regions of high gradient of velocity.

3.3.2 Computational modeling

The 3-D computational fluid dynamics (CFD) modeling of the flow and sediment transport along the study reach was performed using the commercial software package Phoenics 3.5 (CHAM Ltd.). The model is based on solving the full 3-D Navier-Stokes equations that are based on fundamental physical principles. These equations relate the local pressures and velocities within a body of moving fluid. They consist of the conservation of mass, momentum, and energy. The Cartesian form of the continuity equation and the full three-dimensional Navier-Stokes equations for an incompressible fluid are given below. These are the governing fluid flow equations for the model.

1. Conservation of Mass:

$$\frac{\partial u}{\partial x}+\frac{\partial v}{\partial y}+\frac{\partial w}{\partial z}=0 \tag{3.8}$$

Here, u, v, and w are the components of velocity in the x, y (planform) and z (vertical) directions, respectively.

2. Conservation of Momentum in the three coordinate directions x, y and z:

$$x\text{-}direction: \quad \rho\left(\frac{\partial u}{\partial t}+u\frac{\partial u}{\partial x}+v\frac{\partial u}{\partial y}+w\frac{\partial u}{\partial z}\right)=-\frac{\partial p}{\partial x}+\mu\left(\frac{\partial^2 u}{\partial x^2}+\frac{\partial^2 u}{\partial y^2}+\frac{\partial^2 u}{\partial z^2}\right)$$

$$y-direction: \quad \rho\left(\frac{\partial v}{\partial t}+u\frac{\partial v}{\partial x}+v\frac{\partial v}{\partial y}+w\frac{\partial v}{\partial z}\right)=-\frac{\partial p}{\partial y}+\mu\left(\frac{\partial^2 v}{\partial x^2}+\frac{\partial^2 v}{\partial y^2}+\frac{\partial^2 v}{\partial z^2}\right)$$

$$z-direction: \quad \rho\left(\frac{\partial w}{\partial t}+u\frac{\partial w}{\partial x}+v\frac{\partial w}{\partial y}+w\frac{\partial w}{\partial z}\right)=-\frac{\partial p}{\partial z}+\mu\left(\frac{\partial^2 w}{\partial x^2}+\frac{\partial^2 w}{\partial y^2}+\frac{\partial^2 w}{\partial z^2}\right)-\rho g$$

(3.9 a, b, c)

Here, μ is the coefficient of dynamic viscosity (in $kgm^{-1}s^{-1}$) and p is the pressure (Pa).

Analytical solution of partial differential equations involves closed form expressions that yield dependent variables that are continuous throughout the domain. However, numerical solutions can give answers only at discrete points such as grid points. Following discretization, the partial differential equations can be readily solved for the values of the flow field variables at the discrete grid points only. This discretization requires the definition of discrete time-steps and the division of space into discrete units.

3.3.2.1 Numerical solution

The variables used in this study were pressure, velocity, shear stress, and turbulence intensity. Distinctive characteristics of the meandering rivers are turbulent flows and secondary flows. Turbulence is inherently 3-D, time dependent, dissipative, and strongly diffusive (Wilcox, 1998). The Navier-Stokes equations combined with the continuity equation are considered a valid description of both laminar and turbulent flows. Various methods are used to simulate turbulent flow. A common approach is the Reynolds averaged Navier-Stokes (RANS) equation. The velocity is decomposed into a mean and a fluctuating part:

$$u_i = \overline{u}_i + u_i' \tag{3.10}$$

Here, u_i is the instantaneous value of one of the velocity component (u, v, or w) $\overline{u}_i$ is the time averaged value and u_i' is the time variant component. One gets these mean values of

the parameters by averaging over a time scale, *dt*, which is long compared to the time scale of turbulent motion, and in unsteady problems small compared with the unsteadiness of the mean motion. The definitions of instantaneous quantities are substituted into the equations of the instantaneous motion, which are then averaged to produce the equations of the mean motion.

The averaged equations using equation 3.9 are:

$$\frac{\partial \overline{u}}{\partial x}+\frac{\partial \overline{v}}{\partial y}+\frac{\partial \overline{w}}{\partial z}=0 \tag{3.11}$$

$$\rho\left(\frac{\partial \overline{u_i}}{\partial t}+\overline{u}_i\frac{\partial \overline{u_i}}{\partial x}+\overline{u}_i\frac{\partial \overline{u_i}}{\partial y}+\overline{u}_i\frac{\partial \overline{u_i}}{\partial z}+\frac{\partial \overline{u_i'u'}}{\partial x}+\frac{\partial \overline{u_i'v'}}{\partial y}+\frac{\partial \overline{u_i'w'}}{\partial z}\right)=-\frac{\partial \overline{p}}{\partial x_i}+\mu\left(\frac{\partial^2 \overline{u_i}}{\partial x^2}+\frac{\partial^2 \overline{u_i}}{\partial y^2}+\frac{\partial^2 \overline{u_i}}{\partial z^2}\right) \tag{3.12}$$

The time-averaged conservation of mass, equation (3.10), is identical to the instantaneous equation (3.6) with the mean velocity replacing the instantaneous velocity (Wilcox, 1998). However, the statistical-averaging process has introduced unknown turbulent correlations ($\overline{u'_i u'_j}$) into the mean–flow equations, which represent the turbulent transport of momentum and mass (Wilcox, 1998). The unknown turbulent correlations are called the Reynolds or turbulent shear stresses. A turbulence model is required to determine the turbulent shear stress. Phoenics has various turbulence models but for this study the RNG k-ε (renormalization group) model was adopted. This model is derived from mathematical methods. It gives improved performance for separated and curved flows as well as for flows with moderate swirl (Yakhot and Orszag, 1986; Versteeg and Malalasekera, 1995; Dargahi, 2004).

The momentum and continuity equations are linked. The momentum equations share pressure, and the velocities enter in the continuity equation. There is no direct equation for the pressure. Therefore, the task of the CFD code is to join the variable without an equation (pressure), to the equation without variable (continuity). Phoenics does this using SIMPLEST, a variant of the SIMPLE algorithm (Pantankar and Spalding, 1972).

3.3.3 Boundary conditions of 3-D simulation

As described earlier in section 2.3.2, a good knowledge of boundary conditions, particularly in terms of inflow data, is required in order to have accurate model predictions. The necessary boundary conditions related to this study are water surface, bed surface, extent of domain, outlet, and inflow characteristics. Some of these boundary conditions were extracted from field measurements carried out by Christian Latulippe (2004). The water surface was defined as a plane of symmetry having a gradient of 0.3 %. Method such as the porosity correction method (Ouillon and Dartus, 1997; Bradbrook et al., 2000a, b) relating water surface to flow field was not used for this study due to time constraints. A roughness height (z_o) of 30 mm was used for the bed surface, based on measurement of bed particle size of the study reach. The extent of domain, which is described by the river bed and the water edges, was kept fixed as described in Lane et al. (1999), Ferguson et al. (2003), and Dargahi (2004). A relative static pressure of 1000 Pa was specified at the outlet.

Inflow conditions are very important factors in the predictive ability of a model as illustrated by Lane et al. (1999). A good knowledge of the inflow velocity is required in

this study. The velocity distribution across the inflow plane was interpolated from the field measurements described in section 3.2.1 above. However, this procedure was not as straightforward as expected due to various reasons such as the upstream river geometry and the mid-channel bar downstream of the bridge as seen in Fig. 3.2. Different approaches were tested in order to make a proper representation of the inflow velocity with respect to the actual field measurements. These approaches include 1) the simulation using the study section where the inlet velocities were separated into one, two, or three separate vertical panels of constant velocity and 2) the use of outlet velocities from different sections of the upstream simulation as inlet velocities for simulations on the study reach.

3.3.3.1 Downstream simulations

The downstream simulations were carried out on the study reach (AA′ - BB′ of Fig. 3.10) with constant inlet velocities in panels (Fig. 3.11). In order to have a more realistic

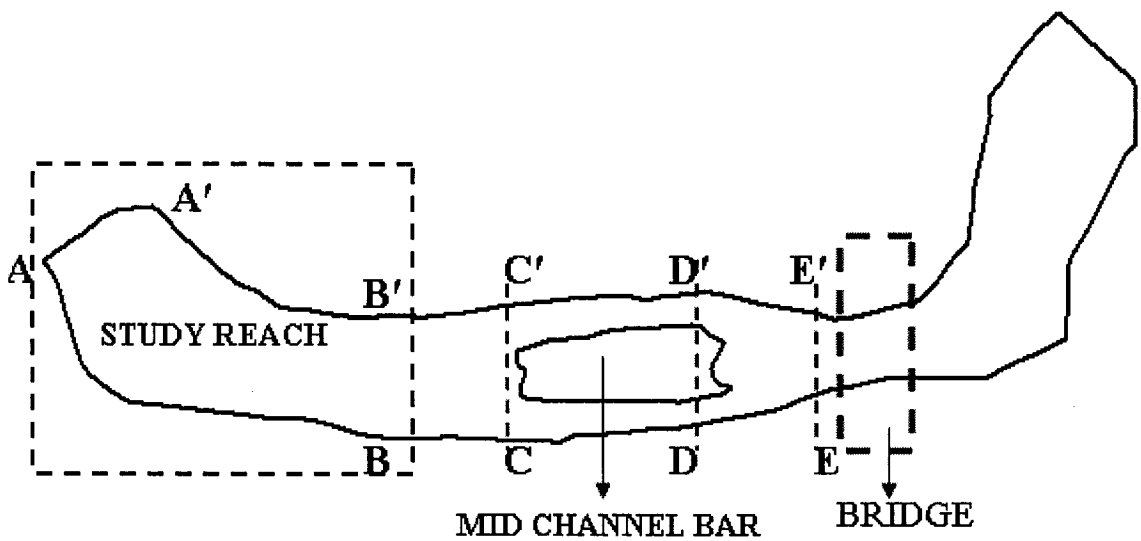

Figure 3.10 Study section and the upstream section

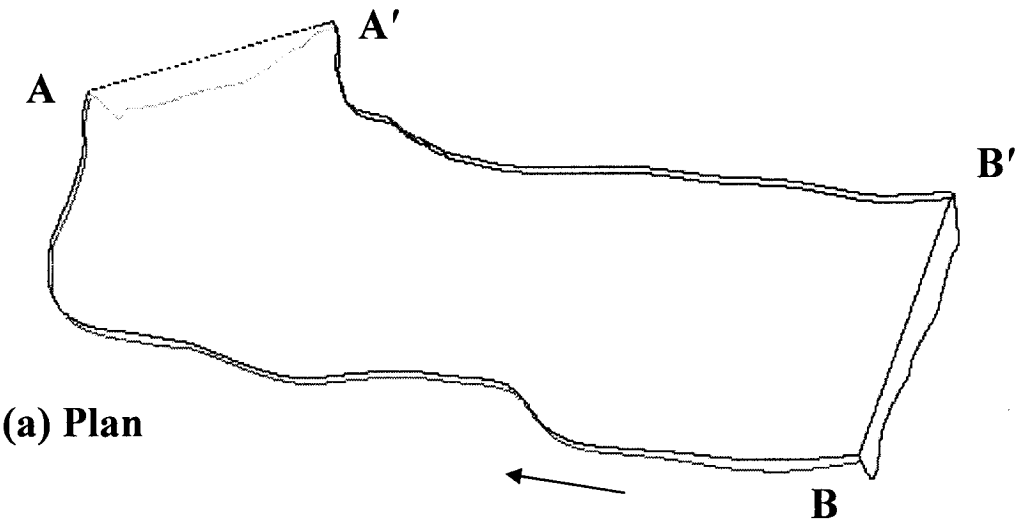

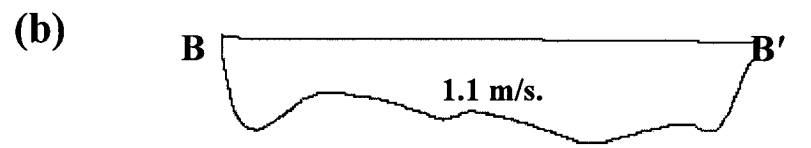

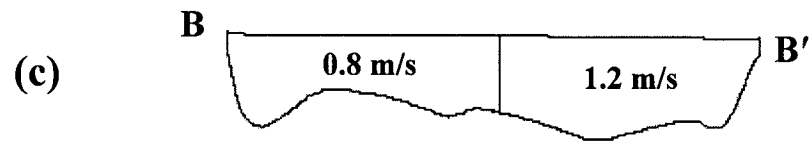

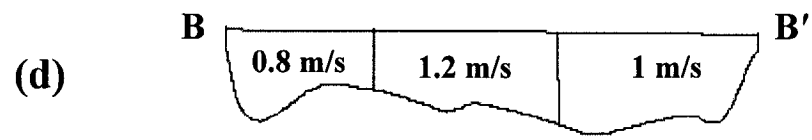

Figure 3.11 (a) Study reach as in Fig.3.10 (b) uniform inlet velocity (c) dual inlet velocities (d) three inlet velocities

model, series of inflow velocities were used at the inlet of the study reach section B-B′ (Fig.3.11). Fig. 3.11a shows the 3-D plan form view of the study reach. Fig 3.11b, c, and d show the different velocity combinations used at the inlet of the study reach. The overall discharge was kept constant for all the simulations when using different inlet conditions. However, to have a proper representation of the inlet conditions at the study reach, slight variation in the discharge (less than 8%) had to be used during the course of the study.

3.3.3.2 Upstream simulations

Since it is known that the upstream flow dynamics influences markedly the downstream reaches in a complex flow field (Lane et al., 1999), attempts were made to simulate the flow field upstream, and to use the outlet velocities as inlet values for the downstream simulations. The difficulty in modeling the upstream reach is the presence of the mid-channel bar (Fig. 3.2), which is partly above the water level. This creates numerical instability in a 3-D model. Three approaches were adopted in considering the inlet velocities of the downstream simulations using the outlet velocities of the upstream simulations.

To begin with, the entire upstream section of the study reach (BB′ - EE′ of Fig. 3.10) was simulated using a uniform inlet velocity of 1.1 m/s at section E-E′ (Fig. 3.12). The mid-channel bar, which is above the water surface (Fig.3.2), was considered as a simple object in the river section during these simulations. Secondly, upstream simulations considering

the section from the mid-channel bar to the inlet of the study reach (BB′ - DD′ of Fig. 3.10) were used with slight modifications of the object's shape to avoid numerical errors during discretization (Fig. 3.13). This modification involves the reduction of sharp points of the mid-channel bar to curves as seen in Fig.3.13. Based on the overall discharge, it was estimated that a higher velocity of 1.2m/s had to be introduced into the right channel (looking downstream) and 0.6m/s in the left channel of the study reach (section D-D′).

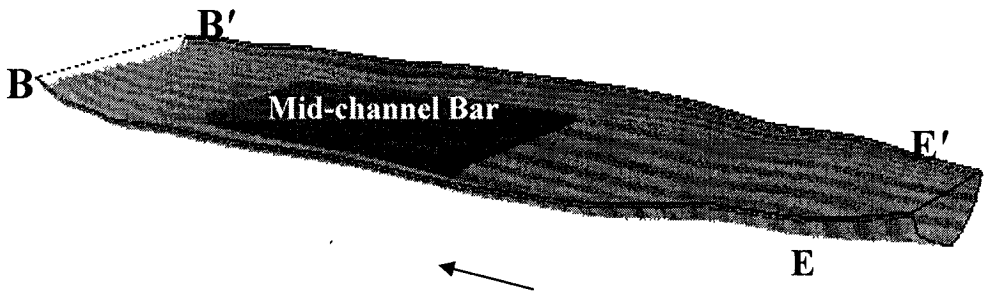

Figure 3.12. Entire upstream section of study reach

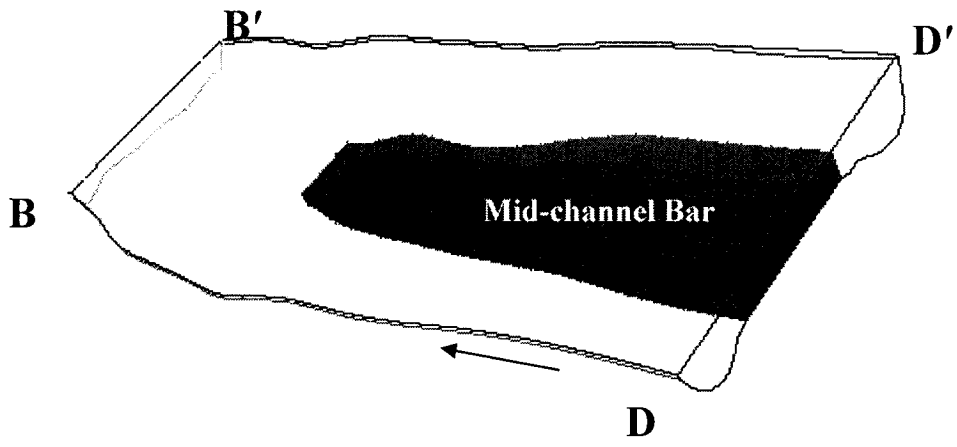

Figure 3.13. Upstream simulation from mid-channel bar

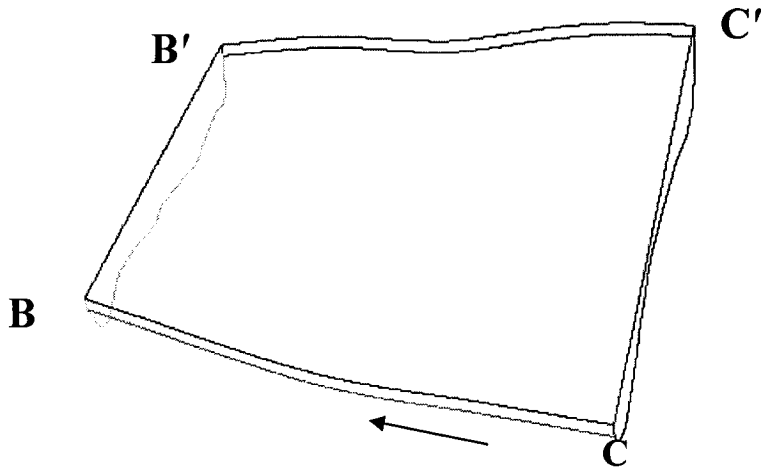

Figure 3.14. Upstream simulation without mid-channel bar

Lastly, the upstream section was simulated from the zone where the mid-channel bar was no longer above the water surface (BB′ - CC′ in Fig. 3.10) using the actual bed topography measurements to build the body fitted coordinate grid. Fig. 3.14 illustrates the 3-D form of this simulation. A uniform velocity of 1.1 m/s was used at the inlet of Fig.3.15 (C-C′). All these three approaches to specify the inlet conditions were adopted to enable a fully developed log profile of the velocity to be present at the inlet of the study reach (B-B′ in Fig. 3.10).

3.3.3.3 Combined simulations

Different inlet velocities were also used in a combined simulation section (AA′ - CC′ of Fig. 3.10). Fig. 3.15a illustrates the 3-D form of the combined simulation section. Fig. 3.15b, c and d shows the trial inlet conditions for the study using uniform velocity, dual velocity and three inlet velocities at section C-C′ of Fig. 3.15a.

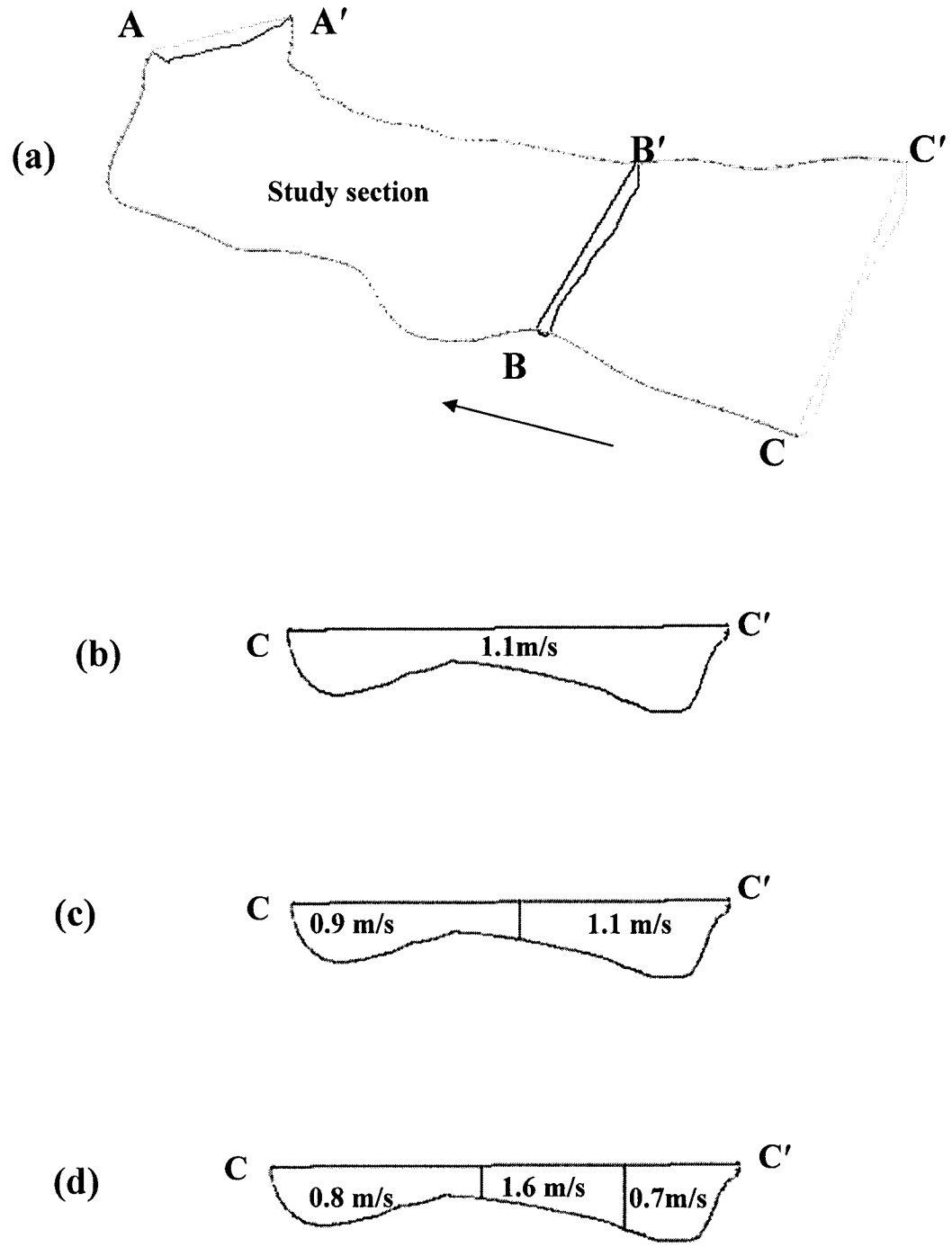

Figure 3.15 (a) Combined simulation section as in fig. 3.11 (b) uniform inlet velocity (c) dual inlet velocity (d) three inlet velocities at section C-C′ of Fig.3.16a

3.3.4 Bed load equations

To estimate the bed load transport different equations are available. These equations are based on the shear stress approach, stream power approach or the parametric approach as stated in section 2.5. The following equations were used here are:

(i) The DuBoys equation:

$$q_b = C_d \tau_o (\tau_o - \tau_c) \tag{3.13}$$

Here, q_b is the bed load discharge, C_d is the characteristic sediment coefficient ($0.17/d^{3/4}$) in $m^3/kg/sec$, τ_o is the bed shear stress, τ_c is the critical shear stress in N/m^2, $\tau_c = 0.0125 + 0.019d$ (kg/m^3), and d is bed grain size diameter in mm.

(ii) The Meyer-Peter and Muller equation

$$\left[\frac{q_b(\gamma_s - \gamma)}{\gamma_s}\right]^{2/3}\left(\frac{\gamma}{g}\right)^{1/3}\frac{0.25}{(\gamma_s - \gamma)d_m} = \frac{\left(k/k'\right)^{3/2}}{(\gamma_s - \gamma)}\frac{\gamma RS}{d_m} - 0.047 \tag{3.14}$$

(I) (II) (III)

Here q_b is in weight per unit time and unit channel width, γ_s and γ are specific gravity of sediment and water respectively, k and k' are reciprocals of Manning roughness coefficient, d_m is the effective grain size of the sediment, R is the hydraulic radius and S is the total energy gradient. Expressions I, 11, and III in 3.13 are described as the bed load discharge, the effective shear stress, and the critical shear stress respectively.

(iii) The Shield equation:

$$\frac{q_b \gamma_s}{q_s \gamma} = 10\frac{\tau_0 - \tau_c}{(\gamma_s - \gamma)d} \tag{3.15}$$

Here, q_b is in kg/m/s

(iv) Sato et al. equation:

$$\frac{q_b}{\tau_o V_* f(\tau_c/\tau)} = 1 \tag{3.16}$$

(v) The Meyer-Peter equation:

$$\frac{q_b}{\sqrt{(s-1)gd^3}} = \left(\frac{4\tau_o}{\rho(s-1)gd} - 0.188\right)^{3/2} \tag{3.17}$$

(v) The Nielsen equation:

$$\frac{q_b}{\sqrt{(s-1)gd^3}} = \left(\frac{12\tau_o}{\rho(s-1)gd} - 0.05\right)\sqrt{\frac{\tau_0}{\rho(s-1)gd}} \tag{3.18}$$

In equations 3.17 and 3.18, q_b is the bed load discharge in m^2/s, and s is ratio of mass density of sediment to mass density of water. To use these equations for model validation the grain size distributions of the trapped sediment data is needed. However, for the course of this study 20 mm and 40 mm grain size diameters were used in the various equations. This was based on the median diameter of the bed sediment for the upstream (40 mm) and the downstream (20 mm) of the study reach as described in section 3.1.

(vi) Engelund-Hansen stream power equation

$$f'\phi = 0.1(\tau_*)^{5/2} \tag{3.19}$$

$$f' = 2gRS/U^2 \tag{3.20}$$

$$\phi = \frac{q_s}{\gamma_s\left[(s-1)gd^3\right]^{1/2}}, \quad \tau_* = \frac{\tau_0}{(\gamma_s - \gamma)d} \tag{3.21}$$

Here, f' is the friction factor, ϕ is the dimensionless sediment discharge, and τ_* is the dimensionless shear stress or the shields stress.

4.0 RESULTS

4.1 Flow field

Fig. 4.1 shows the results for the depth-averaged velocity (0.4 of the flow depth) distribution for the downstream simulations (study reach) using different trial inlet velocities as in Fig. 3.11. Fig. 4.1a, b, and c show different flow field patterns and velocity magnitudes, when the inlet condition, were varied for the simulations. However, all three simulations in Fig. 4.1 showed zones of highest velocity towards the centre of the study reach, a low velocity zone at the left side and center of the study reach section towards the outer bank of the river curvature (Fig. 4.1). This was a result of the complex geometry of the river section and the nature of the deep section at the region. The various simulation results shown in Fig. 4.1 also displayed secondary flows across the river section. Fig. 4.2 shows the secondary flows at sections 1-1′, 2-2′, and 3-3′ of Fig. 4.1. These denote the velocity components at right angles to the channel axes. All sections in Fig. 4.2 had similar secondary flow patterns, but had different velocity magnitudes. Section 3-3′ showed the strongest secondary flow compared to the other two sections.

Fig 4.3 shows the results of the velocity distribution for depth-averaged studies for the downstream simulations. Here, the outlet velocities from the simulation of the upstream sections (Fig. 3.12, Fig. 3.13, and Fig. 3.14) are used as inlet velocities for the downstream section (study reach) simulations. The results of the three simulations in Fig. 4.3 showed the highest zones of velocity at the centre of the channels at a position

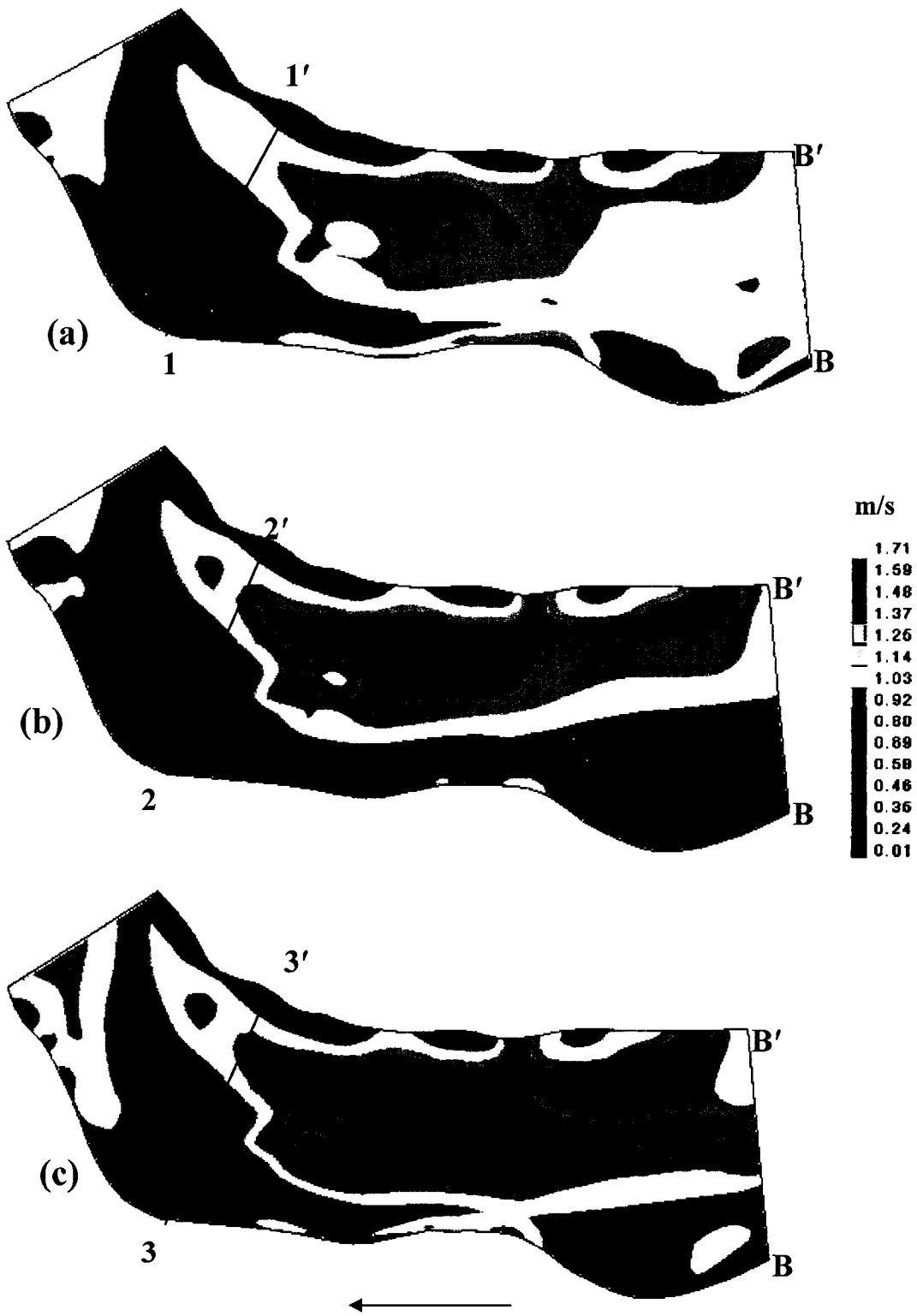

Figure 4.1. Depth-averaged velocity distribution for the study reach using (a) uniform velocity (b) dual velocity (c) three velocity values at the inlet as in Fig. 3.12.

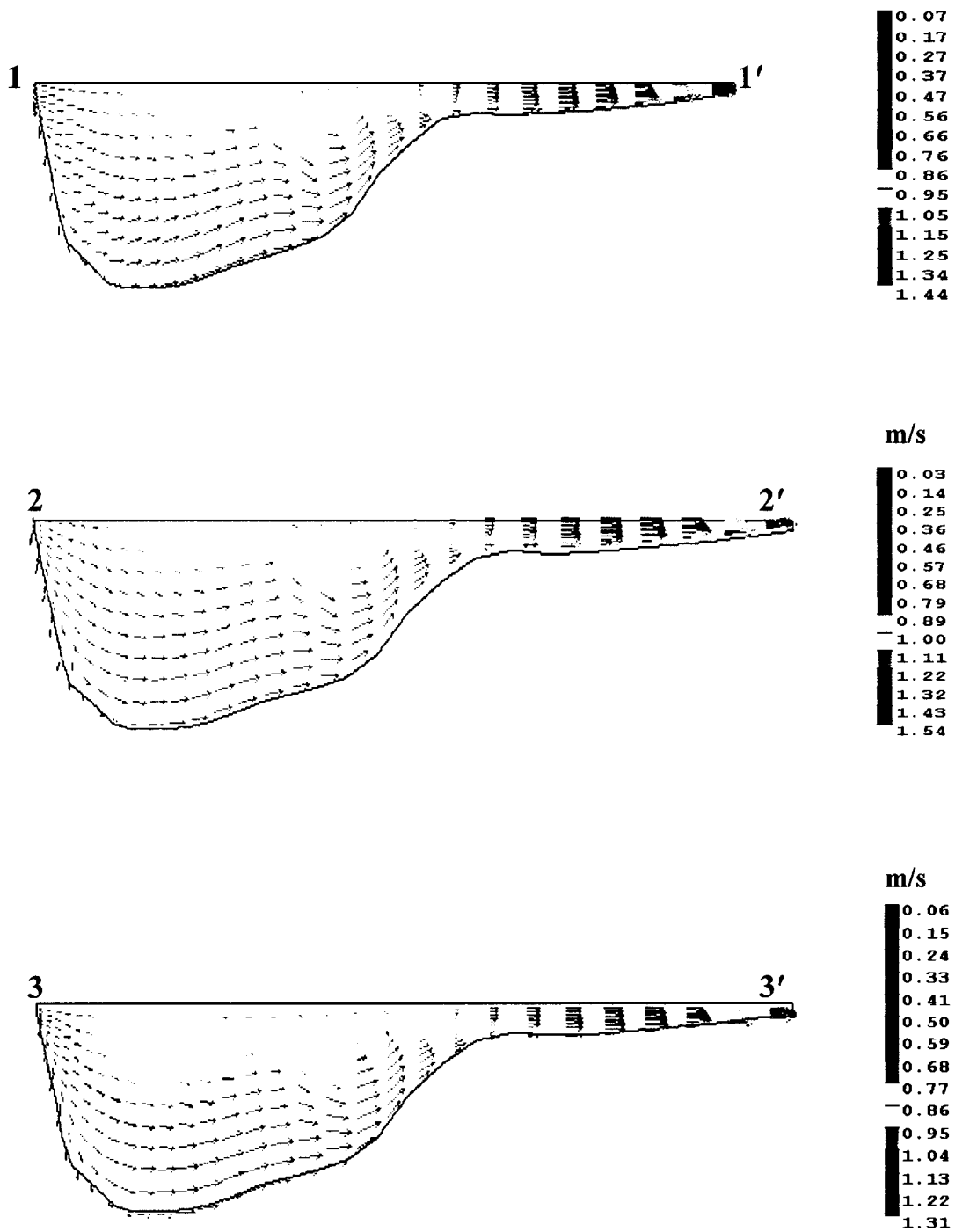

Figure.4.2. Cross-sections showing secondary flow for sections (a) 1-1′ (b) 2-2′ and (c) 3-3′ of fig.4.1

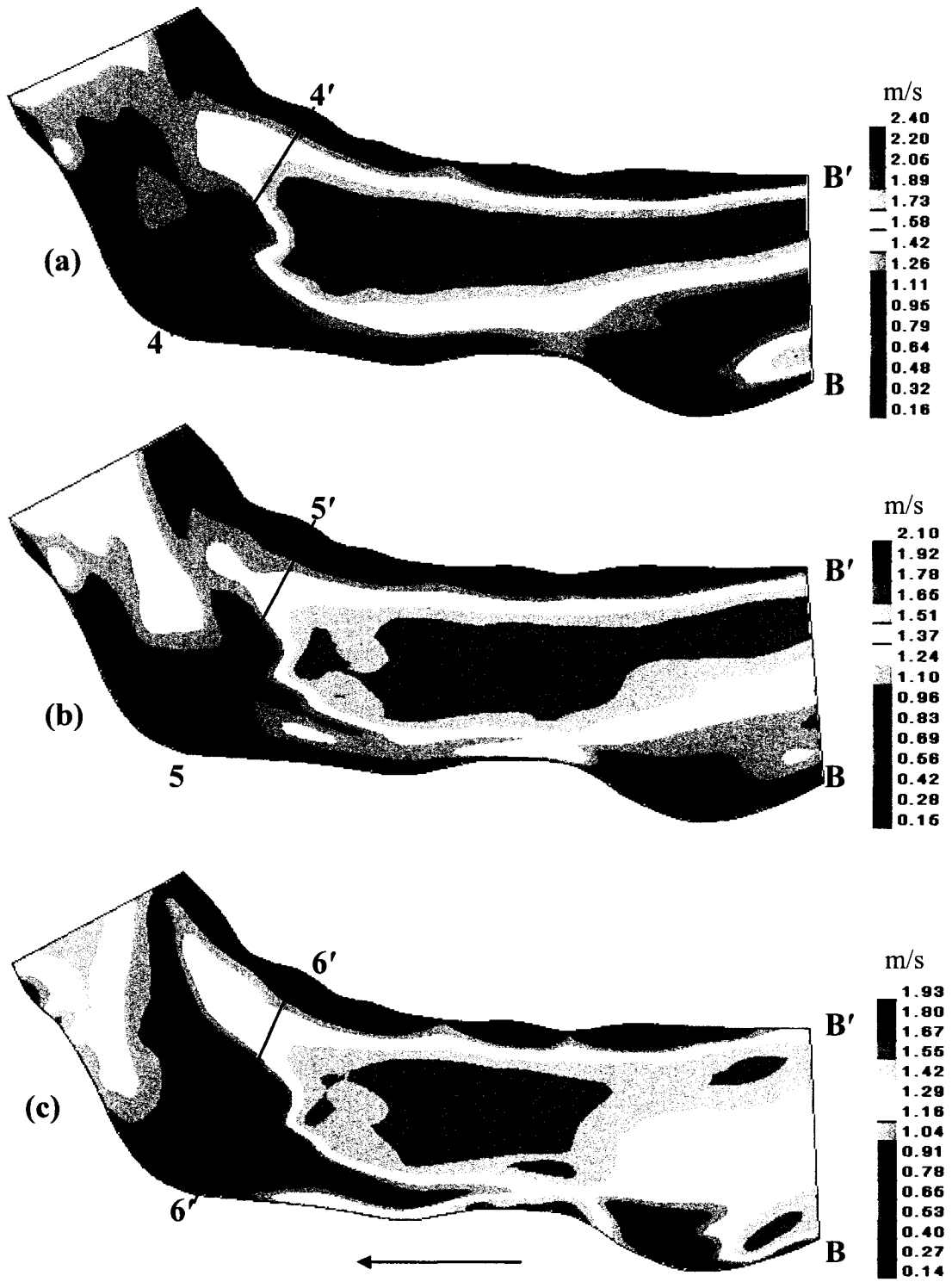

Figure 4.3. Depth-averaged velocity distribution using outlet velocities from upstream section as inlet velocities of study reach for (a) entire upstream section (Fig. 3.12) (b) from the mid-channel bar (Fig. 3.13) (c) before mid-channel bar (Fig. 3.14)

similar to that of Fig. 4.1. However, the velocity magnitudes for these figures were slightly different compared with the results in Fig. 4.1. Fig. 4.3a, b, and c had a maximum velocity of 2.3 m/s, 2.1 m/s and 1.93 m/s respectively. Fig. 4.3a and b showed low velocity zones on both sides of the channel section. Fig. 4.3a has the largest low velocity zone close to the right bank at the downstream end of the study reach. Fig. 4.3c shows a low velocity zone on the right side, the left side, and at the center of the study reach section. Secondary flows obtained from the simulations are illustrated in Fig. 4.4 for sections 4-4′, 5-5′, and 6-6′ of Fig. 4.3. At sections 4-4′ and 5-5′ of Fig. 4.4, a different recirculation pattern (secondary flow) is exhibited in the deep region compared to Fig. 4.2, indicating a marked impact of the upstream condition on the meandering flow dynamics. Section 6-6′, however, showed a similar secondary flow pattern as that described in Fig. 4.2. The strongest secondary flow was found at section 5-5′.

Fig 4.5 shows the depth-average velocity distribution from the simulation of the combined section using three different inlet conditions as seen in Fig. 3.15. The simulation results in the Fig. 4.5 also illustrate a high velocity zone at the center of the study reach. The maximum velocities for the three trials (Fig. 4.5a, b, and c) were almost the same compared with the results in Fig. 4.2, which were much more variable. Despite markedly different velocities close to the cross-section B-B′, the three simulations had similar flow characteristics of low velocity zones, particularly near the left side and center of the study reach section, towards the outer bank of the river curvature. These zones were similar to those present in Fig. 4.1. Secondary flows were also seen in the simulation results of Fig. 4.5.

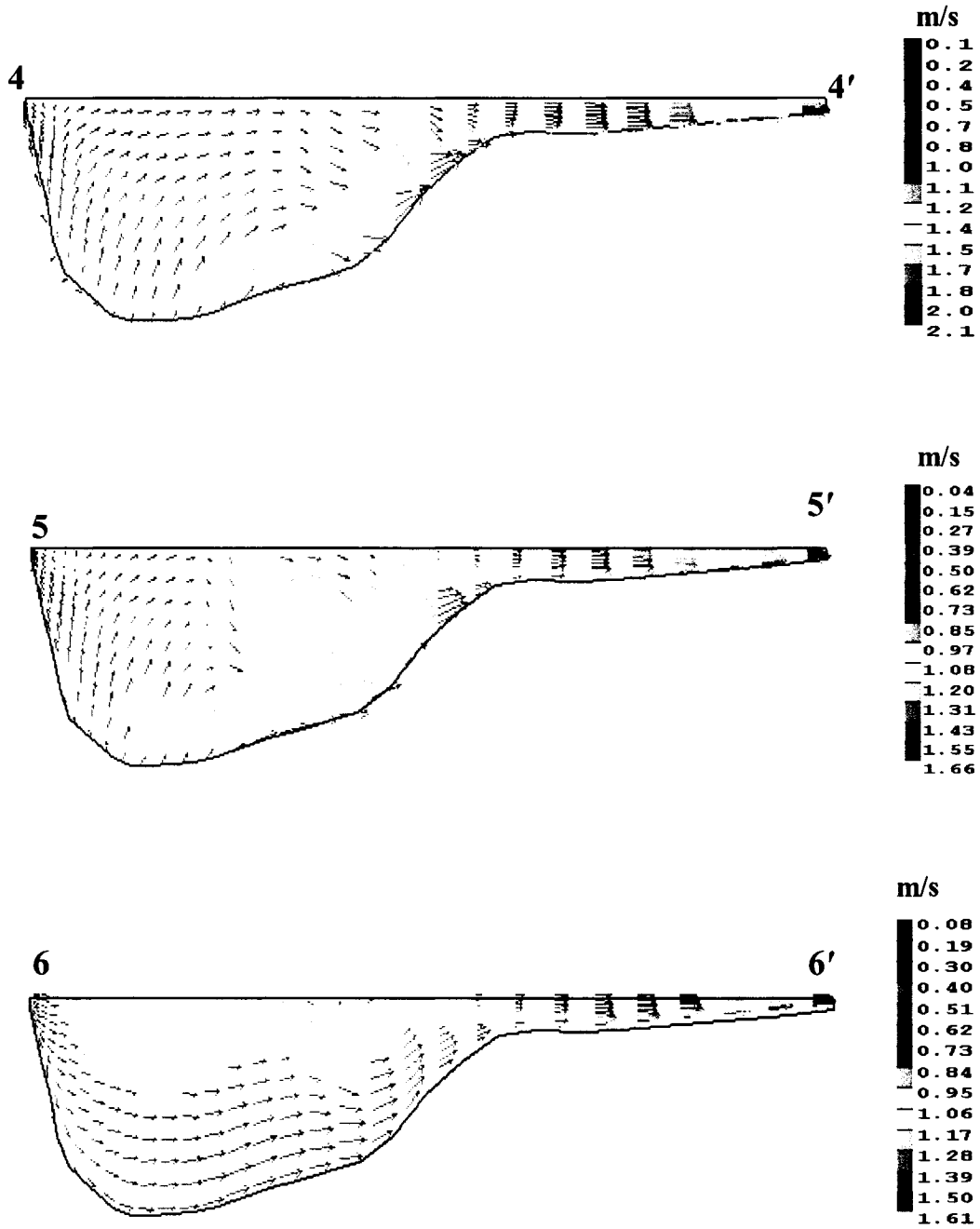

Figure.4.4. Cross-sections showing secondary flow for sections (a) 4-4′ (b) 5-5′ and (c) 6-6′ of fig.4.3

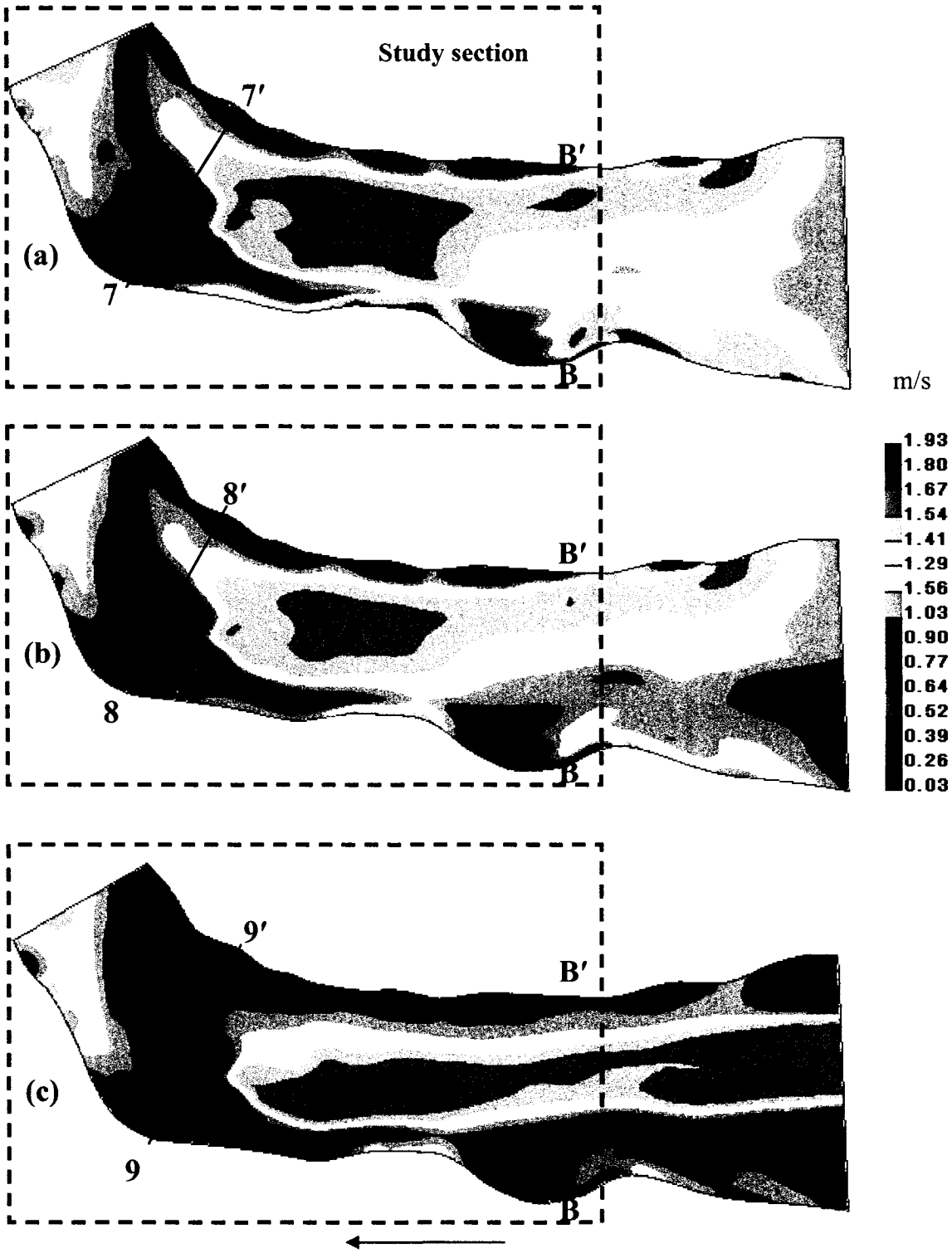

Figure 4.5. Depth-averaged velocity distribution using inlet velocities as in (a) Fig 3.15b (b) Fig 3.15c and (c) Fig 3.15d

Sections 7-7′, 8-8′, and 9-9′ in Fig. 4.6a, b and c illustrates the secondary flow patterns of Fig. 4.5. The secondary flow patterns in Fig. 4.6 compared to the flow patterns in Fig. 4.2 and 4.4 had different velocity magnitudes and stronger secondary flows. Table 4.1 summarizes the conditions used in simulations carried out in this study.

4.2 Validation of results

4.2.1 Velocity data

Results of the different trial inlet velocities were compared with the field measurements to determine the proper inlet velocity scheme that was the most appropriate for the analysis. Visual comparison of the simulated velocity distributions using the field measurements (Fig. 3.3b) as a reference was carried out for this purpose. The simulation shown in Fig. 4.5c provided the best qualitative match with the field measurements (Fig. 4.7). Following this, a regression analysis was performed to get a quantitative estimate of the agreement. Again, Fig. 4.5c simulation, with the three inlet velocities of 0.8 m/s, 1.6 m/s and 0.7 m/s respectively (Fig 3.15d) in the simulation of the combined section (Fig. 3.15a), gave the best results in terms of correlation coefficient (R = 0.86, Fig. 4.8).

A correlation coefficient of 0.92 was obtained for the 2-D model. It was therefore slightly higher than that for the 3-D model (R = 0.86) as shown in Fig. 4.9. However, the slope (0.70) of the 2-D model was slightly smaller than for the 3-D simulation (0.79). Compared to the 2-D simulation, the 3-D simulation corresponds closer to conditions encountered in streams. Hence, for the velocity data, one expects a better degree of agreement between

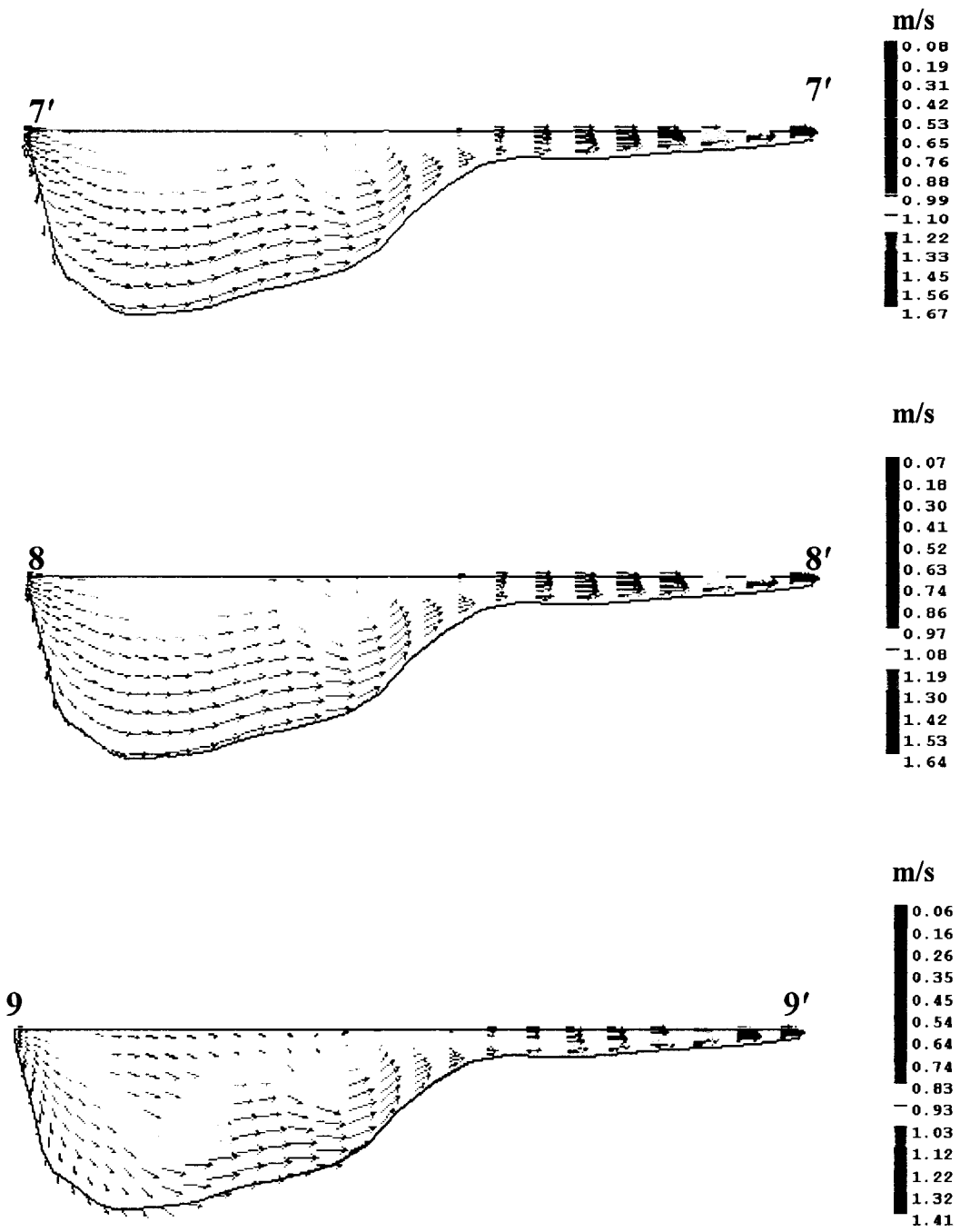

Figure.4.6. Cross-sections showing secondary flow for sections (a) 7-7′ (b) 8-8′ and (c) 9-9′ of fig.4.3

Table 4.1 Summary of the simulations.

Simulation no	Related figure	Area configuration of simulation	Inlet conditions	Description	Remarks
1	4.1a	Downstream (Study section)	Fig. 3.11b	Study section	Uniform velocity of 1.1 m/s at the inlet of study section.
2	4.1b	Downstream (Study section)	Fig. 3.11c	Study section	Dual inlet velocities of 0.8 m/s and 1.2 m/s at the inlet of study section
3	4.1c	Downstream (Study section)	Fig. 3.11d	Study section	Three inlet velocities of 0.8m/s, 1.6 m/s and 0.7 m/s respectively at the inlet of the study section
4	4.3a	Two section (upstream+ study section)	Fig. 3.12	Outlet velocities from entire upstream simulation are used as inlet velocities study for the section simulation.	Uniform velocity of 1.1 m/s at the inlet of the entire upstream.
5	4.3b	Two section (upstream+ study section)	Fig. 3.13	Outlet velocities from upstream simulation from mid channel bar are used as inlet velocities for the study section simulation.	Two inlet velocities of 0.6m/s and 1.2 m/s at the upstream section from the mid channel bar.
6	4.3c	Two section (upstream+ study section)	Fig. 3.14	Outlet velocities from upstream simulation without the mid channel bar are used as inlet velocities for the study section simulation.	Uniform inlet velocity of 1.1 m/s at the inlet of the upstream without the mid channel bar.
7	4.5a	Combined	Fig. 3.15b	Study section combined with the upstream section (without the mid channel bar).	Uniform inlet velocity of 1.1m/s at the inlet of the combined section.
8	4.5b	Combined	Fig. 3.15c	Study section combined with the upstream section (without the mid channel bar).	Two inlet velocities of 0.9m/s and 1.1 m/s at the inlet of the combined section.
9	4.5c	Combined	Fig. 3.15d	Study section combined with the upstream section (without the mid channel bar).	Three inlet velocities of 0.8 m/s, 1.6 m/s and 0.7 m/s at the inlet of the combined simulation.

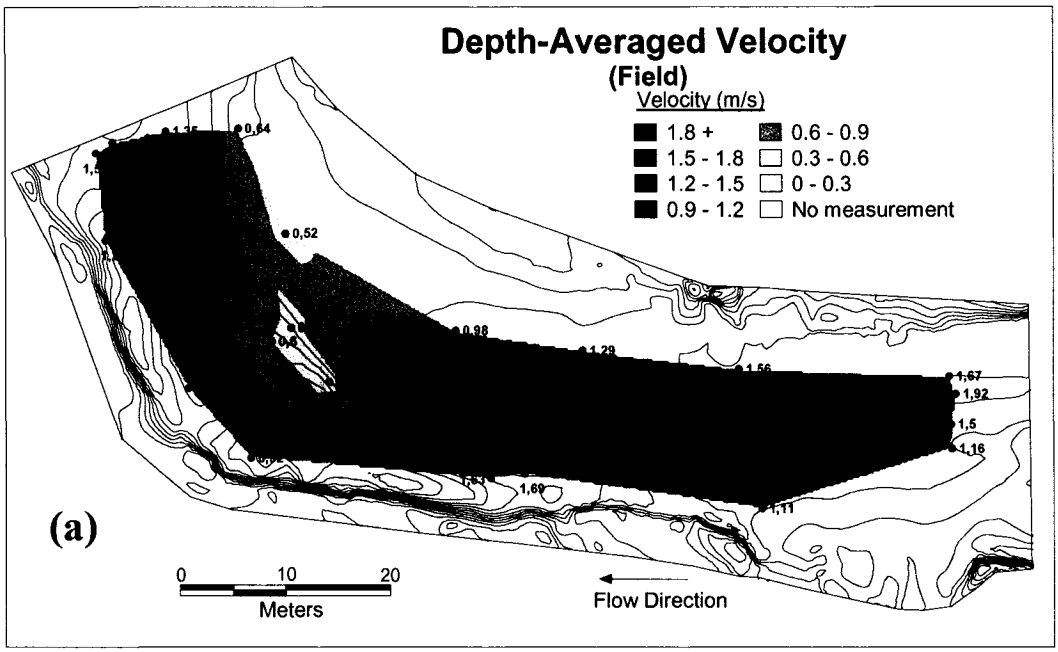

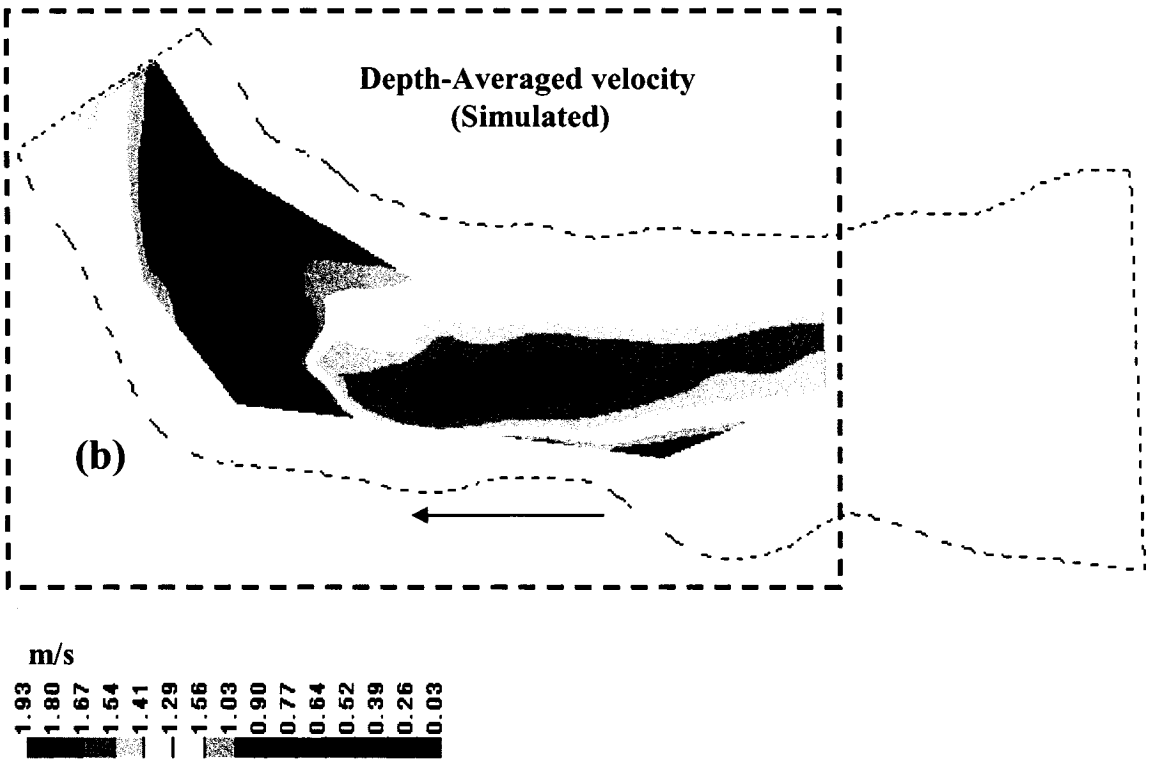

Figure 4.7. Comparison of interpolated filled contours of the depth-averaged velocity distribution of (a) the field measurements and (b) the 3-D simulation for study section with inlet conditions as in Fig. 4.5c.

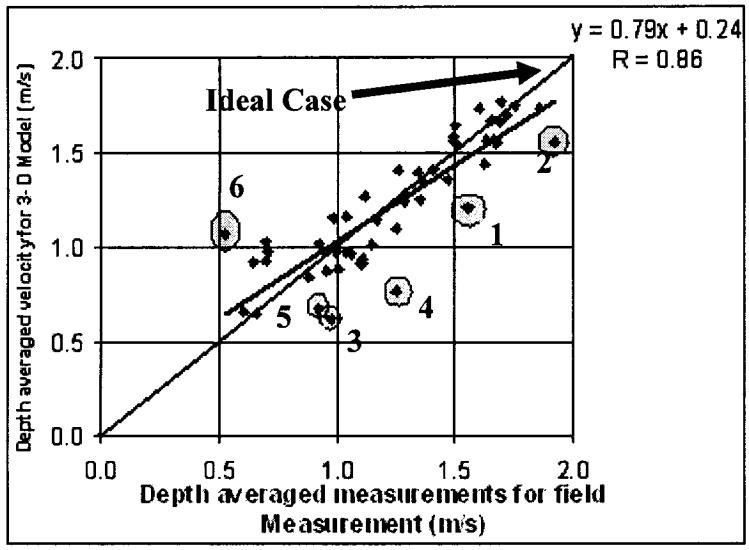

Fig. 4.8 Correlation result of the depth-averaged velocity between the field measurements and the 3-D model results

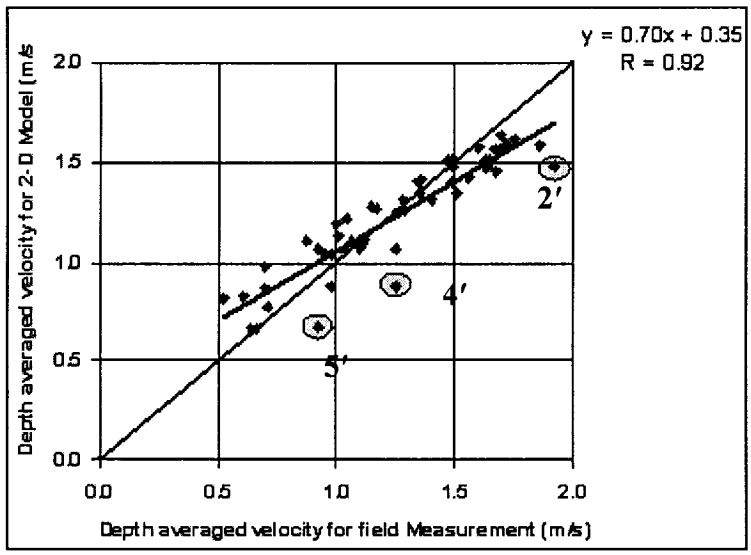

Fig. 4.9 Correlation result of the depth-averaged velocity between the field measurements and the 2-D model results

predictions and field data. Various reasons appear to be responsible for the slightly weaker correlations obtained from the 3-D simulation in the present case. Some of the reasons contributing to a relatively lower R-value for 3-D case are listed below.

1. Inlet conditions: In a 2-D model, inlet conditions are specified as a discharge (or water level) at the upstream cross-section. In a 3-D model, the ideal situation is to provide the 3-D velocity for each cell at the inlet cross-section. As it is virtually impossible to obtain such detailed field measurements, uniform velocity value is sometimes used, as in simulation 1 (Table 4.1, Fig. 4.1a). This is far from ideal, however, and using upstream reaches to obtain more reliable simulations in the study section is the alternative chosen in this study. However, the complexity of the bed topography upstream of the study section, with a mid-channel bar, greatly complicated the task of making sure the inlet conditions were appropriate for the 3-D simulation.
2. Errors in field measurements: Even though the measurements were taken in a control situation, the velocity measurements were not taken simultaneously at all the points. It is therefore possible that secondary circulation would produce some differences over a period of time in field measurements, thus increasing the error when comparing with the simulated flow field.
3. More than other factors, the validation had to be confined to a single sample of field measurements.

In Fig. 4.8, there are six outliers, which markedly affect the correlation results. These points are shown in Fig. 4.10 along the study reach section. Some of these outliers (2, 4,

and 5 of Fig. 4.8) correspond to the zone of the three outliers seen in the correlation results of the 2-D model with the field measurements (2′, 4′, and 5′ of Fig. 4.9). This indicates that the field measurements in these zones may be problematic. Fig. 4.11 shows a correlation result of the depth-averaged velocity between the field measurements and the 3-D model results without these outliers. This gave a correlation coefficient of 0.93, and the slope is much closer to 1 (0.86) for the 3-D case. If circumstances permitted, one would repeat some of the field measurements to ensure that the collected data at some locations were not influenced by extraneous factors. However, the R-value obtained in the present case (0.86) is in the general range of the R-values reported in other field studies related to 3-D simulation of river flows (Table 4.1).

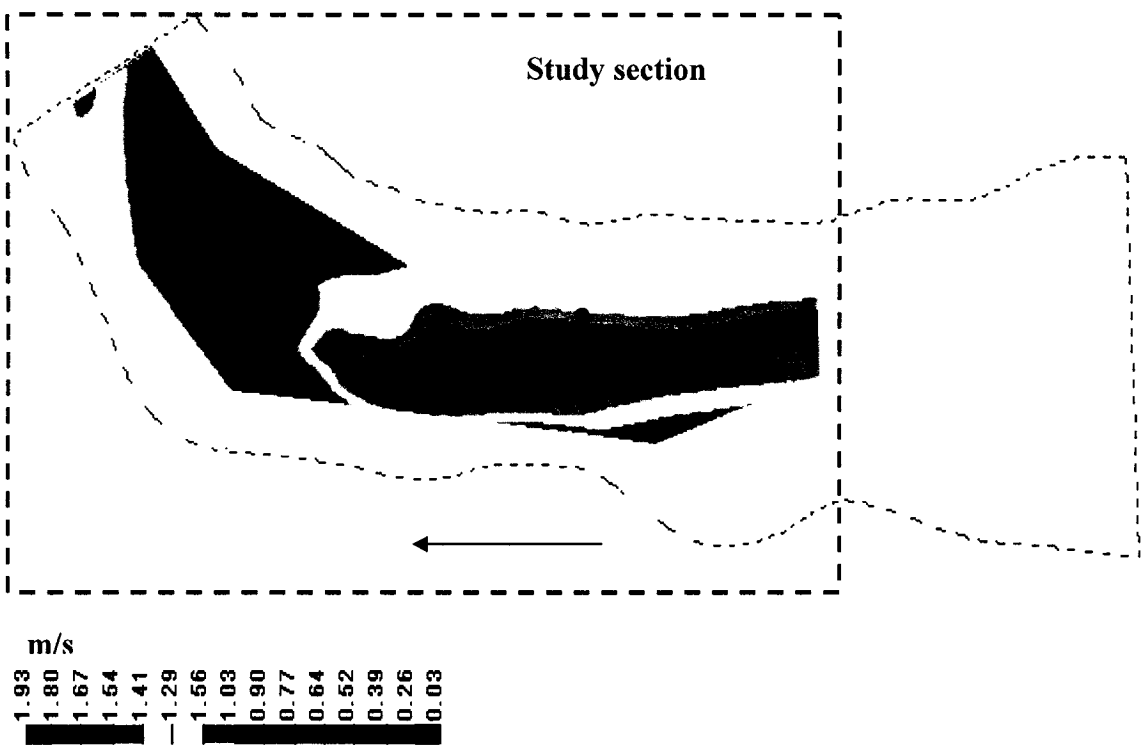

Fig. 4.10 Study reach section showing the outliers of Fig. 4.8

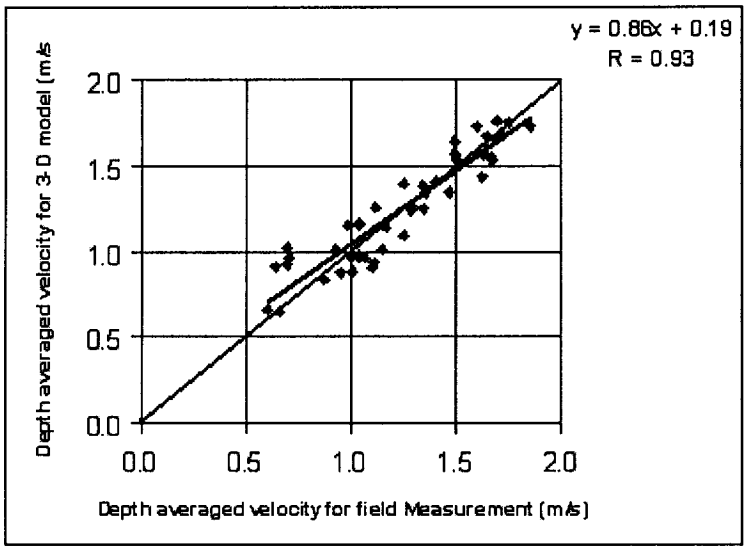

Fig. 4.11 Correlation result of the depth-averaged velocity between the field measurements and the 3-D model results after the elimination of the outliers.

Table 4.2 Correlation results of 3-D models of natural rivers

	3-D model	**R**
1	Hodskinson and Ferguson (1998)	0.94
2	Lane et al. (1999)	0.77
3	Nicholas and Sambrook-Smith (1999)	0.88
4	Booker et al. (2001)	0.88
5	Ferguson et al. (2003)	0.95
6	Present study	0.86

The near bed velocity is very important to estimate the bed shear stress. Therefore, a comparison of the simulated and measured near bed velocity was also carried out. The filled contours of the near bed velocity distribution obtained from field measurements (Fig. 4.12a) are compared with the velocity predictions from the 3-D model simulation (4.12b). It may be noted that the near bed velocity filled contours for the 3-D model

corresponds to the values at the third cell in the study reach. This was done to ensure that the predicted near bed velocity was taken at a location that corresponded to the field measurements of near bed velocity, which were taken at 22cm from the bed in all cases. Fig. 4.13 shows the correlation coefficient value for the near bed velocity to be 0.81 with a slope of 0.69. Fig. 4.14 shows a correlation result of the near bed velocity after eliminating the same outliers as in Fig. 4.10. This gave a correlation coefficient as 0.84 and a slope of 0.73.

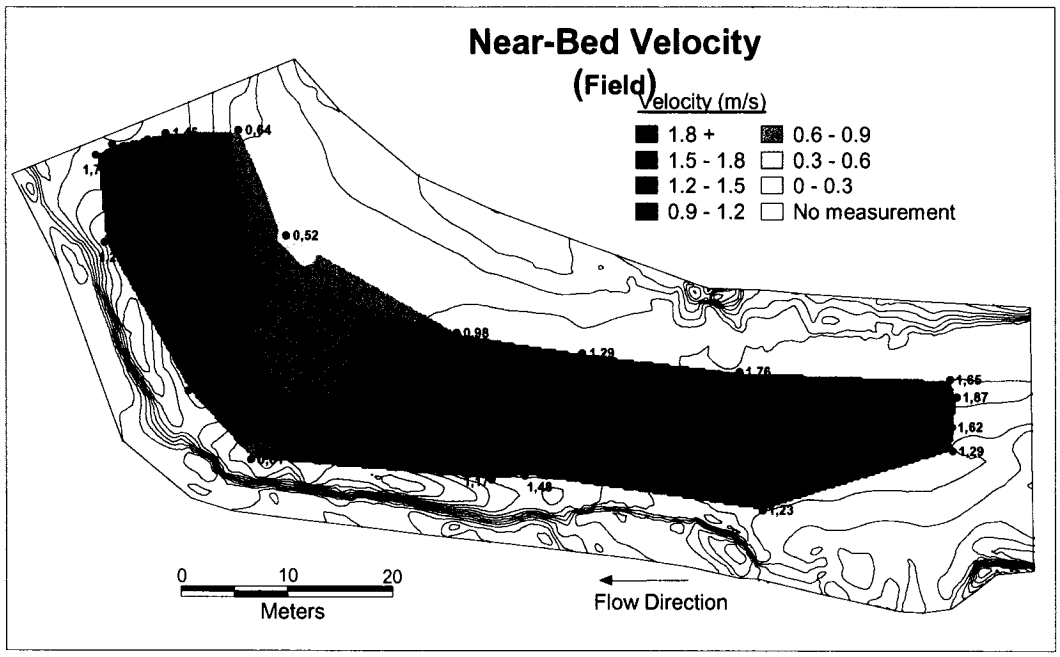

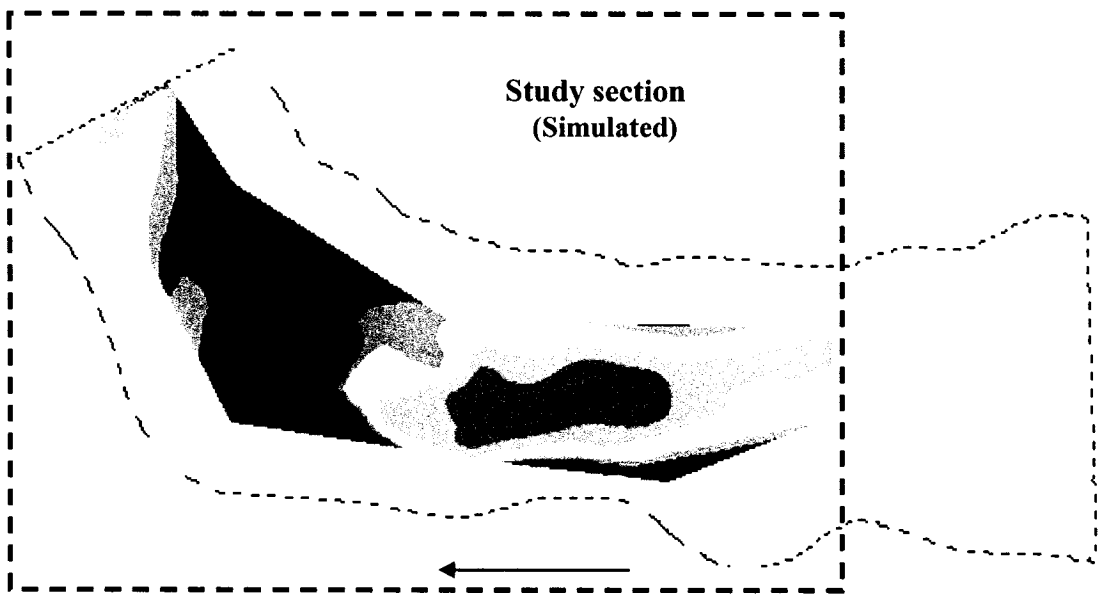

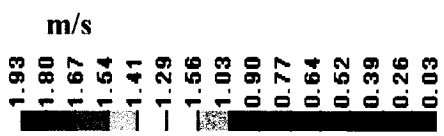

Figure 4.12. Interpolated filled contours of the near bed velocity distribution for (a) the field measurement (b) 3-D model for study section

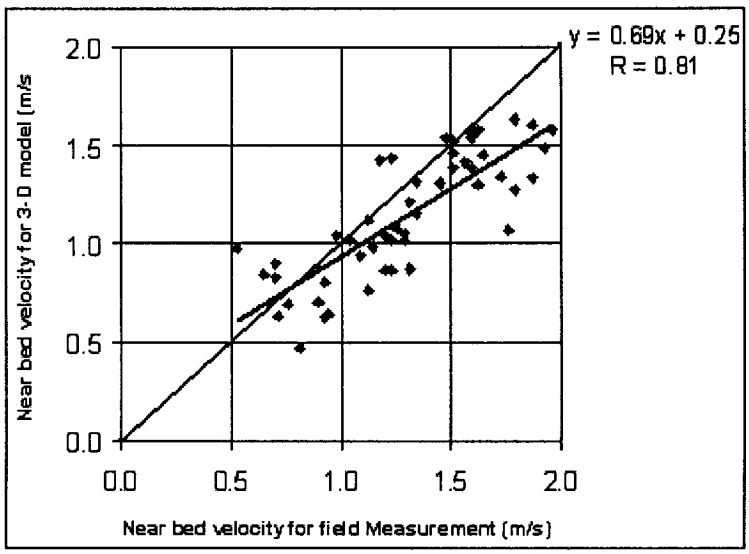

Fig. 4.13 Correlation between the field near bed velocity measurements and 3-D model results

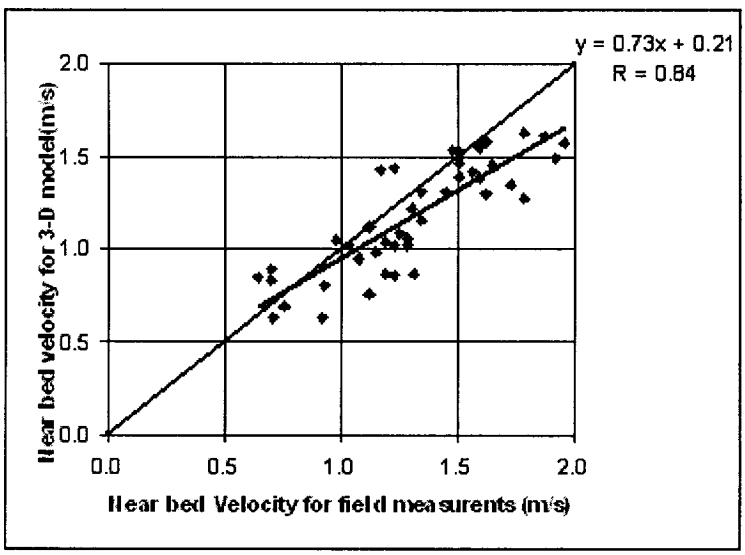

Fig. 4.14 Correlation between the field near bed velocity measurements and 3-D model results after the elimination of the same outliers as in Fig. 4.10

4.2.2 Bed shear stress distribution

4.2.2.1 Shear stress based on Log-law

Estimates of bed shear stresses were required in order to estimate the bed load transport as earlier described in section 2.5. The bed shear stresses were estimated using the same inlet conditions that produced the best match with field velocity measurements (Simulation 9, Table 4.1). Fig. 4.15 presents the bed shear stress distribution and a comparison with the shear stress estimated from field measurements using the near bed method. High estimates of bed shear stresses were seen at regions A and B of the study section only in Fig. 4.15b. Further, the model seems to have under-estimated the bed shear stress compared with the estimated bed shear stresses obtained from field measurements, although there was a slight similarity in terms of the distribution pattern and magnitude in some regions of the study section. The Phoenics software calculates the bed shear stress values by using the log-law wall functions applied to the bottom cell, which is:

$$\frac{V}{V^*} = \frac{In(Ez+)}{\kappa} \tag{4.1}$$

Here, E (roughness parameter) = b/k_s^+, b = 29.7, and $k_s^+ = V^* k_s / \upsilon$ (Phoenics manual). A very good estimate of the representative roughness for the entire study reach is a prerequisite to obtain a reasonable estimate of the bed shear stress.

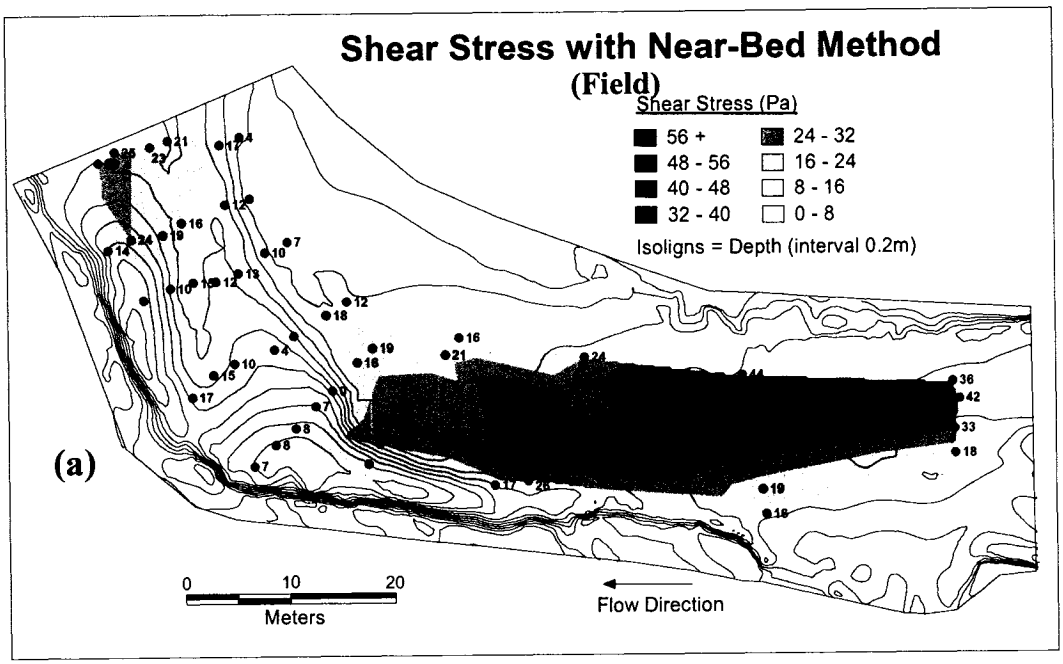

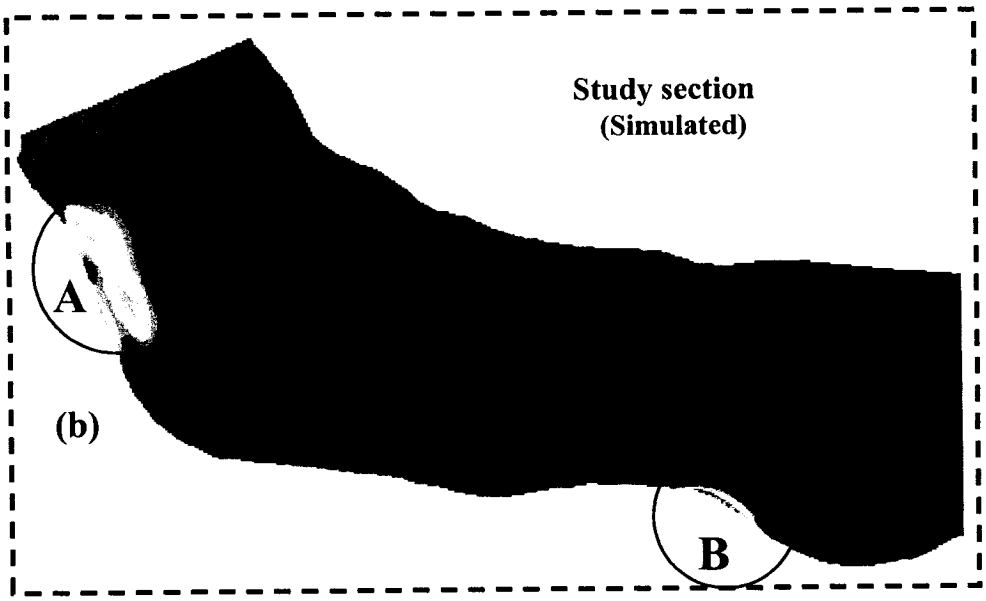

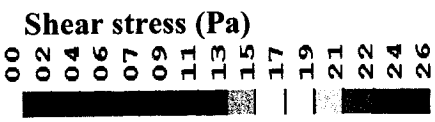

Figure 4.15. (a) Estimated bed shear stress from field measurements using the depth average method compared with (b) the estimated bed shear stress result using combined simulation results as in Fig. 4.5c

4.2.2.2 Shear stress based on quadratic stress law

An alternative way to obtain the estimate of bed shear stress is to use the quadratic stress law. This relates the average shear stress at the bed to the square of the average velocity (Schlichting, 1987).

$$\tau_0 = \rho C_D V^2 \tag{4.2}$$

Where C_D is the drag coefficient. A similar approach was adopted by Lane et al. (1999) who used the quadratic stress law to determine the shear stress instead of the Phoenics shear stress output. The drag coefficient adopted for the bed shear stress estimate for the study reach was 0.01, based on Lisle et al. (2000).

The bed shear stress was estimated using the depth-averaged velocity and the velocity values at the third cell (assumed near bed velocity). The interpolated filled contour plot for estimated bed shear stress using the third cell (Fig. 4.16a) and the depth-averaged velocity (Fig. 4.16b) were obtained from the 3-D simulation. The two figures in Fig. 4.16 gave similar estimated bed shear stress pattern having the highest bed shear stress values at the centre of the study, which matched the estimated field data (Fig. 3.4b). The only difference between the interpolated filled contours for the estimated bed shear stresses using the third and fourth cells (depth averaged) was the difference in magnitude. As expected, for the quadratic stress law, the estimated bed shear stresses using the fourth cell gave a higher estimate since the velocity was greater. The estimated bed shear stresses using the third cell were comparable to the estimated bed shear stresses obtained from field measurements using the near bed method (Fig. 4.17a) and the depth-averaged method (Fig.4.17b). Compared to the estimate of bed shear stresses based on the third

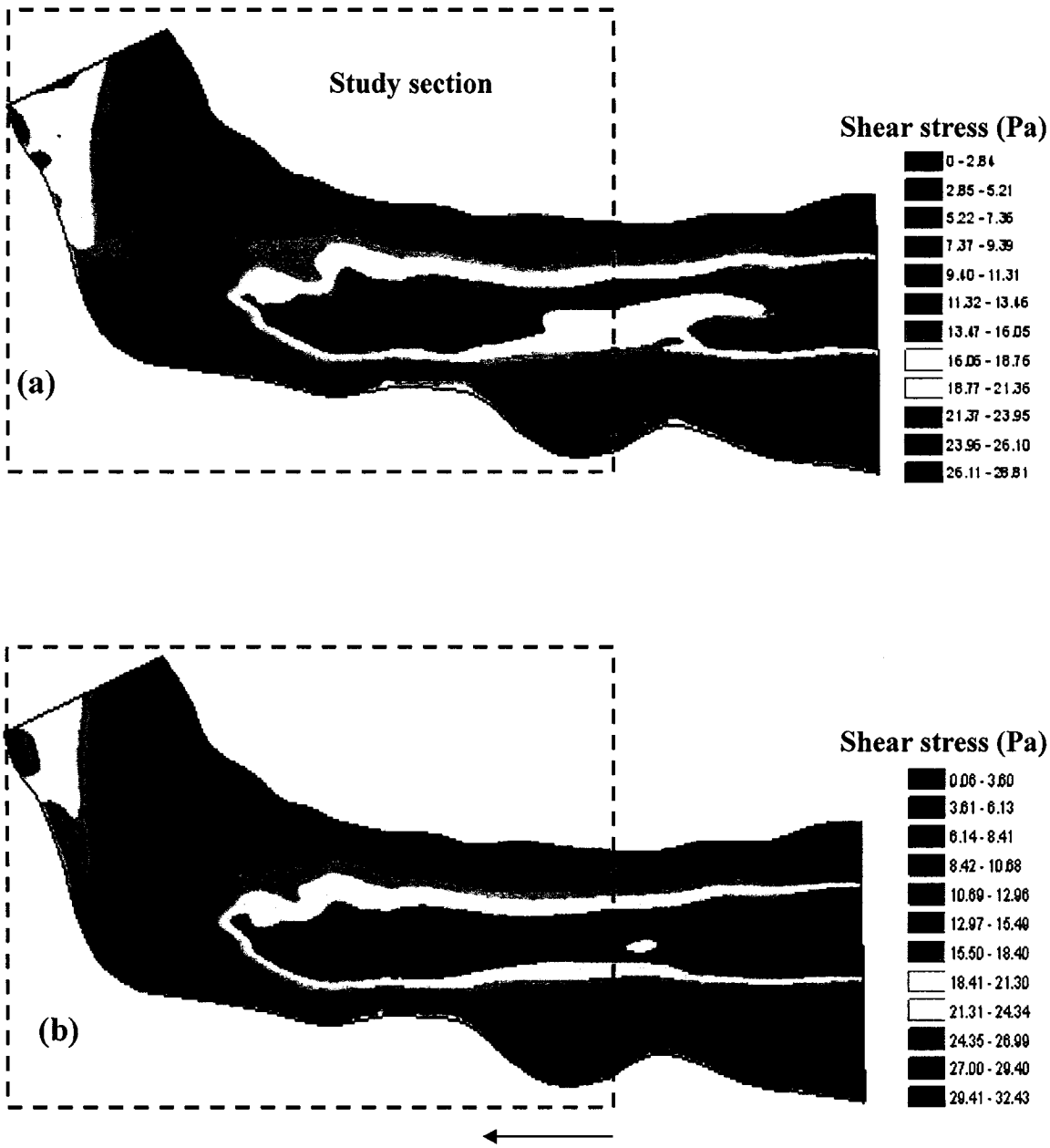

Fig. 4.16. Interpolated filled contour estimated bed shear stress using the (a) third cell (assumed near bed) (b) fourth cell (depth-averaged).

(a)

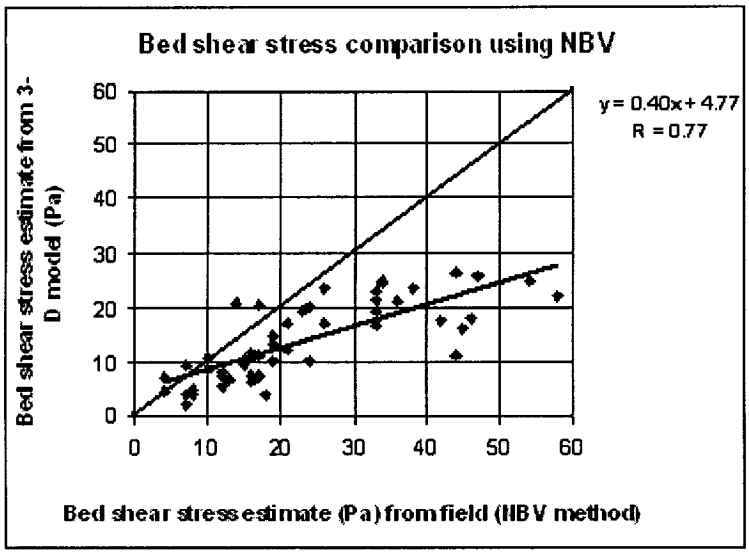

(b)

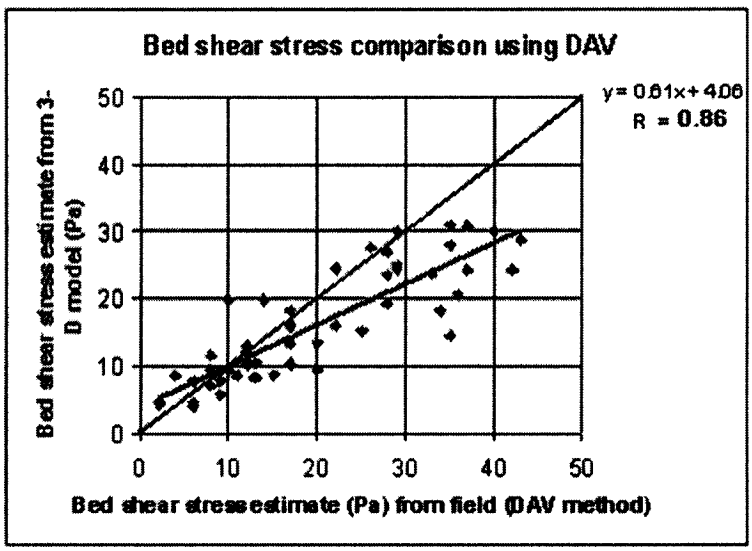

Figure 4.17. Correlation results between the estimated bed shear stresses from 3-D model and field measurements (a) using the third cell (assumed near bed) velocities and comparing with results in field measurement using equation 4.2 (b) using the depth-averaged velocities (fourth cell) and comparing with results in field measurement using equation 3.2.

cell velocities (Fig. 4.17a), shear stresses obtained from the depth-average velocities (Fig. 4.17b) yielded a better correlation (0.86), with a slope of 0.61 (Fig. 4.17b), whereas, the correlation coefficient of using the near bed velocities was 0.77 with a slope of 0.40 (Fig. 4.17a).

4.3 Bed load transport

The bed load transport was computed using the different bed load equations as stated in section 3.3.4. To estimate the bed load, one applies the estimated bed shear stresses obtained from the quadratic stress law substituted into the different equations. These equations were applied for the 20 mm and 40 mm grain size diameters as seen in Table 4.2. Table 4.2 shows a comparison between the total bed load transport obtained from field measurements, and that obtained using the various bed load transport equations. The equations used for the computation of the bed load transport all gave very different results. Most of them showed zero transport rates, while some over-estimated and under-estimated the bed load transport compared to the field measurements of the different traps.

Table 4.2 shows that when the bed load equations based on critical shear stress were used, they gave highly inconsistent results (DuBoys equation, the Shields equation, and

Table 4.3 Estimates of bed load transport using different equations

D=20mm Field (g/m/s)

Traps	Stress	>2mm	Total	Shields	Meyer- Peter	MPM	Nielsen	Sato et al.	Duboys	Eugelund
	(N/m^2)	(g/m/s)	(g/m/s)	(g/m/s)	(g/m/s)	(g/m/s)	(g/m/s)	(g/m/s)	(g/m/s)	(g/m/s)
1	23.53	9.7	10.56	-	996.80	10.13	6691.73	-	20.72	235.94
2	25.76	3.26	3.88	-	1422.77	797.37	7705.53	-	33.43	323.90
3	14.67	35.17	36.94	-	-	-	3173.35	-	-	45.13
4	22.26	34.26	44.05	-	777.77	-	6136.00	-	14.31	194.29
5	2.65	1.45	10.15	-	-	-	131.86	-	-	0.11
6	6.51	10.1	12.25	-	-	-	819.16	-	-	2.63
7	8.52	7.55	9.01	-	-	-	1301.99	-	-	6.74

D=40mm Field (g/m/s)

Traps	Stress	>2mm	Total	Shields	Meyer- Peter	MPM	Nielsen	Sato et al.	Duboys	Eugelund
	(N/m)	(g/m/s)	(g/m/s)	(g/m/s)	(g/m/s)	(g/m/s)	(g/m/s)	(g/m/s)	(g/m/s)	(g/m/s)
1	23.53	9.7	10.56	-	-	-	2222.17	-	-	117.97
2	25.76	3.26	3.88	-	-	-	2573.94	-	-	161.95
3	14.67	35.17	36.94	-	-	-	1008.47	-	-	22.56
4	22.26	34.26	44.05	-	-	-	2029.62	-	-	97.14
5	2.65	1.45	10.15	-	-	-	-	-	-	0.06
6	6.51	10.1	12.25	-	-	-	214.02	-	-	1.13
7	8.52	7.55	9.01	-	-	-	373.84	-	-	3.37

Sato et al.). This was anticipated as stated in section 2.5. In many instances, no bed load transport was predicted. The Nielsen equation, which gave an estimate for all the traps, greatly over-estimated the bed load transport compared to the field measurements. The Eugelund-Hansen stream power equation was used to validate the simulation data. Although this equation over-estimated and under-estimated the bed load transport rates, the bed load estimate ranges were comparable to the field measurements. Bold numbers in Table 4.2 indicate the most appropriate traps associated with the chosen grain size diameter (d). For instance, Traps 1 and 2, d = 40mm was chosen because the region close to the upstream traps (1 and 2) contained sediment transported from upstream which had a d_{50} of 40mm. Similarly for the downstream traps 3 to 7, d = 20 mm was chosen.

Fig. 4.18 shows a comparison between the bed load transport rate from field measurements and predictions using the different estimated bed shear stresses (field, 2-D, 3-D) in the Eugelund-Hansen stream power equation. Fig. 4.18a shows that, comparing the bed load transport rates obtained using the three (field, 2-D, 3-D) estimated bed shear stresses, the 3-D bed load transport rate predictions for traps 1, 3, 5, 6, and 7 were the closest to the bed load transport rates obtained from field measurements. The figure also shows that, though the 2-D bed load transport rate predictions were relatively better for traps 2 and 4 compared to the field and 3-D, the bed load transport rates obtained were still much greater than the actual bed load transport rates obtained from the field measurement. No cases where the estimated bed shear stresses measured in the field gave a better match for the actual bed load transport rates. Overall, all bed load transport rates obtained from the various estimates of bed shear stresses gave poor correlation results

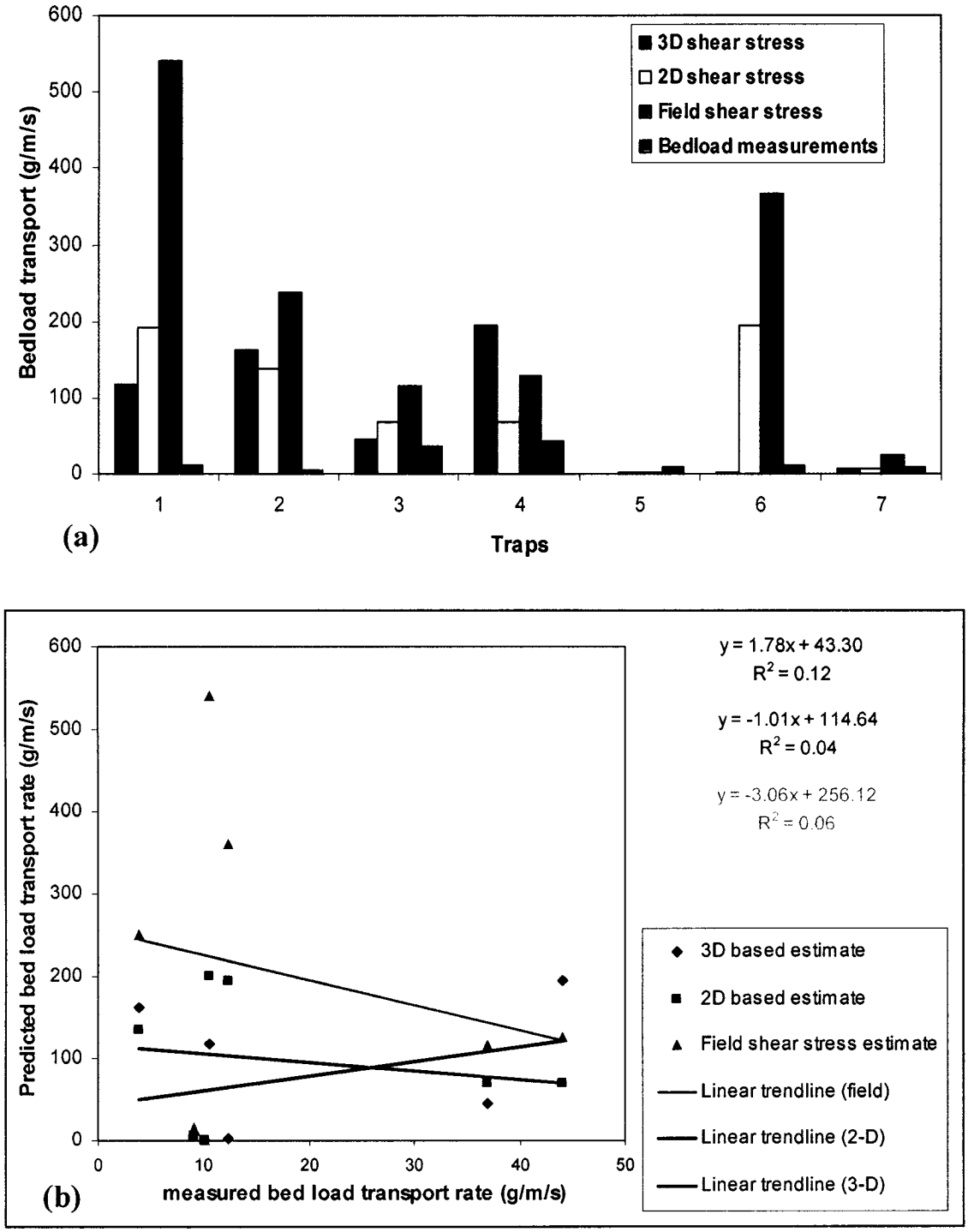

Fig. 4.18 Bed load comparison between using the different bed shear stresses in the Eugelund-Hansen stream power equation and the actual field measurement (a) for the traps (b) correlation results

when compared to the actual bed load transport rates from field measurements. The coefficient of determination (R^2) for the 3-D, 2-D and the field when compared to the actual bed load transport rates from field are 0.12, 0.04, and 0.06 respectively (Fig. 4.18b). These results show that the estimated bed shear stresses from the 3-D (quadratic stress law) had a better bed load transport predictions compared to using estimated bed shear stresses from field measurements and 2-D.

Various reasons appear to contribute to the discrepancies between the estimated bed load transport from the field measurements and the estimated bed load transport obtained from the various equations. These reasons include the following:

1. Bed load heterogeneity in size.
2. Bed armoring: Due to the effect of armoring in a gravel bed river, bed load transport rates might not be a direct function of the bed shear stress.
3. The type of conditions under which these equations were developed (flume experiments mostly).
4. The flow conditions of the upstream part of the study reach in this study.
5. Sediment supply into the river bed: In a natural river it is practically impossible to have sediment equilibrium (inflow of sediment = outflow of sediments). In the effect of this when more sediment is removed than supplied to an upstream region of a natural river, one expects a higher bed load transport rate to be measured downstream during field measurements.
6. Inadequate specification of flow conditions (velocity).
7. Errors associated with bed load field measurement rates.

As earlier discussed in section 2.5, high bed shear stresses should be associated with high bed load transport rates. Fig. 4.19, Fig. 4.20, and Fig. 4.21 show the bed load transport rates from field measurements for the traps and the estimated bed shear stresses obtained from the field measurements, the 2-D model, and the 3-D model. The three figures show that traps 1 and 2, which are located in a zone of high shear stress estimates, did not show the highest bed load transport rates. Conversely, traps 3 and 4, which have the largest transport rates, are located in a zone of lower shear stress for the 2-D and field estimates (Fig. 4.19, Fig. 4.20). Only in the 3-D simulation is there an apparent increase in bed shear stress close to the trap 3 (Fig. 4.21).

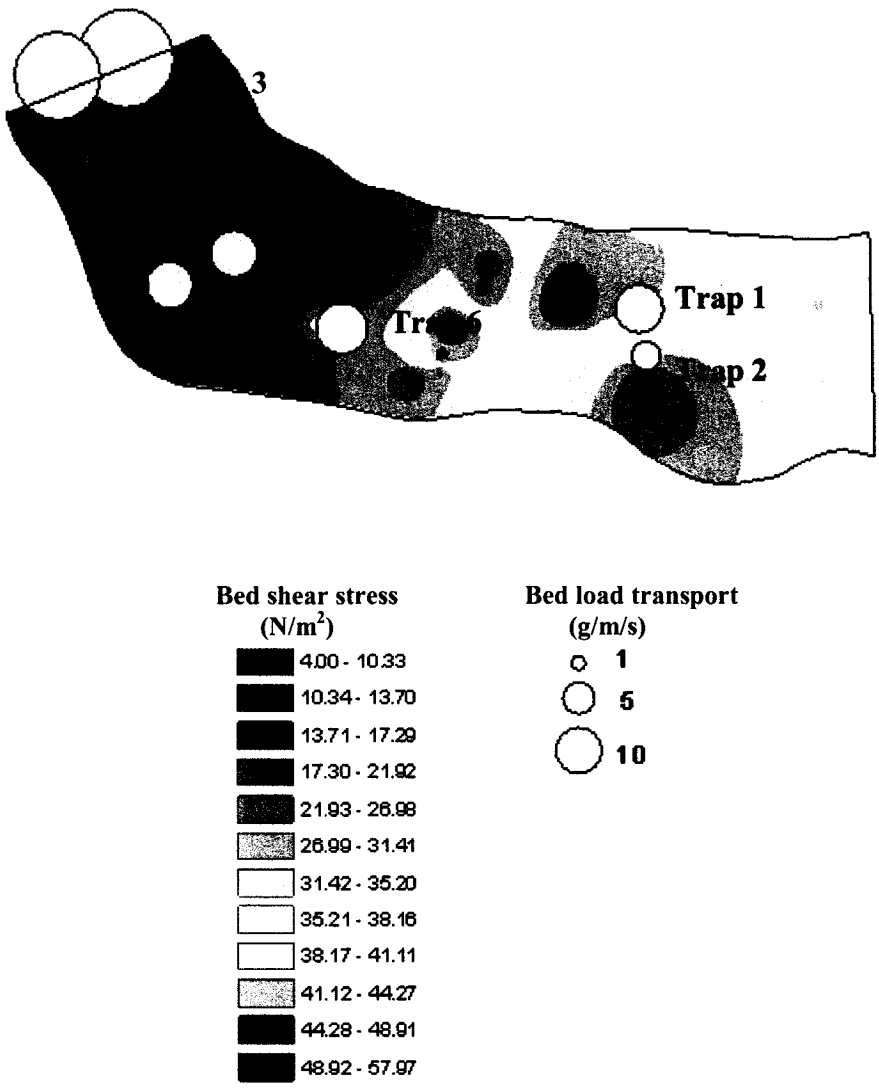

Fig. 4.19 Field measurements of the bed load transport for the traps and the estimated bed shear stress from field measurements.

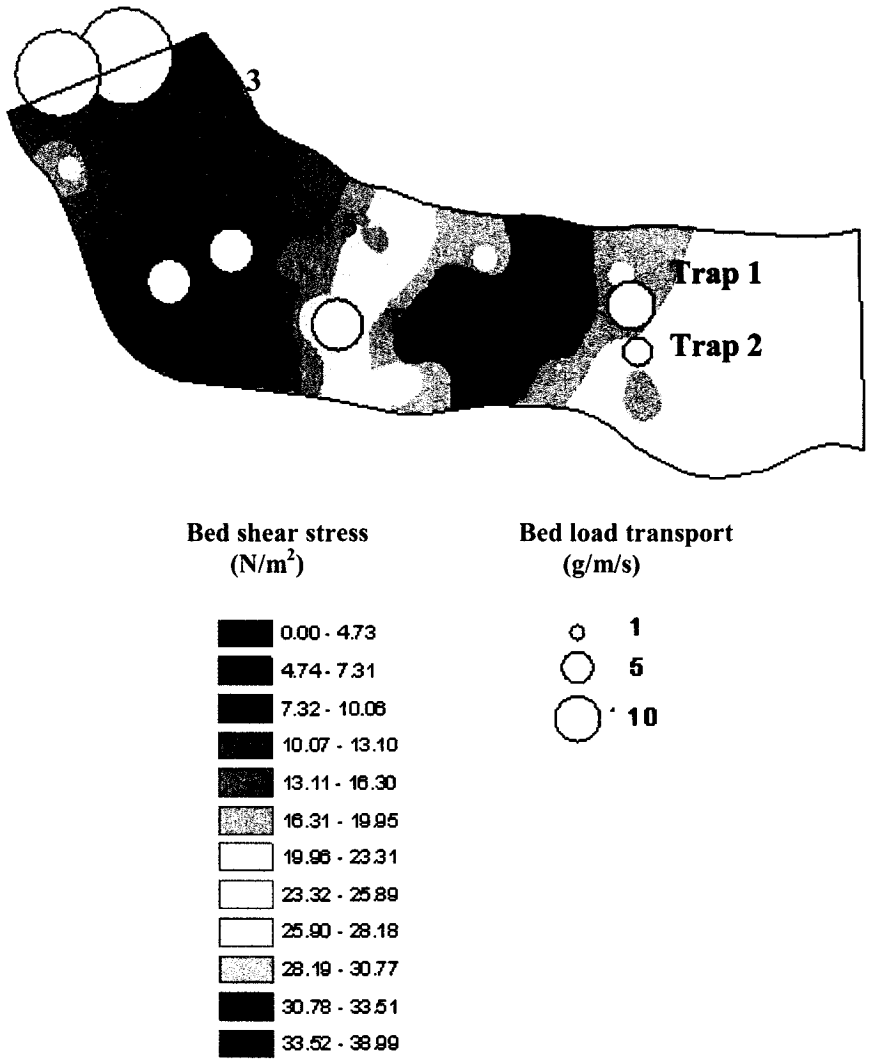

Fig. 4.20 Field measurements of the bed load transport for the traps and the estimated bed shear stress from 2-D model.

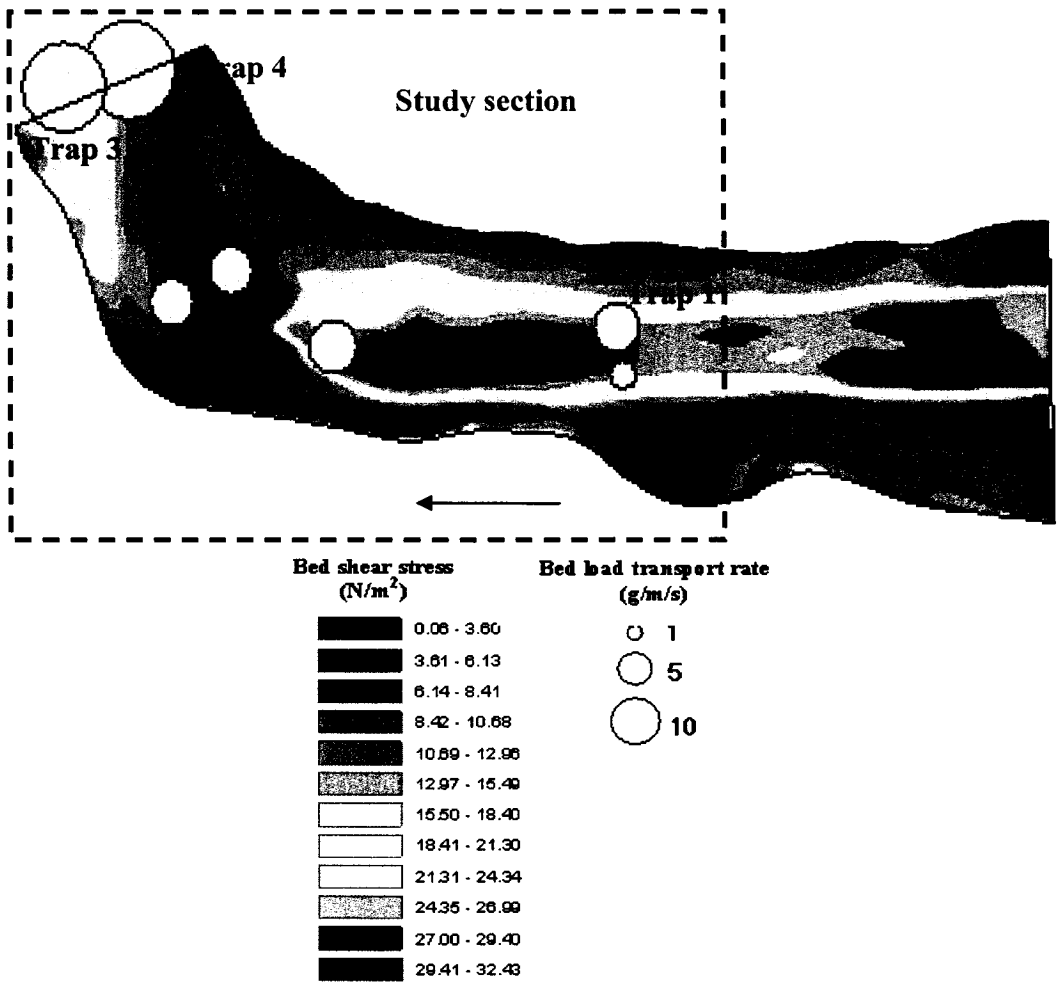

Fig. 4.21. Field measurements of the bed load transport for the traps and the estimated bed shear stress from 3-D model.

5.0 DISCUSSION OF RESULTS

5.1 Discussion

5.1.1 Flow field

When compared to the previous work (field measurements and 2-D model), the 3-D model was able to reproduce the overall flow pattern relatively well. The results were dependent on the conditions at the inlet to the study section. However, the quantitative predictions in this study were less satisfactory than expected. This may have been caused by numerous factors, which include the specification of the inlet conditions, the specification of the roughness coefficient, the complexity involved in the mesh generation of the study reach, especially at regions of shallow to deep transitions, inaccuracies in the location of measuring points, errors due to field measurements and possibly unsteadiness in flow conditions. These factors may be responsible for the outliers seen in Fig. 4.10.

The 3-D model showed the main features of a meandering river such as the secondary flow (Hodskinson and Ferguson, 1998; Butler et al., 2001; Korman et al., 2004). Figures 4.2, 4.4 and 4.6 effectively illustrate this. These secondary flow features could not be produced in the 2-D model. This aspect of 3-D simulation represents a key advantage in using the 3-D model (Fig.3.3).

5.1.2 Bed shear stress

Bed shear stress is a fundamental variable in river studies to link flow conditions to sediment transport (Biron et al., 2004). Direct measurements of bed shear stresses acting

on the bed of a river are very difficult to obtain. Therefore, it is extremely difficult to truly validate bed shear stress data in the field, especially for erodible bed. However, indirect methods are being used to estimate bed shear stress (Dietrich and Whiting, 1989). Bed shear stress predictions will differ fundamentally for a complex flow field with recirculation, between a 3-D and a 2-D model. This is because the 3-D model calculates the shear directly from the velocity of the bottom cell with respect to the bed, while the 2-D calculates the shear based on the depth-averaged velocity (Lane et al., 1999).

The quadratic stress law was used to estimate the bed shear stresses in this study due to the under-estimated bed shear stress results obtained from Phoenics. Assessing which predictions (Phoenics or quadratic stress law) are correct is difficult because of problems of shear stress measurement in natural channels and rivers with complex bed topographies. In a gravel-bed river, both models are likely to under-estimate shear stress variability, and both under-and over-estimate individual bed shear stress magnitudes due to the effects of individual grains and grain arrangements upon local velocities, and hence, shear stresses (Lane et al., 1999).

5.1.3 Bed load transport

The bed load transport obtained from the 3-D model bed shear stress estimates showed different results when using different transport equations (Tables 4.2). This would agree with previous studies that transport equations, which relate sediment transport to stream, flow hydraulics and sediment characteristics generally fail to predict the bed load

transport accurately (Gomez and Church, 1989; Ham and Church, 2000; Habersack and Laronne, 2002; Barry et al., 2004). The reason for this is that all transport equations has been established relying on calibration using flumes and field data, supposedly under steady uniform flow conditions. In addition, the effect of armoring that is present in a gravel bed river cannot be reproduced in flume tests. Other factors responsible for the inadequacy for the transport equations to predict bed transport for natural rivers include the bed topography, the flow pattern, the specifications for sediment characteristics (diameter), sediment supply in the river, and assumptions made in the use of the equations. The zero transport rates experienced during the course of this study were also experienced in previous studies (Martin and Church, 1995; Martin, 2003; Barry et al., 2004) because most bed load transport equations contain transport threshold (Barry et al., 2004). Despite these limitations in the use of bed load equations to predict bed load transport, the results from this study showed that the Eugelund-Hansen stream power equation performed better in the bed load transport prediction compared to other equations. This is in agreement with previous studies (Habersack and Laronne, 2000; Barry et al., 2004), which showed that stream power equations are more reliable for bed load predictions compared to shear stress based formulae.

Bed shear stress has been associated with bed load transport in previous studies (Dietrich, 1989; Dargahi, 2004). However, using any of the estimated bed shear stresses from field measurements, 2-D models, and 3-D models in this study did not agree with the fact that a higher bed shear should produce a larger bed load transport (Fig. 4.19, Fig. 4.20, and Fig. 4.21). Even though the bed load transport rate predictions obtained from the

estimated bed shear stresses of the 3-D had a correlation result, which was slightly better, no bed load equation model provided a satisfactory prediction of bed load transport. Regardless of the shear stress estimate method (field, 2-D, or 3-D), the Eugelund-Hansen equation was still the closest range to the measured bed load transport rates (Tables 5.1 and 5.2).

Table 5.1 Estimates of bed load transport using estimated bed shear stress from field measurements

D = 20 mm

Traps	Stress	>2mm	Total	Shields	Meyer-Peter	Nielsen	MPM	Sato	Duboys	Eugelund
	(N/m)	(g/m/s)	(g/m/s)	(g/m/s)	(g/m/s)	(g/m/s)	(g/m/s)	(g/m/s)	(g/m/s)	(g/m/s)
1	41.4	9.7	10.56	120194.81	5560.58	45333.16	16812.96	-	165.15	1080.60
2	31.68	3.26	3.88	-	2773	30029.35	5243.18	-	71.01	474.48
3	18.62	35.17	36.94	-	262.67	13114.25	-	-		115.87
4	20.51	34.26	44.05	-	506.95	15281.85	-	-	4.78	129.58
5	9.28	1.45	10.15	-	-	4253.47	-	-	-	2.55
6	28.74	10.1	12.25	-	2065.73	25831.04	2715.68	-	49.23	367.02
7	12.97	7.55	9.01	-		7366.46	-	-	-	25.43

D = 40mm

Traps	Stress	>2mm	Total	Shields	Meyer-Peter	Nielsen	MPM	Sato	Duboys	Eugelund
	(N/m^2)	(g/m/s)	(g/m/s)	(g/m/s)	(g/m/s)	(g/m/s)	(g/m/s)	(g/m/s)	(g/m/s)	(g/m/s)
1	41.4	9.7	10.56	-	1512.96	15488.49	-	-	15.89	540.30
2	31.68	3.26	3.88	-	60.01	10145.31	-	-		237.24
3	18.62	35.17	36.94	-	-	4274.94	-	-	-	57.94
4	20.51	34.26	44.05	-	-	5016.39	-	-		64.79
5	9.28	1.45	10.15	-	-	1248.5	-	-	-	1.28
6	28.74	10.1	12.25	-	-	8683.4	-	-	-	183.51
7	12.97	7.55	9.01	-	-	2302.59	-	-	-	12.72

Table 5.2 Estimates of bed load transport using estimated bed shear stress from 2-D

D = 20mm Field

Traps	Stress	>2mm	Total	Shields	Meyer-Peter	Nielsen	MPM	Sato	Duboys	Eugelund
	(N/m)	(g/m/s)	(g/m/s)	(g/m/s)	(g/m/s)	(g/m/s)	(g/m/s)	(g/m/s)	(g/m/s)	(g/m/s)
1	29.19	9.7	10.56	-	2170.44	9356.95	3069.2	-	52.39	386.82
2	25.89	3.26	3.88	-	1448.1	7763.75	861.6	-	31.06	275.01
3	14.63	35.17	36.94	-		3159.3	-	-	-	68.76
4	15.62	34.26	44.05	-	11.38	3508.74	-	-	24.22	67.59
5	5.64	1.45	10.15	-		633.67	-	-	-	1.34
6	24.67	10.1	12.25	-	1208.62	7204.87	315.16	-	-	193.70
7	7.26	7.55	9.01	-		990.02	-	-	-	6.76

D = 40mm

Traps	Stress	>2mm	Total	Shields	Meyer-Peter	Nielsen	MPM	Sato	Duboys	Eugelund
	(N/m^2)	(g/m/s)	(g/m/s)	(g/m/s)	(g/m/s)	(g/m/s)	(g/m/s)	(g/m/s)	(g/m/s)	(g/m/s)
1	29.19	9.7	10.56	-	-	3148.1	-	-	-	193.41
2	25.89	3.26	3.88	-	-	2594	-	-	-	137.51
3	14.63	35.17	36.94	-	-	1003.66	-	-	-	34.38
4	15.62	34.26	44.05	-	-	1123.42	-	-	-	33.80
5	5.64	1.45	10.15	-	-	153.68	-	-	-	0.67
6	24.67	10.1	12.25	-	-	2400.14	-	-	-	96.85
7	7.26	7.55	9.01	-	-	270.21	-	-	-	3.38

6.0 SUMMARY, CONCLUSIONS AND RECOMMENDATIONS

6.1 Summary

Rivers have a complex and three-dimensional form, which makes it difficult to adequately characterize channel boundary conditions, flow conditions, and sediment properties. Several studies have shown that 3-D models have the ability to predict the flow field distribution more accurately than the 2-D models in natural rivers. However, this accuracy is dependent on several factors. These factors are related to the accuracy of the field measurements used for inlet conditions, the complexity of the river geometry, which affects the mesh generation, the boundary conditions, and the type of inlet conditions specified. The bed shear stress estimates of natural rivers can be obtained in several ways, which gives very different results (Biron et al., 2004). This complicates shear stress validation.

The bed load transport of a natural river does not only depend on the bed shear stress but to a large extent depends on the river geometry, flow pattern, sediment characteristics, sediment supply in the river, and armoring in the case of gravel bed rivers. The difficulty of predicting bed load transport rate is well known, and the advantage of the 3-D over a 2-D model is not that obvious given the large error in bed load predictions. However, 3-D model is required to properly characterize secondary circulation, which occurs in curved channels, and which significantly affect sediment transport (Odgaard, 1989a, b; Shams et al., 2002; Ferguson et al., 2003; Olsen, 2003; Dargahi, 2004)

6.2 Conclusions

The following conclusions are drawn from the present study.

1. The 3-D model developed predicted the flow field of the Escoumins River reasonably well.

2. Unlike the 2-D model, the 3-D model developed successfully predicted the secondary flow present in a meandering river.

3. The depth-average velocity provides better correlation with field data for the bed shear stress distribution.

4. The bed shear stress was estimated using the following: (i) indirect field measurements (ii) 2-D model (iii) 3-D model. The bed load transport rates obtained using the estimated bed shear stresses from the 3-D model was better than the bed load transport rates obtained using the estimated bed shear stresses from the indirect field measurements and the 2-D model.

5. The bed load transport equations under-predicted, over-predicted, and also showed zero transport rates when compared to the sediment data. However, some reasonable agreement was obtained using the Eugelund-Hansen stream power equation to predict the bed load transport of a natural river.

6.2 Recommendations

1. Further studies should be carried out on the grid generation of natural rivers with complex geometries.

2. Further studies should be carried out in obtaining good knowledge of the boundary and inlet conditions.

3. Further studies should be carried out in obtaining the best approach to estimate bed shear stresses, especially in natural rivers with complex geometries.

4. Studies should be carried out on the derivation of bed load transport equations for natural rivers. This can be accomplished by carrying out more bed load transport field measurements, grain size distribution of sediments and relating them to the hydraulic and sediment parameters.

5. Further studies should be carried out on the use of the stream power equations to predict bed load transport.

REFERENCES

Alexander, G.R., and Hansen, E.A., 1986. Sand bed load in a brook trout stream. *North American Journal of Fisheries Management*, 6, 9-23.

Andrews, E. D., and Nelson, J. M., 1989. Topographic response of a bar in the green river, Utah, to variation in discharge. In Ikeda, S., and Parker, G. (eds), *River meandering: American Geophysical Union*, Water Resource Monograph, 12, 463-485.

Andrews, E.D., and Pizzi, L.A., 2000. Origin of the Colorado River experimental flood in Grand Canyon. *Hydrological Sciences*, 45, 607-627.

Barry, J.J., Buffington, J.M., and King, J.G., 2004. A general power equation for predicting bed load transport rates in gravel bed rivers. Water Resources Research, 40, W10401.

Bathurst, J.C., Benson, I.A., Valentine, E.M., and Nalluri, C., 2002. Overbank sediment deposition patterns for straight and meandering flume channels. *Earth Surfaces Processes and Landforms,* 27, 659-665.

Bennett, J.P., 1995. Algorithm for resistance to flow and transport in sand-bed channels. *Journal of Hydraulic Engineering, 121,* 578-590.

Best, J. L., and Reid, I., 1984. Separation zone at open channel junctions. *Journal of Hydraulic Engineering,* 110(11), 1588-1594.

Biron, P.M., Richer, A., Kirkbride, A.D., Roy, A.G., and Han, S., 2002. Spatial patterns of water surface topography at a river confluence. *Earth Surface Processes and Landforms*, 27, 913-928.

Biron, P.M., Robson, C., Lapointe, M.F., and Gaskin, S.J., 2004. Comparing different methods of bed shear stress estimates in simple and complex flow fields. *Earth Surfaces Processes and Landforms,*29, 1403-1415.

Booker, D.J., Shear, D.A., and Payne, A.J., 2001. Modelling three-dimensional flow structures and patterns of boundary shear stress in a natural pool-riffle sequence. *Earth Surface Processes and Landforms,* 26, 553–576.

Bradbrook, K.F., Biron, P., Lane, S.N., Richards, K.S., and Roy, A.G., 1998. Investigation of controls on Secondary circulation and mixing processes in a simple confluence geometry using a three-dimensional numerical model. *Hydrological Processes*, 12, 1371-96.

Bradbrook, K.F., Lane, S.N., and Richards, K.S., 2000a. Numerical simulation of time-averaged flow structure at river channel confluences. *Water Resources Research*, 36, 2731-46.

Bradbrook, K.F., Lane, S.N., Richards, K.S., Biron, P.M., and Roy, A.G., 2000b. Large Eddy Simulation of periodic flow characteristics at river channel confluences. *Journal of Hydraulic Research*, 38, 207-16.

Bridge, J. S., and Gabel, S. L., 1992. Flow and Sediment dynamics in a low sinuosity, braided river: Calamus River, Nebraska Sandhills. *Sedimentology*, 39, 125-142.

Butler, J.B., Lane, S.N., and Chandler, J.H. 2001. Application of two-dimensional fractal analysis to the characterisation of gravel-bed river surface structure. *Mathematical Geology*, 33, 301-30.

Chang, H.H., 1988. *Fluvial Processes in River Engineering*. John Wiley: New York. 81-137.

Chanson, H., 1999. *The Hydraulics of Open Channel Flow*. Arnold: London. 149-209.

Church, M., Hassan, M., and Wolcott, J., 1998. Stabilizing self-organized structures in gravel-bed stream channels: field and experimental observations. Water Resources Research, 35, 3169-3179.

Conti, C., Morandi, R., and Spitaleri, R.M., 2004. An algebraic-elliptic algorithm for boundary orthogonal and grid generation. *Applied Mathematics and Computation* (in press).

Dargahi, B., 2004. Three-dimensional flow modeling and sediment transport in River Klaralven. *Earth Surfaces Processes and Landforms*, in press.

Demuren, A.O., 1989. Calculation of sediment transport in meandering channels. *Tech. Session A, Proc., 23rd IAHR Congr.,* International Association of Hydraulic Research, Delft, The Netherlands.

Demuren, A.O., 1991. Development of a mathematical model for sediment transport in meandering rivers. *Rep. No 693*, Inst. for Hydro-mechanics, University of Karlsrushe, Germany

Dietrich, W. E., and Whiting, P. J., 1989. Boundary shear stress and sediment transport in river meanders of sand and gravel. In Ikeda, S. and Parker, G. (eds), *River meandering*, AGU Water Resour. Monog. 12, 1-50.

Dietrich, W.E., and Smith, J.D., 1983. Influence of the point bar on flow through curved channels. *Water Resources Research*, 19, 1173-1192.

Dietrich, W.E., Smith, J.D., and Dunne, T., 1979. Flow and sediment transport in a sand bedded meander. *Journal of Geology*, 87, 305-315.

Ferguson, R.I., Parsons, D.R., Lane, S.N. and Hardy, R.J., 2003. Flow in meander bends with recirculation at the inner bank, *Water Resources Research* 39, 2003WR001965.

Garde, R.J., and Ranga Raju, K.G., 1985. *Mechanics of sediment transportation and alluvial stream problems*. Halsted Press, New Delhi. 177-179.

Ghanem, A., Steffler, P., and Hicks, F., 1996. Two-dimensional hydraulic simulation of physical habitat conditions in flowing streams. *Regulated Rivers: Research and Management*, 12, 185-200.

Gomez, B., and Church, M., 2000. Bed–material transport estimated from transport formulae for gravel bed rivers. *Water Resources Research* 25, 1161-1186

Graf, W.H., 1971. Hydraulic of Sediment Transport. McGraw-Hill: New York, pp 101.

Guo, Q-C., and Jin, Y-C., 1999. Modelling sediment transport using depth-averaged and moment equations. *Journal of Hydraulic Engineering*, 125, 1262-9.

Habersack, H.M., and Laronne, J.B., 2002. Evaluation and Improvement of Bed Load Discharge Formulas based on Heley-Smith Sampling in an Alpine Gravel Bed River. *Journal of Hydraulic Engineering*, 128. 484-499.

Ham, D.A, and Church, M., 2000. Bed material transport estimated from channel morphodynamics: Chilliwack River, British Columbia. *Earth surface processes and landforms* 25, 1123-1142

Hattingh, J., and Rust, I.C., 1993. Flood transport and deposition of tracer heavy minerals in a gravel-bed meander bend channel. *Journal of Sedimenaryt Petrology*, 63, 828-834.

Heede, B.H., and Rinne, J.N., 1990. Hydrodynamic and fluvial morphologic processes: Implications for fisheries management and research. *North American Journal of Fisheries Management*, 10,249-268.

Heggberget,T.G., 1988. Timing of spawning in Norwegian atlantic salmon (Salmo salar). *Canadian Journal of Fisheries and Aquatic Science*, 45, 845-849.

Heniche, M., Secretan, Y., Boudreau, P., and Lecler, M., 2000. A two-dimensional finite element drying-wetting shallow water model for rivers and estuaries. *Advances in Water Resources* 23, 359-372

Hickin, E.J., 1977. Hydraulic factors controlling channel migration. In Davidson-Arnott, R. and Nickling, W. (Eds), *Proceedings of the 5th Guelph Geomorphology Symposium.* Geobooks, Norwich. 59-72

Hickin, E.J., 1986. Concave-bank benches in flood plains of Muska and Fort Nelson Rivers, Bristish Columbia. *Canadian Geography*, 30, 111-122

Hodskinson, A., and Ferguson, R. I., 1998. Numerical modelling of separated flow in river bends: Model testing and experimental investigation of geometric controls on the extent of flow separation at the concave bank, *Hydrological Processes,* 12, 1323-1338.

Hubbell, D.W., 1987. Bed load sampling and analysis. In: Thorne, C., Bathurst, J., Hey, R. (Eds.), Sediment Transport in Gravel-Bed Rivers. Wiley, Chichester, pp. 89-106

Hughes, S.A., 1993. Physical models and laboratory techniques in coastal engineering. *Advance Series on Ocean Engineering*, Volume 7. World Scientific, Singapore, pp 568

Jackson, R.G., 1975. Velocity bedform texture patterns of meander bends in the lower Wabash River of Illinois and Indiana. *Geological Society of America Bulletin*, 86, 1511-1522.

Jordan, S.A., and Spaulding, M.L., 1993. A Fast Algorithm for Grid Generation. *Journal of Computational Physics*, 104, 118-128.

Khamayseh, A., Kuprat, A., and Mastin, C.W., 1999. Boundary orthoganility in elliptic grid generation. In Thompson, J.F. (Ed.), Soni, B.K., Weatherill, N.P. (Eds.), Handbook of grid generation, CRC Press, Boca Raton, Florida.

Korman, J., Wiele, S.M., and Torizzo, M., 2004. Modeling effects of discharge on habitat quality and dispersal of juvenile humpback chub (Gila Cypha) in the Colorado River, Grand Canyon. *River Research and Apllications*, 20, 379-400.

Lane, S.N., and Ferguson, R.I. (forthcoming). Modeling reach-scale fluvial flows. In: Bates, P.D., Lane, S.N., and Ferguson, R.I. (eds). CFD Applications in Hydrology and Hydraulics: Theory and Pratice. Wiley.

Lane, S.N., Bradbrook, K.F., Richards, K.S., Biron, P.M. and Roy, A.G., 1999. The application of computational fluid dynamics to natural river channels: three-dimensional versus two-dimensional approaches. *Geomorphology*, 29, 1-20.

Lane, S.N., Bradbrook, K.F., Richards, K.S., Biron, P.M. and Roy, A.G., 2000. Secondary circulation in river channel confluences: measurement artefacts or coherent flow structure. *Hydrological Processes*, 14, 2047-2071.

Lane, S.N., Richards, K.S., 1995. Within-reach spatial patterns of process and channel adjustment. In Hickin, E.J. (Ed.), *River Geomorphology*, Wiley, Chichester, 105-130.

Latulippe, C., 2004. Private Communication.

Latulippe, C., Lapointe, M.F., and Talbot, T., 2001. Visual characterization technique for gravel-cobble river bed surface sediments; Validation and environmental applications contribution to the programme of CIRSA (centre interuniversitaire de recherché sur le saumon atlantique). *Earth Surface Processes and Landforms* 26, 207-318.

Launder, B. E., and D. B. Spalding, 1974.The numerical computation of turbulent flows. *Computer Methods in Applied Mechanics and Engineering,* 3, 269-289.

Lee, H.Y., Hsieh, H.M., Yang, J.C., and Yang, C.T., 1997. Quasi-two-dimensional simulation of scour and deposition in alluvial channels. Journal of Hydraulic Engineering, 123, 600-609.

Leopold, L.B., and Emmett, W.W., 1984. Bedload movement and its relation to scour, in River meandering. *Proceedings of the conference*, Rivers '83, edited by Elliot, C.M., pp 640-649, American Society of Civil Engineering, New York.

Leopold, L.B., and Wolman, M.G., 1960. River meanders. *Geological Society of America Bulletin*, 71, 769-794.

Lin, B.L., and Falconer, R.A., 1996. Numerical modeling of three-dimensional suspended sediment for estuarine and costal waters. *Journal of Hydraulic Research*, 34(4), 435-456.

Lisle, T.E, Nelson, J.M, Pitlick, J., Madej, M.A, and Barkett, B.L., 2000. Variability of bed mobility in natural, gravel-bed channels, and adjustments to sediment load at local and reach scales. *Water Resources Research*, 36(12), 3743-3755.

Ma, L., Ashworth, P.J., Best, J.L., Elliott, L., Ingham, D.B, and Whitcombe, L.J., 2002. Computational fluid dynamics and the physical modeling of an upland urban river. *Geomorphology*, 44, 375-391.

Markham, A.J., and Thorne, C.R., 1992. Geomorphology of gravel bed river bends. In *Dynamics of Gravel Bed Rivers*, Billi, P., Hey, R.D., Thorne, C.R., Tacconi, P. (Eds). Wiley, Chichestes, 433-456.

Martin, Y., 2003. Evaluation of bed load transport formulae using filed evidence from the Vedder River, British Columbia. Geomorphology, 53, 75-76.

Meselhe, E.A., and Sotiropolous, F., 2000. Three-dimensional numerical model for open-channels with free surface variations. *Journal of Hydraulic Research*, 38, 115-121.

Milhous, R.T., 1998. Modeling of instream flow needs: The link between sediment and aquatic habitat. Regulated Research: *Research and Manangement*, 14, 79-94

Nagata, N., Hosoda, T., and Muramoto, Y., 2000. Numerical analysis of river channel processes with bank erosion. *Journal of Hydraulic Engineering*, 126, 243-252.

Nicholas AP, Sambrook-Smith GH. 1999. Numerical simulation of three-dimensional flow hydraulics in a braided river. *Hydrological Processes* 13, 913–929.

Odgaard, A.J. and Bergs, M.A., 1988. Flow processes in a curved alluvial channel. *Water Resources Research*, 24, 45-56.

Odgaard, A.J., 1989a. River meander model. I: Development. Journal of Hydrologic Engineering, 115(11), 1433-1450.

Odgaard, A.J., 1989b. River meander model. II: Applications. Journal of Hydrologic Engineering, 115(11), 1451-1464.

Olsen, N. R. B., 2003. Three-dimensional CFD modelling of self-forming meandering channel, *Journal of Hydraulic Engineering*, 129, 366-372.

Ouillon, S., and Dartus, D. ,1997. Three-dimensional computation of flow around groyne. *Journal of Hydraulic Engineering*, 123, 962-970.

Page, K., and Nanson, G., 1982. Concave-bank benches and associated floodplain formation. *Earth surface and Processes Landforms*, 7, 529-543

Paquier, A., and Khodashenas, S.A., 2002. River bed deformation calculated from boundary shear stress. *Journal of Hydraulic Research*, 40(5), 603-609

Patankar S.V, and Spalding D.B., 1972. Heat and Mass Transfer in Boundary Layers, 3rd edn. London.

Perkins, H.J., 1970. The formation of streamwise vorticity in turbulent flow. *Journal of fluid Mechanics*, 44, 721-740.

PHOENICS manual, concentration, heat and momentum (CHAM).

Reid, J.B., 1984. Artificial induced concave bank deposition as a means of floodplain erosion control. In Elliot, M. (Ed), *River Meandering. Proceedings of the conference Rivers '83,* ASCE. 295-304.

Rhoads, B.L., 1996. Mean structure of transport-effective flows at an asymmetrical confluence when the main stream is dominant. In Ashworth, P.J., Bennett, S., Best, J.L., and McLelland, S.M. (Eds.) *Coherent Flow Structures in Open Channels*, 459-490, Wiley, Chichester, 459-90.

Rinne, J.N., and Medina, A.L., 1989. Factors influencing salmoid populations in six headwater streams, central Aizona, USA. Polskie Archiwum, 35(3-4), 515-532.

Rodi, W., 2000. Numerical calculations of flow and sediment transport in rivers. *Scochastic Hydraulics*, Wang, Z.Y., and Hu S.X. (eds). Balkema, Rotterdam, 15-30.

Schlicting, H., 1987. Boundary Layer theory (7^{th} edition). McGraw Hill: New York

Schmidt, J.C., Parnell, R.A., Grams, P.E., Kaplinski, M.A., Stevens, L.E, and Hoffnagle, T.L., 2001. Ecological Applications, 11(3), 657-671.

Schoonees, J.S., and Theron, A.K., 1994. Accuracy and applicability of the SPM longshore transport formula. Proc. 24th ICCE, Kobe. ASCE, pp. 2595-2609.

Scrivener, J.C., and Brownlee, M.J., 1989. Effects of forest harvesting on spawning gravel and incubation survival of chum (*Oncorhynchus keta*) and coho salmo (*O. kisutch*) in Carnation Creek, British Columbia. *Canadian Journal of Fisheries and Aquatic Science*, 46, 681-696.

Shams, M., Ahmadi, G., and Smith, D.H., 2002. Computational modeling of flow and sediment transport and deposition in meandering rivers. *Advances in Water Resources*, 25, 689-699.

Shapiro, G.I., 2004. A 2.5D model for sand transport in a shallow sea: effect of Ekman veering. *Continental Shelf Research*, 24, 659-671.

Shimizu, Y., and Itakura, T., 1989. Calculation of bed variation in alluvial channels. *Journal of Hydraulic Engineering*, 115, 367-84.

Shiono, k., and Muto, Y., 1998. Complex flow mechanisms in compound meandering channels with overbank flow. *Journal of Fluid Mechanics,* 376, 221-261.

Sinha, S.K., 1997. An algebraic grid generation technique for three-dimensional Natural River reaches. *Communication in Numerical Methodes in Engineering*, 13, 475-485

Spitaleri, R.M., and Micacchi, V., 1998. A mulitiblock multigrid grid generation method for complex simulations. *Mathematics and Computer Simulation*, 46, 1-12.

Tappel, P.D., and Bjornn, T.C., 1983. A new method of relating size of spawning gravel to salmonid embryo survival. *North American Journal of Fisheries Management*, 3, 123-135

Thorne, C.R., Zevenbergen, L.W., Pitlick, J.C., Bradley, J.B., and Julien, P.Y., 1985. Direct measurements of secondary currents in a meandering sand-bed river. *Nature,* 316(6022), 746-747.

Tingsanchali, T., and Maheswaran, S., 1990. Two-dimensional depth-averaged flow computation near groynes. *Journal of Hydraulic Engineering*, 116, 103-125.

Van Rijn, L.C., 1987. Mathematical modeling of morphological processes in the case of suspended sediment transport. Delft Hydraulic Communication No. 382.

Vanoni, V.A. ASCE sedimentation engineering, Manual and Report on Engineering Pratice, No 54, 1975.

Vanoni, V.A., 1984. Fifty years of sedimentation. *Journal of Hydraulic Engineering*, 110, 1021-57.

Versteeg, H.K., and Malalasekera, W., 1995. *An Introduction to Computational Fluid Dynamics*. Longman. Harlow, London. 103-134, 134-155

Wang, S.Y., and Adeff, S.E., 1986. Three-dimensional modeling of river sedimentation processes. *Proc., 3rd int. Symp. on River sedimentation*, University of Mississipi, Mississipi.

Weerakoon, S.B., and Tamai, N., 1989. Three-dimensional calculation of flow in river confluences using boundary fitted co-ordinates. *Journal of Hydroscience and Hydraulic Engineering*, 7, 51-62.

Weerakoon, S.B., Kawahara, Y., and Tamai, N., 1991. Three-dimensional flow structure in channel confluences of rectangular section. *Proceedings of the 25th I.A.H.R. Congress A*, IAHR, Madrid 373-380.

White, T.E., 1994. Field tests of radiation-stress estimators of longshore sediment transport. Proc. 24th ICCE, Kobe. ASCE, pp. 2799-2812

White, T.E., 1998. Status of measurement techniques for coastal sediment transport. *Costal Engineering* ,35, 17-45

White, T.E., and Inman, D.L., 1989a. Application of tracer theory to NSTS experiments. In : Seymour, R.J. (Ed.), Nearshore Sediment Transport, Chap. 6B. Plenum, NY, pp. 115-128

White, T.E., and Inman, D.L., 1989b. Measuring longshore transport with tracers. In: Seymour, R.J. (Ed.), Nearshore Sediment Transport, Chap. 13. Plenum, NY, pp. 287-312

Whiting, P. J., and Dietrich, W. E, 1993, Experimental studies of bed topography and flow patterns in large-amplitude meanders, 1. Observations, *Water Resources Research* 29, 3605-3614.

Wilcox, D.C., 1998. *Turbulence modeling for CFD*. DCW Industries.

Wu, W., Rodi, W., and Wenka, T., 2000. 3D numerical modelling of flow and sediment transport in open channels. *Journal of Hydraulic Engineering*, 126, 4-15.

Yakhot, V., and Orszag, S.A, 1986. Renormalization group analysis of turbulence. I. Basic theory. *Journal of Scientific Computing* 1(1), 1-51.

Yu, L., Zhu, Y., and Righetto, A.M., 1997. Hybrid grid- A specialized mesh system for full three-dimensional numerical simulation in natural waters. *Mathematical Computation Modeling,* 26, 81-95.

Zhu, J., 1990. A hybrid differential-algebraic method for three-dimensional grid generation. *International Journal of Numerical Methods Engineering*, 29, 1271-1279.